Perturbation Analysis of Colorectal Cancer Cell Plasticity and Therapy Resistance at Single Cell Resolution

Dissertation

zur Erlangung des akademischen Grades

Doctor rerum naturalium

(Dr. rer. nat.)

eingereicht an der Lebenswissenschaftlichen Fakultät der Humboldt-Universität zu Berlin von

Mareen Lüthen

Präsidentin der Humboldt-Universität zu Berlin
Prof. Dr. Julia von Blumenthal
Dekan der Lebenswissenschaftlichen Fakultät der Humboldt-Universität zu Berlin
Prof. Dr. Dr. Christian Ulrichs

1. Gutachter: Prof. Dr. Monilola Olayioye
2. Gutachter: Prof. Dr. Nils Blüthgen
3. Gutachter: Prof. Dr. Ulrike Stein

Eingereicht am: 04.05.2023
Mündliche Prüfung am: 09.10.2023

Durchgeführt an der Charité-Universitätsmedizin Berlin
Laborgemeinschaft Molekulare Tumorpathologie
Chariteplatz 1, 10117 Berlin

Für meine Eltern,
Victor & David
und meine ganze Familie.

"*We live on an island surrounded by a sea of ignorance. As our island of knowledge grows, so does the shore of our ignorance.*"

- John Archibald Wheeler, *theoretical physicist*

Contents

Acknowledgments

I would like to express my heartfelt gratitude to Dr. Markus Morkel, my supervisor, for providing me with the opportunity to pursue this fascinating research topic. I would also like to extend my thanks to Prof. Christine Sers for allowing me to work in her lab to become a part of the AG Sers. Throughout my doctoral studies, Dr. Morkel's scientific expertise and guidance have been invaluable. His patient teaching on organoid handling and colorectal cancer, in particular, has been extremely helpful. I also appreciate his trust and the independence he afforded me in the lab.
I extend my thanks to Natalie Bublitz and Alexandra Trinks for their invaluable assistance in the lab, especially on those long 10-hour cell culture days. Their presence made the work more enjoyable and rewarding.
I would also like to express my gratitude to the lab technicians, particularly Conny, Kerstin, Silvia, and Andrea, for their help in finding things and answering lab-related questions. I am grateful for the support and camaraderie I received from Pamela Riemer, Julia Hoffmann, Teresa Börding, Tincy Simon, Sylvia Ispasanie, Kathleen Klotz-Noack, and Soulafa Mamlouk throughout my four years in the lab.

I would also like to thank Prof. Nils Blüthgen for his productive and enjoyable collaboration, and Thomas Sell for his assistance with R-related questions and establishing the CyTOF panel. My appreciation also goes to Florian Uhlitz and Stefan Peidli for their assistance with data analysis.

Finally, I would like to express my gratitude to my parents for their unwavering support over the past five years and to my husband, Victor, for his insightful scientific input. Last but not least, I am grateful to my baby David, whose unequaled cuteness made up for the work he prevented me from completing sooner.

Abstract

Normal colon epithelium has a strict cell hierarchy consisting of well-known cell types. In colorectal cancer (CRC) the structure is less conserved and poorly understood. Cancer driver mutations may modulate the prevalence of cell types, and cells may also dedifferentiate to overcome targeted cancer therapy.
My aim is to confirm the existence of heterogeneous cell types in organoids and investigate signaling networks in CRC by targeting specific signaling pathways with pharmacological intervention, which control cell hierarchies in the normal intestine. Strategically selected drugs were used to inhibit nodes in different signaling pathways relevant to the progression of CRC. I explored whether signaling inhibition changes cell type composition and differentiation state, or which inhibitor combinations might induce plasticity or apoptosis. Patient-derived organoids with different oncogenic diver mutations were cultured and treated with a panel of inhibitors and inhibitor combinations for 48 hours. These organoids were mainly examined on two levels: by scRNA seq to assess their transcriptome and by CyTOF, which measures protein abundance to assess the activity of pathways. Both methods were used to quantify CRC heterogeneity.
I was able to see that organoids with the same driver mutations behave more similarly and that the molecular underpinnings of the different lines drive differences in therapy response. Heterogeneous transcriptomes and protein expression were affected by a differentiation gradient and could be altered by inhibitor addition. MAPK activity was graded along this differentiation gradient, and MAPK inhibition reduced cell heterogeneity and induced plasticity. Additionally, I found that a fraction of cells undergo apoptosis, and the remaining cells adopt a non-proliferative stem cell state, which allows cells to recover after suspension of treatment. *In silico* and *in vitro* analyses were performed to find novel inhibitor combinations to maximize apoptosis in CRC organoids to further reduce the emergence of therapy-resistant subpopulations. However, effective treatment combinations remain cell-line dependent.
By separately analyzing cell differentiation state and cell signaling state I contributed to our understanding of how tumor cells can evade targeted therapy by non-genetic resistance mechanisms. Using MAPK inhibition to reduce cell heterogeneity in combination with other inhibitors may be used in the future to optimize therapy success.

Zusammenfassung

Das normale Kolonepithel weist eine strenge Zellhierarchie auf, die aus bekannten Zelltypen besteht. Bei Darmkrebs (CRC) ist die Struktur weniger konserviert und nicht gut verstanden. Krebsauslösende Mutationen können die Prävalenz von Zelltypen verändern, und Zellen können sich auch dedifferenzieren, um einer gezielten Krebstherapie zu entgehen.
Mein Ziel ist es, die Existenz heterogener Zelltypen in Organoiden zu bestätigen und Signalnetzwerke in CRC zu untersuchen, indem ich mit pharmakologischen Eingriffen spezifische Signalwege inhibiere, die Zellhierarchien im normalen Darm kontrollieren. Strategisch ausgewählte Medikamente wurden eingesetzt, um Knotenpunkte in verschiedenen Signalwegen zu hemmen, die für das Fortschreiten von Darmkrebs relevant sind. Ich untersuchte, ob die Inhibition von Signalwegen die Zusammensetzung der Zelltypen und den Differenzierungszustand verändert oder welche Kombinationen von Inhibitoren Plastizität oder Apoptose auslösen könnten. Von Patienten stammende Organoide mit verschiedenen onkogenen Treibermutationen wurden kultiviert und 48 Stunden lang mit einer Reihe von Inhibitoren und Inhibitorkombinationen behandelt. Diese Organoide wurden hauptsächlich auf zwei Ebenen untersucht: durch scRNA seq zur Ermittlung ihres Transkriptoms und durch CyTOF, das die Proteinhäufigkeit pro Zelle misst, um die Aktivität von Signaltransduktionskaskaden zu beurteilen. Beide Methoden wurden eingesetzt, um die Heterogenität des CRC zu quantifizieren.
Ich konnte feststellen, dass sich Organoide mit denselben Treibermutationen ähnlicher verhalten und dass die molekularen Grundlagen der verschiedenen Linien Unterschiede im Therapieerfolg bedingen. Heterogene Transkriptome und Proteinexpression wurden durch einen Differenzierungsgradienten beeinflusst und konnten durch die Zugabe von Inhibitoren verändert werden. Die MAPK-Aktivität folgt diesem Differenzierungsgradienten und eine MAPK-Inhibition verringerte die Zellheterogenität und führte zu Plastizität. Darüber hinaus stellte ich fest, dass ein Teil der Zellen in Apoptose geht und die verbleibenden Zellen einen nicht-proliferativen Stammzellzustand annehmen, der es den Zellen ermöglicht, sich nach Aussetzung der Behandlung zu erholen.
Es wurden *in silico* und *in vitro* Analysen durchgeführt, um neuartige Inhibitorkombinationen zur Maximierung der Apoptose in CRC-Organoiden zu finden, um die Entstehung therapieresistenter Subpopulationen weiter zu reduzieren. Wirksame Behandlungskombinationen bleiben jedoch zelllinienabhängig.
Durch die getrennte Analyse des Zelldifferenzierungszustands und des Zellsignalisierungszustands habe ich dazu beigetragen zu verstehen, wie Tumorzellen einer gezielten Therapie durch nicht-genetische Resistenzmechanismen entgehen können. Die MAPK-Inhibition zur Verringerung der Zellheterogenität in Kombination mit anderen Inhibitoren könnte in Zukunft zur Optimierung des Therapieerfolgs eingesetzt werden.

1 Introduction: homeostasis of colonic epithelium

Colorectal cancer (CRC) is the third most commonly diagnosed cancer and the second leading cause of cancer deaths globally right after lung cancer (Xi and Xu, 2021). CRC develops from the deregulation of cell development in the intestinal epithelium, providing cancer cells a growth and fitness advantage over non-cancer cells. This malignant transformation can lead to cells being able to grow unrestricted, evade the immune system, and even death itself (Hanahan and Weinberg, 2000).
The human gut is a tightly regulated system of cells kept in homeostasis by intrinsic and extrinsic signals (van der Flier and Clevers, 2009). The normal intestinal epithelium is a self-renewing tissue with fast cell turnover. It consists of invaginations, called crypts, and protrusions into the gut lumen, called villi. The small intestine has crypts and villi, whereas the large intestine only consists of a folded epithelium with invaginated crypts. Stem cells reside at the crypt bottom. When dividing, stem daughter cells move upwards into the transit amplifying (TA) compartment, where they continue to divide and move towards the intestinal lumen, differentiating on the way into absorptive enterocytes and multiple secretory cell types, including goblet cells and enteroendocrine cells. When these adult cells have reached the top of the crypt they undergo apoptosis and are shed into the lumen to be excreted. Another secretory cell type is developing from TA cells mostly in the small intestine: CD24+ Paneth cells, which migrate towards the crypt bottom where they reside in between approximately six stem cells for up to two months to produce stem cell niche factors (Sato et al., 2011b). Division, maturation/differentiation and apoptosis are tightly orchestrated processes, regulated by a network of signaling pathways, further described below.

1.1 Emergence of conventional colorectal cancer and signaling pathways involved

Current data supports two distinct ways of CRC development. Both progression pathways are based on a model where normal colon epithelial cells acquire mutations, which leads to the formation of aberrant crypts, then adenoma, and subsequently cancer, termed conventional and serrated pathways of CRC development (Fearon, 2011). Furthermore, less defined pathways of CRC initiation exist, such as via chronic inflammation (Chen et al., 2005). Progression of CRC along the conventional pathway follows multiple steps of signaling pathway deregulation that are correlated with local tumor progression and, in some cases also with therapy resistance, as outlined below. Pathways involved in metastatic dissemination are however poorly understood. A recent publication suggests that the metastatic potential is specified very early on and dissemination can take place

even before the primary tumor is detectable (Hu et al., 2019), which highlights the need to further the understanding of the emergence, development, and adaptability of CRC.

1.1.1 Wnt pathway

The most common conventional way of CRC development follows the adenoma-carcinoma sequence (see fig. 1), which starts most often with a loss of function mutation in the tumor suppressor gene *adenomatous polyposis coli* (APC) in intestinal epithelial (stem) cells, resulting in adenoma formation (Fearon and Vogelstein, 1990; Fearon, 2011). APC is a negative regulator of the Wnt signaling pathway, which controls tissue homeostasis and stemness in intestinal epithelial cells by regulating cell proliferation and fate specification (Pinto et al., 2003). When Wnt signaling is inactive, β-catenin (gene name *CTNNB1*) is phosphorylated by a destruction complex consisting of the scaffold Axin, APC, glycogen synthase kinase 3β (GSK3β), casein kinase (CK1α) and β-transducin repeat-containing protein (βTrCP), which is an E3 ubiquitin ligase. The kinases CK1α and GSK3β phosphorylate β-catenin and then βTrCP ubiquitinates it which leads to its proteasomal degradation in the cytosol (Rao and Kühl, 2010). Without β-catenin in the nucleus, a T cell factor/lymphoid enhancer factor (TCF/LEF) complex recruits histone deacetylases (HDACs) to repress gene transcription (Billin et al., 2000).
However, if Wnt ligands are present at the extra-cellular membrane, the frizzled (Fzd) receptors and lipoprotein receptor–related protein (LRP) co-receptors get activated, which leads to recruitment of the Axin complex to the receptors and their phosphorylation by GSK3β and subsequent activation by phosphoprotein Dishevelled (Dvl), which deactivates the destruction complex. In this state βTrCP is not bound to the complex anymore thus β-catenin does not get ubiquitinated and degraded. β-catenin accumulates and translocates to the nucleus, where it binds as a co-activator to TCF/LEF transcription factors and initiates transcription of target genes (Behrens et al., 1996; Huber et al., 1996; Novak and Dedhar, 1999), which include LGR5, Olfm4, Nkd1, Axin2, and EphB3. These genes are crucial for the maintenance of stem cell niches in the intestinal epithelial crypts (Barker et al., 2007; Clevers and Nusse, 2012), with LGR5$^+$ cells being the stem cells, as has been shown by lineage tracing experiments in the mouse intestinal epithelium (Barker et al., 2007; Sato et al., 2009). Since LGR5 mRNA or protein expression may be low, expression of Olfm4 can be used as a substitute marker in the small intestine and colon, being expressed in the same crypt base epithelial cells (van der Flier and Clevers, 2009). An EPHB2/3 gradient expression, controlled by β-catenin/TCF signaling, is responsible for the correct allocation of precursor and differentiated cells along the crypt-villus axis (Batlle et al., 2002). High expression of EPHB2 and LGR5, along with other stem cell genes, is associated with poorly differentiated colon tumors and a higher tumor-initiating/metastatic potential with the ability of long-term self-renewal,

as patients with high expression of this EPHB2-ISC gene signature have a higher risk of cancer recurrence after initial treatment (Merlos-Suárez et al., 2011). Among the many Wnt/β-catenin target genes, Axin2 appears to be the most specific. Axin2 encodes a destruction complex component and thus serves to regulate a negative feedback loop by inducing degradation of β-catenin (Lustig et al., 2002). Therefore, Axin2 can be used in experiments to define Wnt pathway activity via the activity of a single target, even though quantification from a signature of Wnt targets, such as from Merlos-Suárez et al. (2011) or Muñoz et al. (2012) is likely more robust.
If APC is lost or mutated, it cannot interact with β-catenin (first mutational hit in fig. 1), losing its tumor suppressor function (Morin et al., 1997). Thus β-catenin is constitutively active leading to continuous transcription of LEF-1 and TCF target genes (Behrens et al., 1996; Korinek et al., 1997) and proliferation of undifferentiated stem-cell-like cells (Van de Wetering et al., 2002). Additionally, Barker et al. (2009) highlighted the importance of proper APC/Wnt function in $LGR5^+$ stem cells, since the abrogation of APC in these cells quickly leads to neoplastic transformation, making $LGR5^+$ stem cells cell-of-origin for intestinal cancer. Another proposed type of intestinal stem cells, the so-called quiescent "+4" stem cells, overlap in gene expression with the $LGR5^+$ stem cells, such as Bmi1, Tert, Hopx, and Lrig1. It appears thus that stemness exists as a gradient in the crypt and the more quiescent stem-like cells act as backup or reserve in case of damage to the cycling stem cells (Muñoz et al., 2012).

1.1.2 MAPK pathway

After the initiating APC or β-catenin mutation and expansion of cells with increased Wnt-activity, the mutation that provides the next advantage for these stem-like cells is often in the Mitogen-activated protein kinase (MAPK) signaling pathway, which stimulates cell survival, growth, proliferation, and differentiation (Pages et al., 1993; Krishna and Narang, 2008). During conventional progression, MAPK mutations, most often in KRAS, can occur in adenoma or at later stages in carcinoma.
In normal intestine, one of the most important receptor tyrosine kinases activating MAPK signaling is the EGF receptor (EGFR), which is activated by ligand binding, which induces conformational changes and enables oligomerization with other EGF family receptors via their tyrosine kinase domains (Liang et al., 2018). One of the kinase domains then phosphorylates multiple sites in both kinase domains, generating binding sites for other signaling molecules like guanosine triphosphate hydrolases (GTPases). In this case, the GTPase belongs to the Ras superfamily and can either be H-, K-, or N-Ras, which act similarly within the pathway. Ras is active when GTP is bound and inactive when GDP (guanosine diphosphate) is bound. The switch is stimulated by Ras guanine nucleotide exchange factors (Ras-GEFs), which mediate the substitution of GDP for GTP. The Ras-GEF

in the MAPK pathway is *Son-of-sevenless* (Sos), which works in conjunction with Grb2, which links the activated receptor to Sos thereby facilitating Ras activation. Once GTP is bound it can be hydrolyzed by Ras GTPase-activating proteins (Ras-GAPs), inactivating Ras.
Ras recruits the MAP kinase kinase kinase (A-, B- or c-Raf) to the plasma membrane, where it gets activated. It then activates MAP kinase kinase (called MEK), which in turn activates MAP kinase (ERK). Downstream of ERK are various protein kinases and transcriptional regulators, facilitating changes in protein activation and gene expression to alter cell decisions. To specify the cellular reaction to the activation of receptor tyrosine kinases (RTKs), there are 12 MAPKs, 7 MAPKKs, and 14 MAPKKKs coming together in different "modules" (Wei and Liu, 2002).
Like many pathways, MAPK signaling has many negative feedback mechanisms regulating almost every component of the cascade. Either a pathway component gets post-translationally modified or the signaling cascade leads to transcription and translation of a pathway inhibitor. For example, ERK can phosphorylate the EGFR at T669, downregulating its signaling capacity and in addition, ERK can activate the phosphatase Cdc25c, which dephosphorylates EGFR. Further downstream ERK also phosphorylates and thereby inactivates Raf (Fritsche-Guenther et al., 2011; Lake et al., 2016). If MEK is inhibited, the feedback loop will lead to an attenuation of pMEK in the cell. Additionally, among the target genes of the MAPK signaling are phosphatases (e.g. dual-specificity phosphatases, DUSPs), which get stabilized to remove phosphate from ERK, inactivating ERK itself (Huang and Tan, 2012).
Following the adenoma-carcinoma sequence (fig. 1), genes that are hit with a gain-of-function mutation are major oncogenic drivers KRAS (40% of cases) or NRAS (2-4%) (Fearon and Vogelstein, 1990). Mutant Ras is locked in an active GTP-bound state, continuously presenting a binding site for Raf kinases. An alternative mechanism is loss-of-function mutations in the tumor suppressor NF1, a negative regulator of Ras activity. BRAF is also frequently mutated in CRC, however, CRCs with BRAF mutation mostly belong to the type progressing via non-conventional serrated precursors, as discussed in chapter 1.2.
Mutations in oncogenic drivers and other early mutations in the progression sequence have a strong impact on therapy options for the affected patients, as discussed in chapter 1.4.

1.1.3 PI3K pathway

As mentioned above Ras can activate Raf in the MAPK cascade, but it can also activate other pathways like PI3K-AKT-mTOR signaling, which is a different pathway that can be activated by EGFR signaling and is involved in regulating cell cycle, proliferation, and

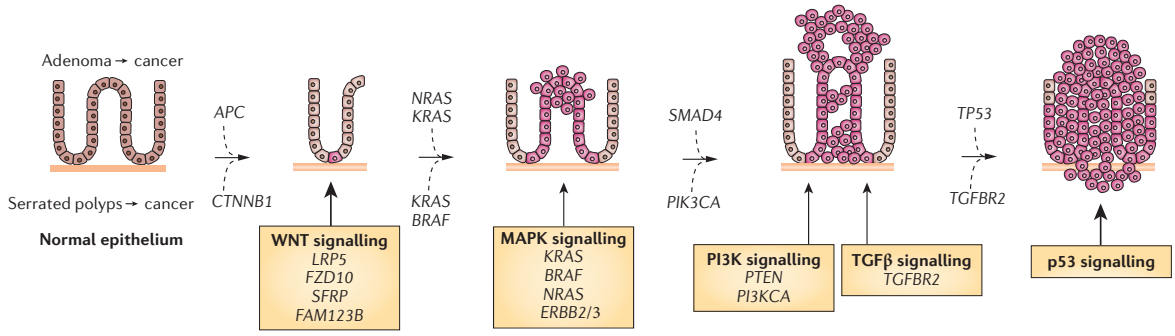

Figure 1: Progression from normal tissue to cancer. **Top.** Adenoma-carcinoma sequence starting from an APC loss. **Bottom.** Serrated sequence of cancer development starting with a mutation in BRAF. Figure modified from Kuipers et al. (2015)

quiescence of cells. AKT is a downstream effector of PI3K and downstream of AKT is mTOR, which promotes protein translation via 4EBP1 and is involved in growth and metabolism (Parsons et al., 2005).

1.1.4 TGFβ superfamily pathway

Following the canonical adenoma-carcinoma sequence, the next mutational hit can occur in the transforming growth factor-β (TGFβ) pathway, most often in Smad4 (fig. 1, cancerous growth step). The pathway transduces signals elicited by a superfamily of growth factors (Activins, BMPs, and TGFβ family factors) and their receptors. In conjunction with other transcriptional regulators, which vary due to cell type and state, a complex of receptor-activated Smads (R-Smad, either 2 and 3 for TGFβ signals or 1, 5, and 8 for BMP signals) and a co-Smad (Smad4) activate target gene transcription in the nucleus (Alberts et al., 2014; Massagué, 2012). Thus, this pathway is involved in a large number of cellular processes, such as pattern formation during development, extracellular matrix production, cell growth/ differentiation/ apoptosis and homeostasis, EMT, and immune regulation (Alberts et al., 2014). If the TGFβ receptor (TGFBR2) is mutated, signaling is interrupted, losing its tumor suppressor function in normal epithelia. Loss of TGFβ signaling in combination with a BRAF mutation can drive colon tumorigenesis even without activation of the Wnt pathway, as shown in a mouse model (Leach et al., 2021). In CRC subtypes with a poor prognosis, TGFβ signaling was found to be enriched (Guinney et al., 2015). The same phenomenon could be observed in stromal cells (Calon et al., 2015). However, TGFβ has different roles in stromal vs. epithelial cells. It slows down proliferation in epithelial cells, which is circumvented in CRC by mutations that make the cells resistant to TGFβ signals. In stromal cells, on the other hand, TGFβ signaling helps initiate tumor metastasis, which could be abrogated in mice by inhibition of TGFBR1 (Calon et al., 2012). During the same time that Calon et al. (2015) found the link between TGFβ signaling and poor prognosis, Guinney et al. (2015) published another classification system, the

consensus molecular subtypes of CRC. They show that high TGFβ activation is associated with stromal invasion, angiogenesis, and metastasis in subtype CMS4. Additionally, this group of CRC patients shows a low relapse-free and overall survival rate compared to the other three CMS subtypes, which are not characterized by a high TGFβ pathway activation (Guinney et al., 2015), highlighting the importance of this pathway in cancer progression.
There is cross-talk between the TGFβ pathway and other major intracellular signaling pathways. For example, ERKs (from the MAPK pathway) can phosphorylate Smad2/3 or coactivators of R-Smads (Chapnick et al., 2011). A member of the PI3K/AKT pathway, PKB/AKT, is able to decrease TGFβ signaling by binding Smad3, thereby inhibiting phosphorylation and interaction with Smad4 (Remy et al., 2004). AKT can inhibit c-Raf to block ERK signaling (Zimmermann and Moelling, 1999). Furthermore, TGFβ2 protein can activate the NFκB pathway in ligand-dependent receptor interactions (Lu et al., 2007).

1.1.5 NFκB pathway

Nuclear factor-κB pathway activation is found to be enriched in several cancers, including CRC. It consists of canonical and non-canonical pathways. The non-canonical pathway is responsible for the development of immune cells, but the canonical one controls cell proliferation, differentiation, and survival, as well as responses to stress, inflammation, and immune activation (Chen and Greene, 2004; Alberts et al., 2014; Yu et al., 2020).
Activated cell-surface receptors (e.g. Toll-like, TNFα and IL1) trigger the phosphorylation of IκB kinase kinase (IKKα/ IKKβ). IKKβ phosphorylates IκB, which triggers degradation of this inhibitory protein complex and releases NFκB, which translocates to the nucleus to activate transcription. Depending on the proteins and coactivators in the nucleus different target genes are transcribed (Chen and Greene, 2004; Yu et al., 2020).
There is transactivation between pathways, for instance, GSK3β phosphorylates a regulatory subunit NEMO, which activates IKK, triggering NFκB release (Medunjanin et al., 2016). Furthermore, PI3K and AKT activate IKKβ, which fosters the phosphorylation of NFκB subunit RELA and stimulates activity (Madrid et al., 2001). There is also a negative feedback loop regulating the activity of NFκB. Among its target genes is IκBα, which binds to NFκB and inactivates it (Nelson et al., 2004). Another important function of NFκB signaling is in the cross-reaction with the Wnt pathway. Elevated NFκB signaling enhances β-catenin activation and thus Wnt activity and induces dedifferentiation of cells, which are then able to metastasize (Schwitalla et al., 2013).

1.1.6 Role of p53 in cancer progression

One of the last steps in the colorectal cancer progression sequence (fig. 1, right side, (Fearon and Vogelstein, 1990)) involves aberration of p53, which is one of the most important tumor suppressors and is inactivated in many malignancies through mutation or deletion. Cells that have accumulated mutations in Wnt, MAPK, PI3K, and TGFβ are under replication stress due to uncontrolled proliferative signals. This might activate p53-mediated cell cycle arrest before mitosis, senescence, or apoptosis. Due to the missense defects (85% of p53 mutations) cells retain their ability to grow (Fearon, 2011). Therefore, under these circumstances, inactivating p53 mutations might provide a selective advantage to tumor cell clones evading p53-mediated proliferation control. Additionally, mutant p53 prolongs NFκB response in epithelial cells in an inflammatory setting, promoting chronic inflammation and associated carcinogenesis (Cooks et al., 2013). Interactions with other pathways include MAPK signaling, which can regulate p53 phosphorylation by CK1ε/δ, which enables p53 to interact with Smad2/3 and thus regulate TGFβ target genes (Chapnick et al., 2011).

1.1.7 Hippo pathway

Mutations in genes of the Hippo pathway lead to increased cell growth, proliferation, and resulting organ size, while restricting apoptosis (Harvey et al., 2003). The core of the signaling cascade consists of the Sterile 20-like kinases MST 1 and 2, which are serine/threonine kinases and can activate large tumor suppressor kinase 1 and 2 (LATS1/2). Additionally, there are adaptor proteins Salvador 1 (SAV1), MOB1A and MOB1B, the transcriptional co-activators YAP and TAZ, and the transcription factors TEAD1 to 4 (Chan et al., 2005; Moya and Halder, 2019). Although the pathway reacts in response to extracellular cell density signals, it is not yet entirely clear which molecules serve as receptors. Once the Hippo pathway gets activated, the transcriptional co-activators get degraded, which suppresses the transcription of Hippo target genes (Liu et al., 2010). It is in an off-state at high cell density, whereas low cell density is turning on Hippo-mediated proliferation. The cell density sensor α-catenin and other cell adhesion molecules serve as receptors of the pathway and ultimately regulate YAP activity by limiting YAP dephosphorylation in a high cell density setting (Schlegelmilch et al., 2011). Also, mechanical strains and cellular energy stress like AMPK and nutrient availability can activate Hippo signaling (Mo et al., 2015).

There is also cross-talk between Hippo and Wnt signaling, as alternative Wnt ligands (Wnt5a/b and Wnt3a) activate YAP/TAZ, which in turn antagonize canonical Wnt/β-catenin signaling (Park et al., 2015). YAP itself can inhibit canonical Wnt signaling in $LGR5^+$ cells to induce the regenerative Hippo program (Gregorieff et al., 2015). However, YAP is considered an oncogene, being essential for tumor initiation, progression, and

metastasis in some solid tumors (Jin et al., 2021; Gregorieff et al., 2015; Piccolo et al., 2014). A highly active YAP, facilitating its target gene expression, is associated with cell proliferation and poor prognosis in CRC patients. The progression-free survival was significantly shorter compared to patients with an inactive YAP target gene expression signature (Lee et al., 2015). Another strong interaction on multiple levels is between p53 and the Hippo signaling pathway (Furth et al., 2018). YAP can bind mutated p53, but not $p53^{wt}$ to enhance pro-proliferative transcripts (Di Agostino et al., 2016). In newly forming organoids a YAP gradient is required for the emergence of Paneth cells among $LGR5^{+}$ cells to break the symmetric structure of spheres. However, both YAP inhibition and YAP overexpression reduces Paneth cell formation (Serra et al., 2019). This highlights the importance of tight Hippo regulation because components of the pathway can hinder normal development and support cancer formation.
In summary, there are many pathways and proteins involved in orchestrating normal intestinal epithelial cell development and differentiation. Since the intestine is a tissue with a very fast cellular turnover, mutations may arise spontaneously and if they are not purged from the system, they will spread and induce the acquisition of other mutations and genetic aberrations leading to cancer formation. However, in addition to alterations in the DNA, there are epigenetic changes, which commonly accompany polyp to cancer progression.

1.2 Emergence of serrated colorectal cancer

A minority of CRCs do not arise via the previously described canonical adenoma-carcinoma sequence, but form from serrated precursor lesions. These precursors have a saw-toothed morphology and belong to one of three categories: hyperplastic, sessile serrated, or serrated polyps. The sessile serrated polyps/adenomas (SSA) are characterized by a mutation in BRAF ($BRAF^{V600E}$), changes in methylation patterns (CIMP, see next chapter 1.3), and activation of the MAPK pathway. The genetic BRAF aberration has been shown to initiate CRC (Rad et al., 2013), and, on its own, can result in serration (Riemer et al., 2015). In the context of CRC initiation via the serrated pathway, BRAF may interact with TGFβ signaling and microbial-driven inflammation (Leach et al., 2021). Serrated progression of CRC may also involve β-catenin activation (Yachida et al., 2009; Rad et al., 2013; Riemer et al., 2015), although newer models of this progression scenario do not strengthen an essential role of Wnt signaling in the formation and progression of CRC via serrated precursors (Leach et al., 2021). Collectively, as also highlighted for conventional CRC progression above, multiple mutations lead to aberrant gene expression and progression of SSAs to carcinoma.
When BRAF itself is mutated, it is also constitutively activated with elevated kinase activity, resulting in MEK binding and downstream signaling (Wan et al., 2004). Mutations in

the tumor suppressor PTEN lead to upregulation of the PI3K pathway. Without the regulatory function of PTEN or other subunits involved in signaling, unhinged signaling promotes angiogenesis, apoptosis inhibition, and tumor progression (Parsons et al., 2005; Koveitypour et al., 2019).
Furthermore, SSAs show high levels of TGFβ pathway activity, which can regulate p53 activity and promote p53/Smad interactions (Fessler et al., 2016; Kawarada et al., 2016). This is also correlated with a dismal patient outcome (Guinney et al., 2015). Advanced CRCs that have emerged via conventional or serrated progression pathways cannot be distinguished very well, although some mutation patterns can hint at the origin, such as APC mutations for the conventional progression pathway and BRAF mutations for the serrated scenario.

1.3 Classes of genetic and epigenetic deregulation

The progressive accumulation of hallmark cancer traits is a combination of genetic and non-genetic alterations. There are three main types of alterations in CRC which foster the activation of oncogenes and inactivation of tumor suppressors (Kuipers et al., 2015).

CIN **c**hromosomal **in**stability is most common in sporadic CRC and arises due to alterations in chromosome number, loss of heterozygosity (one allele is lost) and defects in DNA damage repair. Found in 85% of CRC cases. High frequency of p53 mutations.

CIMP **C**pG **i**sland **m**ethylator **p**henotype tumors can progress because tumor suppressor gene promoters have been permanently silenced by methylation (hypermethylation). Otherwise, the genome is characterized by global hypomethylation, which can lead to genomic instability (Tariq and Ghias, 2016).

MSI **m**icro**s**atellite **i**nstability occurs when DNA replication errors are not corrected due to inactivating methylations of responsible genes (Kane et al., 1997). Found in 15% of CRC cases; has a better prognosis compared to the other subtypes. They have a high frequency of BRAF mutations, but a very low one for APC and KRAS mutations.

These mechanisms may overlap in tumor subtypes, but each has prognostic value, e.g. effects on survival rates (Simons et al., 2013). CIN drives tumor metastasis (Bakhoum et al., 2018) and is an indicator of low progression-free survival and early death (Hveem et al., 2014). On the other hand, MSI tumors present with a less aggressive clinical behavior compared to MSS (microsatellite stable) tumors (Malesci et al., 2007), and their better prognosis over MSS tumors is shown for both 5-FU treated and untreated patients (Klingbiel et al., 2015). Irrespective of MSI status, CIMP is associated with

shorter disease-free and overall survival. However, patients with CIMP tumors have a higher disease-free survival time when treated with adjuvant chemotherapy (Juo et al., 2014).
One epigenetic regulator was associated with poor survival of patients: the histone methyltransferase Mll1 (mixed lineage leukemia). It is highly expressed in LGR5^{+} cells with high Wnt activity and lost upon differentiation. It is an upstream regulator of cancer stemness since excision from the murine genome prevents β-catenin induced tumorigenesis (Grinat et al., 2020).

In summary, the accumulation of genetic and epigenetic alterations mediates CRC formation by deregulating key signaling pathways in epithelial cells, which undergo transformation into cancer cells. Since the mechanisms of emergence and subsequent mutations can vary between patients and even within one tumor, CRC is heterogeneous which makes it plastic and able to become resistant against targeted therapy, which paves the way for metastasis formation and disease exacerbation.

1.4 Current state and challenges of CRC therapy

Due to the highly adaptable and versatile nature of CRC, patients with progressed disease and metastasis have a shortened life expectancy. Advances like chemotherapy (cytotoxic agents) and other medication (small molecule inhibitors) are increasing median survival for patients with advanced CRC. Targeted drugs like the monoclonal antibody Cetuximab, can actively inhibit tumor growth by binding to the extracellular domain of EGFR, blocking receptor signaling (Li et al., 2005; Karapetis et al., 2008). During treatments, a common side effect is toxicity to the skin signaling network in form of a rash, which correlates positively with overall survival time. Even with Cetuximab treatment, the median survival of CRC patients was just 6.1 months, compared to 4.5 months when only receiving supportive care (Jonker et al., 2007). Other monoclonal anti-EGFR antibodies, like Panitumumab, also increase progression-free survival, but no correlation between efficacy and skin rash severity was observed (Van Cutsem et al., 2007). Cetuximab alone or in combination with Irinotecan has emerged as a common initial treatment for patients with metastatic CRC (Van Cutsem et al., 2009; Arena et al., 2015). Predictive mutations such as in KRAS or NRAS serve as biomarkers, e.g. when tumors present such mutations, EGF receptor inhibitors cannot be used for therapy (Misale et al., 2012) and Cetuximab and Panitumumab lose efficacy. Only patients with KRAS^{wt} benefit from Cetuximab treatment, since activating mutations or amplifications of the KRAS gene render upstream EGFR inhibition ineffective (Karapetis et al., 2008). This resistance to treatment is termed primary resistance because it exists prior to any treatment. Numerous mutations in the EGFR-MEK-ERK signaling pathway can contribute to primary resistance (Misale et al.,

2014; Arena et al., 2015). Modifying this simple model of predictive mutations, recent systems biology approaches identified variations between signaling mechanisms of the various KRAS mutations, with potential clinical impact (McFall et al., 2019). Also in BRAF mutated tumors EGFR inhibitors alone do not increase progression-free survival time for patients (Pietrantonio et al., 2015). This highlights why patients are routinely tested for the mutations in their tumors prior to the start of targeted treatment.
Patients which are not primary resistant most often develop secondary resistance during initial therapy. It has been shown that this is caused by a subpopulation of tumor cells that may contain a mutation in KRAS already and thus survive the therapy or by changes in selective pressure elicited by therapy, favoring selection of cells with *de novo* KRAS mutations (Misale et al., 2012). Not only KRAS, but other mutations along the EGFR-MEK-ERK cascade influence treatment efficacy, whereas treatment itself triggers the emergence of subclones with multiple genetic aberrations. Once secondary resistance emerges, the tumor could be treated with a combination of EGFR and MEK inhibitors, which may delay disease progression (Misale et al., 2012). Mathematical modeling, *in vitro* and *in vivo* experiments have shown that specific combinations of inhibitors can be more effective than single inhibition alone to block KRAS^{mut} and BRAF^{mut} cell growth (Klinger et al., 2013). Patients that present with a BRAF^{mut} tumor do not benefit from Cetuximab or Panitumumab treatment alone (Pietrantonio et al., 2015), but they benefit from a combination of Encorafenib, Cetuximab, and Bimimetinib (inhibiting BRAF, EGFR, and MEK, respectively) (Kopetz et al., 2019; Corcoran et al., 2018). This combination reduces the feedback activation of EGFR and thus MAPK reactivation.
However, not only genetic mutations result in the formation of tumor cells with a primary or secondary resistance that can survive EGFR inhibition (e.g. Cetuximab) treatment, but also non-genetic mechanisms contribute to resistance against targeted therapy of CRC. A subpopulation of resistant cells can confer Cetuximab resistance to sensitive surrounding cells by secreting EGFR ligands (e.g. TGFα) to sustain signaling in non-resistant cells (Hobor et al., 2014). In 64% of metastasis biopsies, which acquired resistance to Cetuximab, no genetic driver mutations were found with deep amplicon sequencing (Woolston et al., 2019). Anti-MAPK therapy can still be overcome by the tumor due to plasticity and heterogeneity of cells. Once EGFR is blocked in xenograft models the tumor cannot signal via EGFR, reduces cell proliferation, and a pro-regenerative program is induced as if the intestine had sustained damage. This is followed by pseudo-differentiation to a Paneth cell-like phenotype, which is a plastic phenotypic change that can reverse upon treatment suspension (Lupo et al., 2020). Woolston et al. (2019) characterized some RAS^{wt} Cetuximab resistant CRC samples on a transcriptomic level and found that the resistance to Cetuximab was driven by a switch from sensitive TA-subtype to a stem-like subtype, in which stromal remodeling lead to an increase in fibroblasts and growth factors.

In order to counteract the emerging resistance mechanisms in CRC, multiple drug treatments could be combined. However, this might increase toxicity in patients since the inhibitors might cross-react and inhibit other essential pathways in healthy cells too.

1.5 Organoids in cancer research

To assess the impact of inhibitors and inhibitor combinations, *in vitro* methods have been used. 2D cell lines have been used in research for more than 70 years. However, the advancement of cell culture techniques has yielded the ability to grow 3D structures from single stem cells from different organs, called organoids. Sato et al. (2009) have managed to establish culture conditions for intestinal epithelium. LGR5-positive cells were able to grow out and form crypt-villus structures from a single cell, which were self-organizing and resembled a normal gut. This method was further refined and adapted to accommodate the long-term growth of epithelial cells from murine colon and human small intestine (Sato et al., 2011a). Using the improved culture conditions, differentiation from stem to mature enterocytes was possible. Nicotinamide in the medium inhibited goblet cell differentiation. In general, it is assumed that organoids represent the intestinal epithelium more closely than cell lines such as CaCo2 or DLD1 (Sato et al., 2011a), as organoids preserve a greater part of the *in vivo* cell heterogeneity of CRC. Therefore, cancer material from CRC patients was used to compile organoid libraries and biobanks. Each organoid line can be characterized by sequencing and/or gene expression to get a more comprehensive overview of genetic alterations and their consequences in patients. One of these libraries was assembled by Fujii et al. (2016) and they show that organoids recapitulate clinical phenotypes *in vitro* and *in vivo*. The authors found that with increasing mutational load the organoids become more niche-factor independent, meaning they need fewer growth factors added to their medium. If healthy and tumor samples are taken from the patients, drug screening can be performed to identify associations between genetic mutations and drug sensitivity, which might inform personalized therapies and responses to chemotherapy (van de Wetering et al., 2015; Kolahi et al., 2020).
Instead of studying heterogeneous patient samples, organoids can also be genetically modified to generate isogenic lines, which only differ by one mutation. Drost et al. (2015) modified human normal colon tissue organoids by introducing APC^{KO}, $P53^{KO}$, $KRAS^{G12D}$ and $SMAD4^{KO}$ mutations sequentially, so that the fifth line has all four mutations. With these lines, many aspects of the adenoma-carcinoma sequence could be recapitulated, showing that only these four mutations are necessary for stem-cell niche factor independent growth with invasive phenotype (Drost et al., 2015).
Taken together, organoids are a versatile model for investigating CRC and a middle ground between 2D cell lines and *in vivo* mouse experiments. Even though genetic and xenograft mouse models are crucial in the investigation of CRC growth in a complex *in vivo* mi-

croenvironment, there are multiple drawbacks in mouse experiments, e.g. cost, time, and ethical considerations. It also should not be dismissed that in the mouse adenomas form in the small intestine, whereas in humans they form in the colon, no matter if they arise from hereditary or sporadic cancer (van der Flier and Clevers, 2009), casting doubts on the inter-species conservation of the gut epithelium signaling network.

1.6 Single cell analysis to decipher tumor heterogeneity

In recent years technological advancement has allowed researchers to investigate tumors on a single cell level, a new approach to decipher the cause and outcome of CRC heterogeneity, giving rise to much more detailed studies. Several techniques exist to gain information on single cells at the protein level, for example, flow cytometry or CyTOF. Furthermore, single-cell RNA sequencing can yield information on single-cell transcriptomes. These methods improve former analyses like western blots and bulk sequencing, where only an average of all input cells was received as a read-out. Thus, only the majority of cell types could be analyzed, while information on rare cells was often lost in the noise. In contrast, in single-cell analyses, even small subpopulations can be picked up, which might have acquired a new mutation or have differential drug sensitivity due to epigenetic changes.
Even though the costs for sequencing have been significantly reduced in the last 10 years, preparing libraries is still a costly endeavor. Barcoding or tagging cells of different conditions and then pooling them together in one sample or library, so-called multiplexing, not only reduces the number of library preparations and sequencing costs but also reduces batch effects. Those are variations due to sample handling which produce changes in the experimental data. This technical variance can be reduced by multiplexing or correcting for it in a later data analysis step to be able to compare different experiments.
Sampling multiple developmental time points Fawkner-Corbett et al. (2021) followed the human intestinal morphogenesis on a single cell level (RNA sequencing, scRNA seq). They found location-specific transcription leading to different cell populations and eventually crypt-villus formation. Their detailed cell atlas can be used to better understand neonatal disease stemming from genetic defects and affecting specific cell types at certain time points (Fawkner-Corbett et al., 2021). Looking at adult colon diseases scRNA seq revealed expression patterns and shifting cellular composition in ulcerative colitis (Smillie et al., 2019). E.g. in inflamed tissue, there are metabolic changes and an upregulation of genes associated with the restoration of homeostasis, like activation of innate immunity.
A complementary method to scRNA is single-cell mass cytometry (CyTOF), which is based on heavy-metal conjugated antibody staining, suited to measure between 30 and 50 (phospho)-proteins per cell. This method is also suited for multiplexing by tagging each experimental condition with a different composition of palladium mass tags, creating a

barcode for deconvolution in the analysis step (Zunder et al., 2015). Measuring protein density directly is important since mRNA levels do not always reflect the abundance of translated protein (Schwanhäusser et al., 2011). Using antibodies for cell state and signaling proteins on CRC organoids, signaling network states can be investigated, and analyzed on a cell type-specific level (Qin et al., 2020). Brandt et al. (2019) showed that organoid lines have graded EPHB2 expression in line with the expression of phosphorylated MEK and ERK. At the end of the differentiation axis, marked by low EPHB2, cleaved caspase 3 (cCASP3) expression was high, which is a marker for apoptosis. In combination with transcriptome analysis cell type-specific ERK suppression could be shown and linked to the differentiation state of the cells.

All of these findings indicate the importance of sensitive sequencing technologies to pick up on preexisting or emerging cell populations which may drive resistance and ultimately tumor progression. This can be done by checking cell-free DNA in the blood of patients, since checking one biopsy already neglects the intratumoral heterogeneity and genetic diversity of metastasis. Every lesion could develop a different resistance mechanism independently, which would need to be addressed in order to stop tumor progression (Misale et al., 2014). In research settings, analysis can be performed on a single-cell basis like described above to investigate subpopulations of cells, which might have altered their pathway activities by up- or downregulating signaling proteins or shifted cell differentiation trajectories after being exposed to small molecule inhibitors. Ongoing technical developments of single-cell technologies to measure RNA and proteins have allowed for analysis from immediate transcriptomic responses to later translational effects. During this project, I mainly employed RNAseq and CyTOF techniques on human organoid cultures to investigate cellular responses to pharmacological perturbations.

2 Aims and objectives

CRC is one of the most common malignancies worldwide and a leading cause of cancer-related deaths. According to the World Health Organization, there were an estimated 1.9 million new cases of CRC in 2020, accounting for approximately 10% of all cancer cases (Xi and Xu, 2021). The high incidence and mortality rates associated with CRC result in significant healthcare costs. In the US, the total cost of CRC treatment is estimated to be over $16 billion annually, including both direct medical costs and lost productivity (Mariotto et al., 2011). Therefore, there is an urgent need to improve our understanding of CRC biology and develop more effective therapies to reduce the burden of this disease on both patients and healthcare systems. To date, even targeted cancer therapies are unable to eradicate all cancer cells, leading to recurrence and/or metastasis formation, since small surviving subpopulations can grow out again to form new tumor masses.
In this doctoral work, I, therefore, combined CRC organoid studies with single-cell techniques to determine whether this experimental workflow is suitable to assess CRC cell heterogeneity in greater detail, with the future aim to identify disease-relevant cell subpopulations. In particular, my aim was to contribute to the following questions:

1. Do CRC organoids display heterogeneous cell types?
I used immunohistochemistry and CyTOF to analyze heterogeneous cell type staining, cell state, and - type markers.

2. Does signaling inhibition modulate the prevalence of known cell types and how do signaling pathway activities and differentiation states influence each other?
I used patient-derived organoid lines and analyzed them on a single-cell level using CyTOF and RNA sequencing to assess changes in cell types, signaling activity, and transcriptomes.

3. Which targeted therapies induce homeostasis-related features in CRC organoids, such as differentiation, cellular plasticity, or apoptosis?
I treated the organoid lines with multiple inhibitors and then compared CyTOF and scRNA seq readouts to see changes on transcriptomic and translational levels. *In silico* computation was used to guide inhibitor combination selection for subsequent *in vitro* cell viability and apoptosis experiments. For selected organoid lines and inhibitors RNA velocity was employed to visualize the differentiation trajectories of cells under treatment.

Understanding how CRC organoids cope with inhibition of one or more main signaling pathways, could help identify compelling alternative novel targeted therapy strategies. Knowledge about which cells evade or survive treatment could be used to optimize targeted therapy success in the future.

3 Results

3.1 Genetically heterogeneous organoid lines used in this project

To investigate if patient-derived (PD) organoid lines display heterogeneous cell types, I used organoid lines from different patients with differing mutational patterns. In the course of this project, I have worked mostly with ten CRC organoid lines. Additionally, I cultured two normal colon lines, called NCO and P021N. The table below is summarizing the most important driver mutations of the cancer lines. For specific codon changes and resulting amino acid changes see table 5. OT209 was used in only one experiment and is thus grayed out. The organoid lines were either established in-house in a previous project (all OT lines from Schütte et al. (2017)) or established during the work for Uhlitz et al. (2021), or in the case of IKP007s, B2-040 and C2-019 were obtained commercially or from an MTA from another lab. These organoid lines were chosen, because of their differences in genetic driver mutations and their ability to grow long-term in cell culture.

Table 1: Overview of mutations in organoid lines

Line	APC	TP53	SMAD	ATM	KRAS	BRAF	other
OT108	x	x					
OT326	x	x		x			
P009T	x	x					x
P013T	x						x
OT227	x	x			x		x
OT302		x			x		x
OT238		x	x		x		x
OT209	x	x			x		x
IKP007s						x	x
B2-040		x	x			x	x
C2-019					x	x	x

3.2 Patient-derived organoids showed heterogeneous marker expression in immunohistochemistry

Initially, I used three of the above-mentioned organoid lines to investigate by immunohistochemistry (IHC) if marker distribution in organoids is heterogeneous to confirm the existence of different cell types or states within the organoids. Additionally, two phospho-proteins were stained in this experiment to visualize MAPK signaling activity. OT108 and OT326 which are $KRAS^{wt}$, but harbor APC and TP53 mutations, and OT227, which additionally has a KRAS and KIT (a receptor tyrosine kinase) mutation, were

cultured and harvested after 48 hours of treatment with either DMSO as control, MEK inhibitor (AZD6244) or PI3K inhibitor (GDC0941), embedded in FFPE and sectioned. Three cell state markers were stained: KI67 is a marker for proliferation, Krt20 for differentiation, and cleaved Caspase 3 (cCASP3) marks apoptotic cells (fig. 2, upper row). pMEK and pERK were stained to assess the MAPK pathway activity in those organoids (fig. 2, lower row). I found all three cell state markers were not uniformly distributed

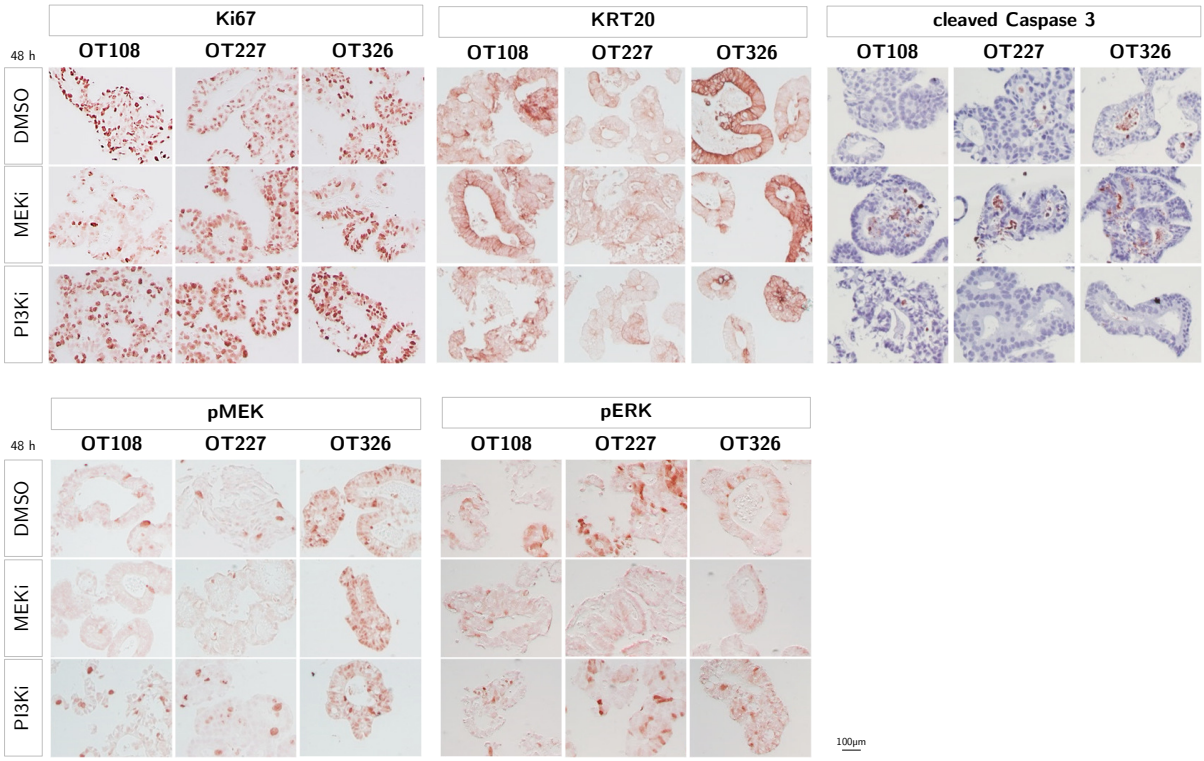

Figure 2: Immunohistochemistry stainings of three organoid lines with three cell state markers and two phospho-proteins to assess signaling. brown = signal, blue = counter staining to visualize organoids, scale bar = 100 µm

among organoid cells, but expression strength (staining intensity) was heterogeneous even within a single organoid. cCASP3 had a very low abundance so counter-staining (blue) was necessary to make out organoid structures. In the DMSO-treated organoids, only a small number of cCASP3-positive cells could be observed in the lumen of organoids. Phosphorylation of signaling molecules MEK and ERK was also heterogeneous between neighboring cells of the same organoid. The presence of pMEK was stronger in the KRAS^{wt} lines compared to KRAS^{mut}, whereas it is the other way around for pERK.
MEK inhibition (MEKi) appeared to downregulate MEK phosphorylation, which was unexpected, as negative feedback of signals within the pathway has previously been shown to result in upregulation in CRC lines (Fritsche-Guenther et al., 2011). However, since I also observed reduced expression of KI67 in KRAS^{wt} lines and increased cCASP3 expression in all three organoid lines, this could mean that reduced MEK phosphorylation

was an indirect result of a decreased proliferative potential.
PI3Ki did not alter pMEK and pERK levels visually, however, the treatment appeared to increase KI67 staining, decreased Krt20, and had no visible effect on cCASP3 expression. Overall, this experiment showed that inhibition of MAPK signaling affected cell proliferation and apoptosis. However, it is complicated and error-prone to quantify proteins from IHC stainings, for instance, because stainings are not normalized to a control. By visual inspection, only strong changes will be observable and changes in subpopulations of cells might go unnoticed due to sectioning. Additionally, the effects could not be observed in the same cells, but could only be compared among organoids that were treated in parallel. Therefore, instead of staining bulk organoids, I now switched to analyzing and quantifying RNAs and proteins in organoids on a single-cell basis.

3.2.1 Patient-derived organoids showed heterogeneous marker expression in CyTOF

In a pilot experiment, I aimed to quantify cell type markers, pMEK and pERK on a single cell level, by using mass cytometry (CyTOF). Organoids were grown for at least eight days to allow cell heterogeneity to develop, then harvested and a single-cell solution was prepared. Organoid cells were stained with Cisplatin to mark dead cells, then barcoded and pooled. This pool of cells was stained with antibody mixtures, which contain markers for cell type (stemness, differentiation, lineage), phenotype (apoptosis, DNA damage), and cell signaling (different pathways, e.g. MAPK, PI3K, TGFβ, WNT). The CyTOF antibody panel was established by Thomas Sell (AG Blüthgen). Cells were stained first for extracellular markers and after permeabilization for intracellular markers. After overnight fixation cells were measured in a mass cytometer to see antibody abundance per cell.
A principal component analysis (PCA) was performed on pre-processed data, described in chapter 3.4.1. PCA plots order the cells according to the main components affecting similarity. We found that the first principal component of the complete dataset strongly correlated with EPHB2, a known graded CRC cell marker. Thus cells were ordered on the PC1 axis from EPHB2-high to EPHB2-low in a gradient, which, according to published data (Batlle et al., 2002; Muñoz et al., 2012) might mean from stem-cell-like to differentiated/apoptotic. cCASP was expressed mostly in EPHB2-low cells, forming a cluster of apoptotic cells in OT302, whereas expression in OT227 was very low overall. Interestingly, pMEK and pERK followed the EPHB2 gradient, meaning MAPK signaling could decrease with the progression of cell differentiation. The CyTOF result, therefore, shows heterogeneous signaling states within CRC organoid cells and hints at connections between MAPK activity and cell differentiation.

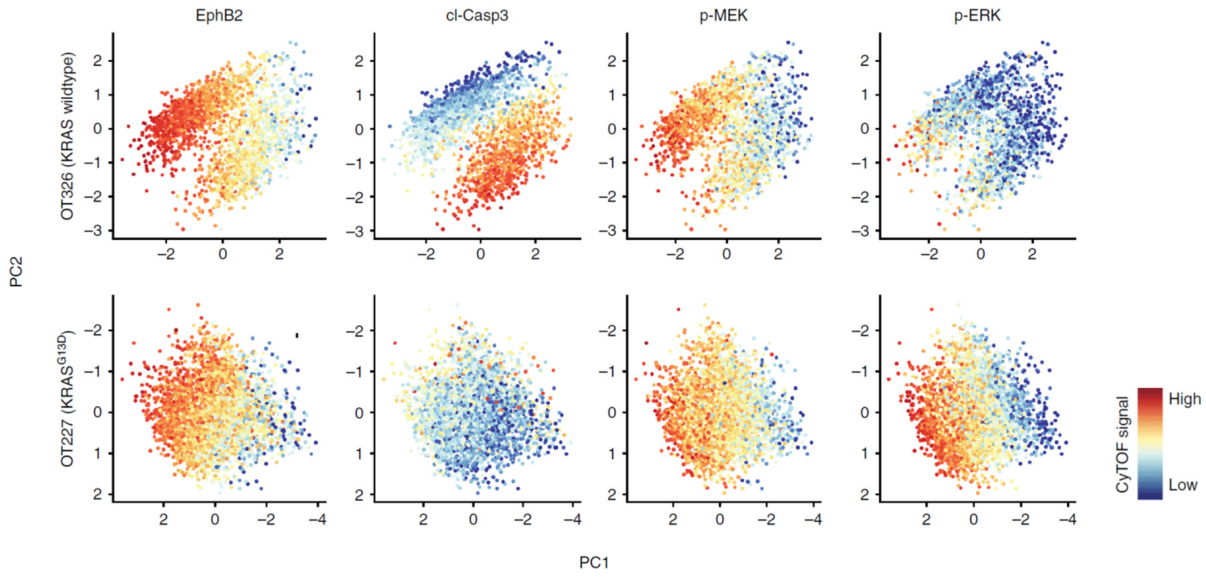

Figure 3: Graded MEK and ERK phosphorylation. Principal component analysis (PCA) on CyTOF data of two organoid lines. Color-coded expression strength of EPHB2, cCASP3, pMEK and pERK are shown per cell. Analysis revealed graded MEK and ERK phosphorylation, which followed a differentiation gradient. Figure modified from data I produced for Brandt et al. (2019).

3.3 Inhibitor panel and workflow for large-scale perturbation experiments

Confirming heterogeneity between some organoid lines in the abundance of cell state and -type markers has affirmed the first question posed in chapter 2 if CRC organoids display heterogeneous cell types. I now turn to question number two, if signaling inhibition modulates the prevalence of cell types and how signaling pathway activities and differentiation states influence each other. To answer this question, pharmacological intervention was required with a focus on the main pathways of CRC emergence and progression. In order to shed some light on the wiring of this interconnected network, we chose sixteen different inhibitors and three combinations at concentrations previously employed in CRC organoids and cell lines.

As MAPK signals play a key role in CRC biology and therapy, we chose several inhibitors in this pathway: We targeted the EGF and FGF receptor tyrosine kinases, as they relay MAPK signals from the extracellular space to the cytoplasm and furthermore are implicated in intracellular feedback regulation of MAPK signals (Fritsche-Guenther et al., 2011). Indeed, inhibition of EGFR is also first-line therapy for RAS/RAF wildtype advanced CRC; however, here we employ a pan-EGFR kinase inhibitor instead of an anti-EGFR antibody to inhibit both, extracellular signaling and intracellular feedback. Targeting of the cytoplasmic MAPK pathway was achieved by inhibitors of BRAF, MEK, and ERK, thus covering all three kinase levels of the core MAPK cascade. It is of note that inhibition of BRAF can also result in MAPK pathway activation, depending on BRAF mutational status, as inactivation of BRAF changes the relative stoichiometries of BRAF and CRAF

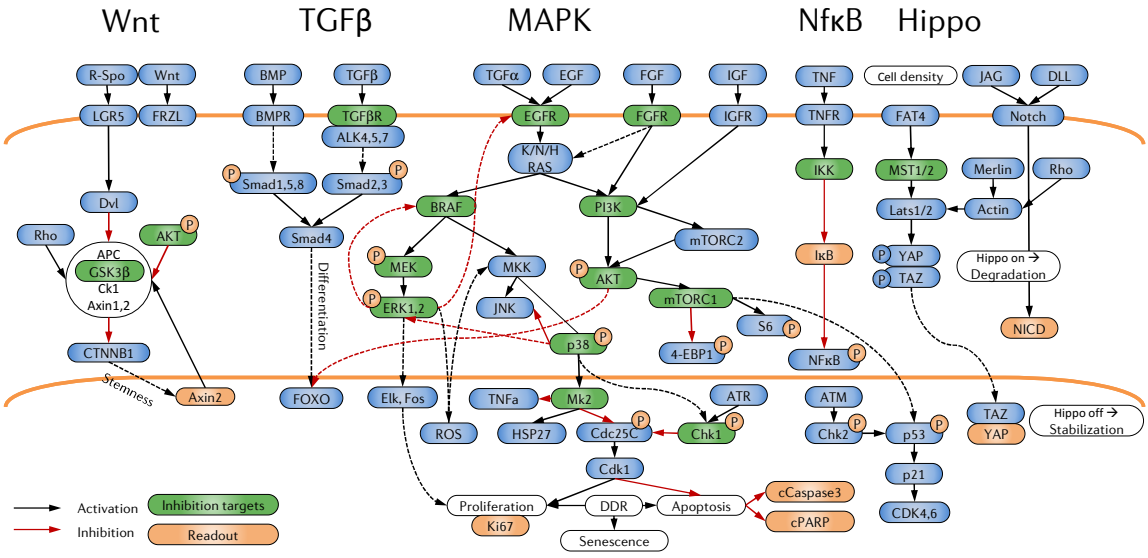

Figure 4: Overview of signaling pathways and inhibitors used in my project. Five main pathways involved in CRC emergence and progression were perturbed with small molecule inhibitors. Inhibitor targets are highlighted in green. The orange infill indicates CyTOF readouts. If not the whole protein, but only an attached circled "P" is highlighted, the CyTOF antibody was specific for the phosphorylated form of this protein.

proteins available for dimerization in the cell (Röck et al., 2019). MEK inhibition can also activate PI3K/AKT signaling by increasing AKT phosphorylation (Turke et al., 2012). To inhibit the PI3K/AKT pathway at different levels, PI3K, AKT, and mTOR inhibitors were used. The pan-PI3K inhibitor inhibits the production of secondary messengers and thus downstream activation of the pathway (Folkes et al., 2008). Interestingly, as MEK inhibition activates PI3K signaling, so does mTORc1 inhibition activate MAPK signaling, specifically it activates ERK (Carracedo et al., 2008). The mTORc1 inhibitor activates AKT signaling via a negative feedback loop in different cancer entities (Sun et al., 2005; Wan et al., 2007). Inhibition of mTOR complexes 1 and 2 was used, since both complexes control activation of AKT and ERK in a concentration-dependent manner (Chen et al., 2010). mTOR also controls the translation of MK2, which is downstream of p38. However, mTOR inhibition only affects the activity of MK2 and not p38 (Herranz et al., 2015). In this screen, p38 is an inhibition target and simultaneously a CyTOF readout for the PI3K pathway. MK2 and Chk1 were inhibited since they play a role in cell cycle checkpoint initiation and maintenance, and their combined inhibition reportedly eradicates $KRAS^{mut}$ cancer cells in a mouse model and patient-derived cells (Dietlein et al., 2015).
The TGFβR inhibitor blocks SMAD2/3 nuclear translocation. However, TGFβ signaling is highly context-specific and there is crosstalk between MAPK and TGFβ, for instance, SMAD2/3 could also be phosphorylated by ERK (Chapnick et al., 2011). ERK or AKT may also phosphorylate GSK3β and thus prime it for subsequent phosphorylation and inactivation (Ding et al., 2005). Inactivation of GSK3β activates Wnt signaling, in this case, the GSK3β inhibitor binds secreted Wnt-protein to its receptor, which leads to β-catenin accumulation and pathway activation. GSK3β itself is involved in NFκB activa-

tion via IKK/NEMO phosphorylation (Medunjanin et al., 2016). Inhibition of IKK blocks phosphorylation of IκBα, keeps NFκB in the cytoplasm, and may lead to an increase in pERK in the cytoplasm, depending on the type of inhibitor (Gilmore, 2006; Klinger et al., 2013).
MST1/2 inhibition blocks its kinase activity, thus reducing the phosphorylation of downstream LATS and YAP, which activates YAP, increases its nuclear translocation, and thereby promotes cell growth (Fan et al., 2016).
All sixteen inhibitors are highlighted in their respective pathways in green (fig. 4), whereas the orange-colored infill indicates CyTOF readout. For all inhibitors, I used concentrations determined in prior publications or other unpublished projects from the laboratory, as referenced in table 2 with corresponding catalog number, concentration, and main pathway of activity. It is of note, that organoid lines are expected to respond to different concentrations of each inhibitor with on-target inhibition, due to differences in signaling molecule concentrations, activities, and/or interactions. Thus, differential effects on the various organoid lines in the assays performed are not necessarily an indication of the essentiality of the target signaling molecule.
This panel of inhibitors was applied to the eight organoid lines previously mentioned: two normal colon organoid lines (no cancer-driver mutation), two KRAS^{wt}, three KRAS^{mut} and one BRAF^{mut} organoid line. Analysis was done by scRNA sequencing to get RNA transcript abundance per cell, and sc-mass cytometry (CyTOF) to get (phospho)-protein abundance per cell. This will allow us to investigate the effect of pharmacological small molecule intervention on changes in signaling, gene expression, and resulting cell type composition.

Table 2: Perturbation inhibitor panel

No.	Cat. No.	Target	Pathway	Final Conc.	Reference
1	AZD8931	EGFR	EGFR-RAS-MAPK	50 nM	Brandt et al. (2019)
2	CH5183284	FGFR	EGFR-RAS-MAPK	200 nM	AG Schulz, personal communication
3	/	EGFR + FGFR	EGFR-RAS-MAPK	/	
4	PLX4032	BRAF	EGFR-RAS-MAPK	3 µM	Corcoran et al. (2012)
5	AZD6244	MEk	EGFR-RAS-MAPK	8 µM	Riemer et al. (2017)
6	/	MEk + EGFR	EGFR-RAS-MAPK	/	
7	SCH772984	ERK	EGFR-RAS-MAPK	100 nM	AG Sers, personal communication
8	LY2228820	P38	MAPK/DDR	200 nM	Cloninger et al. (2011)
9	PF3644022	Mk2	DDR	2,5 µM	Dietlein et al. (2015)
10	PF477736	Chk1	DDR	1 µM	Dietlein et al. (2015)
11	/	Chk1 + Mk2	DDR	/	
12	GDC0941	PI3K	EGFR-PI3K	500 nM	Riemer et al. (2017)
13	MK2206	AKT	EGFR-PI3K-AKT	250 nM	Riemer et al. (2017)

14	AZD8055	mTOR (both) complexes)	EGFR-PI3K-AKT-MTOR	100 nM	Hu et al. (2014)
15	Rapamycin	mTOR → S6	EGFR-PI3K-AKT-MTOR	100 nM	Riemer et al. (2017)
16	Chir99021	GSK3β	Wnt/β-catenin	6 µM	Riemer et al. (2017)
17	SB525334	TGFβ receptor	TGFβ	1 µM	Li et al. (2014)
18	IKK-16	Ikk	NFκB	10 µM	Shashkova et al. (2016)
19	S8334	Mst1/2	Hippo	1 µM	Fan et al. (2016)
20	/	DMSO Control		1:1000	

3.3.1 Workflow for large-scale single-cell analysis

The large-scale perturbation experiment was done with the goal to integrate changes in the transcriptome with signaling changes. Thus one common time point for both methods was used. For proteins in CyTOF, one short time point was additionally harvested: 3 hours to catch fast and therefore potentially direct post-translational modifications and 48 hours to see both direct and indirect effects of signaling node inhibition that may also depend on slow downstream processes such as altered transcription or changes in cell differentiation states. For scRNA seq only the 48-hour time point was investigated since transcriptional changes are slower. For all experiments, large organoids were used to increase the chances of heterogeneous cell types after symmetry breaking (Serra et al., 2019).

Figure 5 depicts a gross overview of the workflow. For detailed information on the methodology see method sections 5.4 (scRNA seq) and 5.3 (CyTOF). In short, organoids were plated in 24-well plates for both scRNA seq and CyTOF at the same time. After eight to eighteen days, depending on the growth rate of the respective lines, organoids were treated with the inhibitor panel (see table 2) for three and forty-eight hours. The organoids were harvested and digested into single cells that were subsequently analyzed by scRNA-seq and CyTOF.

In the case of scRNA-seq, the cells were tagged with antibodies to identify the different perturbations after sequencing and pooled. Each organoid line was split into two pools of ten samples and the half that did not contain the DMSO control, had an extra DMSO control added so that there was one pool with ten perturbations and one pool with eleven perturbations per organoid line. This also meant that for each organoid line, one of the twelve available sample tags from the BD Human-Multiplexing-kit was not used. The pooled samples were fixed in MeOH and stored at -80°C until sequencing library preparation. After all samples for multiplexing were prepared, cells were rehydrated, filtered, and counted. Then the "Chromium Single Cell 3' Reagents Kits v3"-protocol was followed to produce single-cell libraries for sequencing. The sequences were annotated

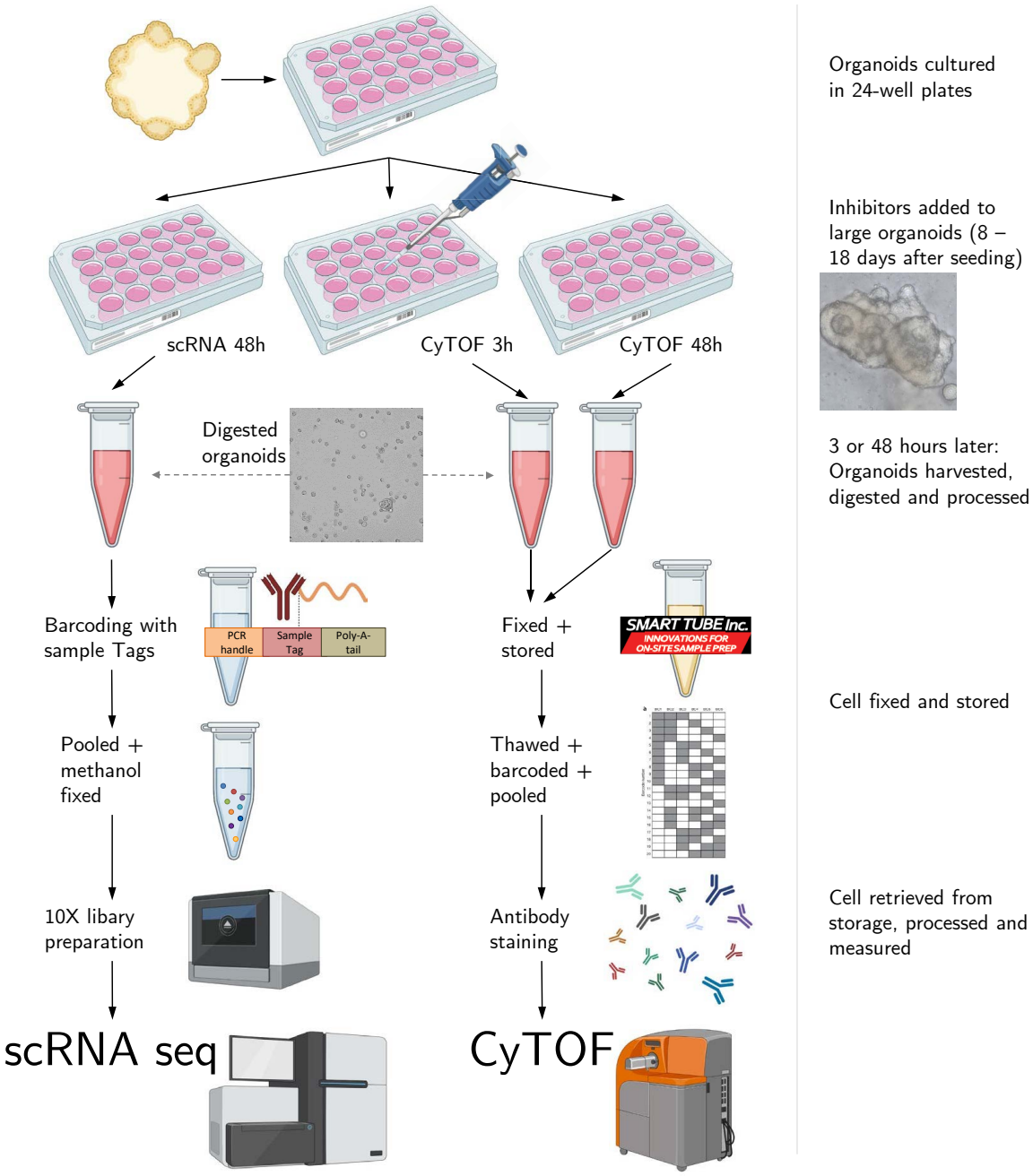

Figure 5: Overview of perturbation screen from organoid culture to both methods of single cell analysis. After harvesting the workflow differed between scRNA seq (on the left) and CyTOF (on the right).

with original organoid line and perturbation by either Dr. Florian Uhlitz or Stefan Peidli (AG Blüthgen).

For CyTOF, cell suspensions were shortly stained with Cisplatin to mark dead cells, and samples were individually fixed and stored at -80°C. A day prior to analysis, cells were thawed, washed, and barcoded with stable palladium isotopes, which covalently bind to an amine group. The barcoding kit from Fluidigm has twenty barcodes with each containing three of the six isotopes and each barcode is either positive or negative for a unique combination of isotopes, which make up the barcode. The distance between

the third- and fourth-highest barcode intensities is termed "barcode separation", which is not only used to match cells to sample conditions but also works as a quality control since samples with a low barcode separation are either doublets or debris (Zunder et al., 2015). Then cell suspensions were pooled into one tube to be stained with extracellular markers, subsequently permeabilized and stained for intracellular markers. Cells were fixed overnight to be measured on a CyTOF 2 Mass Cytometer (Fluidigm) at the BIH Cytometry core facility. Debarcoding and post-processing were done by Thomas Sell (AG Blüthgen).

3.4 Single cell mass cytometry (CyTOF)

3.4.1 CyTOF debarcoding and pre-processing

The perturbation screen was planned with the constraint of twenty palladium-based CyTOF-barcodes in mind, which means that all barcodes were used in each CyTOF run. Barcode separation (fig. 6A) had a high overall yield (around 92%) with the lowest yield in IKP007s of 81.2%. In the right upper panel, the individual barcode isotope densities are shown, clearly separating positively from negatively stained cells. The plot below shows data integrity measuring DNA density over the time of sample measurement. Next, the cerium-bead (^{140}Ce) related events were excluded (fig. 6B), since cerium was not used for antibody labeling of cells, but only to distinguish cell-bead doublets and debris. Beads were DNA-negative, whereas cells were ^{140}Ce-negative. Double positives were bead-cell doublets and double negatives were debris. The right panel in fig. 6B shows singlet gating by plotting a DNA channel against the event length. Again, too-high amounts suggested doublets and too-low values indicated debris. In this case, 92.2% of events were kept and regarded as single cells for further analysis. The last step in post-processing was dead cell removal (fig. 6C) by using the viability stain Cisplatin, which binds to dead cells. The plot shows DNA versus Cisplatin (with beads filtered out). Red outlined are the dead cells (3.50%), leaving 96.5% of the remaining cells as viable single cells. From raw unfiltered data to viable single cells without beads, the total percentage dropped from 100% to 89.4% (average for the other organoid lines 85%).
Fig. 6D shows the filtered channel densities of OT227 for selected cell type markers, which were used for clustering. The x-axis shows signal strength on a log scale and the y-axis shows the density of metal abundance per cell. EpCAM is an epithelial cell marker (Litvinov et al., 1994). CD44 and PROM1 are markers previously published to be expressed in colon or colorectal cancer stem cells (Du et al., 2008; Jing et al., 2015), Krt20 is known to mark differentiated cells (Chan et al., 2009), CD24 could indicate Paneth cell-like differentiation (Sato et al., 2011b), and EPHB2 is known to have a graded expression highest in stem-like and lowest in differentiated cells (Merlos-Suárez et al., 2011). cCASP3 and cPARP mark dead or dying cells (Sabine et al., 2012; Kaufmann et al.,

1993).

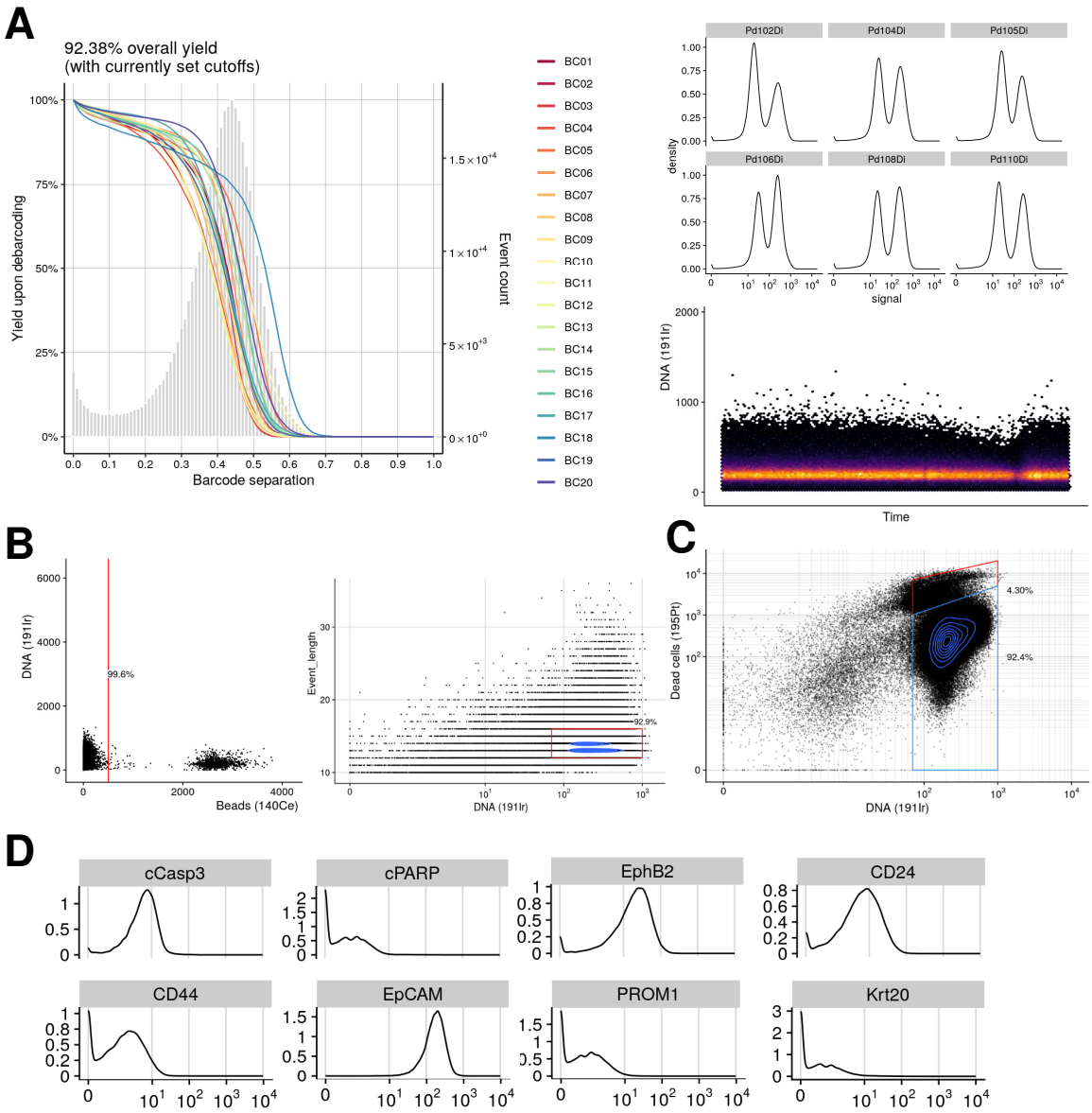

Figure 6: Debarcoding and quality control for CyTOF. Exemplary plots are shown for OT227 **A.** Barcode separation is used to deconvolve samples. Overview showing yield and barcode isotope densities individually. Below is the data integrity plot showing DNA measured over time: yellow indicates high DNA content, measured by intercalating agent Iridium191. Darker spots in the DNA-dense area might indicate a reduced sample flow or a clogging of the machine. **B.** Normalization steps: Cerium-Bead removal and singlet gating. The red square indicated where the majority of events fell. **C.** Debris removal indicated by gating **D.** Density plots for markers that are used for clustering. Plots provided by Thomas Sell

In this case OT227 cells stained all positively for EpCAM, which is expected as organoids consist exclusively of epithelial cells. A major cell population also expressed EPHB2, in line with its known role as a graded marker of the colon differentiation axis (Merlos-Suárez et al., 2011). However, only a few cells expressed PROM1 and CD44, which could mark stem cells, and also only a subset of cells expressed Krt20 and/or CD24, which

could be differentiated cells. There was also a population of cells expressing PARP and/or cCASP3, which could indicate the presence of apoptotic cells in the organoid cultures. Overall this marker expression profile is indicative of a growing and functioning organoid culture since stem cells and differentiated cells are present to uphold long-term *in vitro* culture.

3.4.2 Cellular heterogeneity at single-cell resolution between organoid lines

After observing heterogeneous marker expression in two organoid lines in IHC (fig. 2) and CyTOF (fig. 3), we employed the single cell analysis to more organoid lines to analyze differences among the lines. Here data from all analyzed cells per line is shown. For each line, cells were binned by their EPHB2 level, so that cells high in EPHB2 are located on the left and cells low in EPHB2 are on the right. As EPHB2 expression is known to be graded along a differentiation trajectory, described in chapter 1.1.1, this means that stem cell-like cells are displayed to the left and differentiated cells to the right. Now we can estimate the distribution of all other markers, and as examples, the markers from the previous immunohistochemistry experiment (fig. 2) were chosen. Now, heterogeneity of marker expression along the differentiation axis can be investigated.
The proliferation marker Ki-67 is expressed very lowly in all cancer lines and almost not expressed in the normal lines, however, it tends to be expressed at the beginning of the trajectory in EPHB2-high cells. In contrast, cCasp3 is often higher at the end of the differentiation trajectory, that is, in the EPHB2-low cells. This confirms that the cells are indeed sorted according to a differentiation gradient with proliferation in the beginning and apoptosis at the end of the trajectory. The differentiation marker Krt20 seems to be only highly expressed in OT238 and very little in the normal lines. However, I also see deviations from the differentiation trajectory, like in the BRAF^{mut} line, where EPHB2 and cCasp3 are expressed in the same cells. This might be due to replication stress caused by the BRAF mutation (Klotz-Noack et al., 2020).
Interestingly, pMEK and pERK expression is graded and follows the EPHB2 gradient,

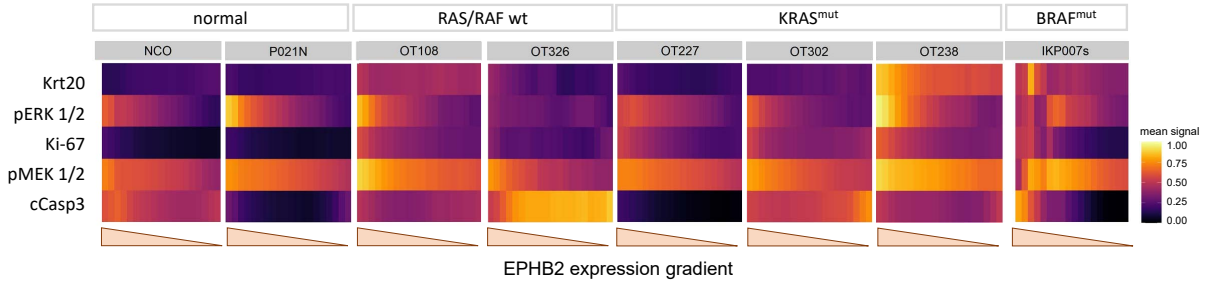

Figure 7: Heterogeneous marker expression between organoid lines. Cells are binned along an EPHB2 marker gradient so marker expression of cell type or signaling markers could be compared along the putative differentiation axis.

being expressed more in EPHB2-high cells and decreasing along the trajectory. Like I previously showed in chapter 3.2.1 for only two organoid lines, MAPK signaling decreased with the progression of cell differentiation in all tested organoid lines, even in the normal colon organoid lines.
In summary, CyTOF is a powerful method to assess organoid cell heterogeneity on a single cell level and I can detect heterogeneous signaling states within the organoids. This analysis could be widened, so that several conditions can be compared.

3.4.3 Perturbations affect cellular hierarchies

Next, I wanted to assess how perturbations affect the EPHB2 axis analyzed for the untreated condition above. For this analysis I only used selected perturbations, showing mainly MAPK inhibitions and two non-MAPK examples. I again used CyTOF EPHB2 expression strength to sort cells by their differentiation. The cells of each organoid line were sorted into twenty bins according to their EPHB2 expression strength from high to low, and the distribution of cells belonging to the various perturbations was analyzed (fig. 8). I then compared how the perturbations for 48 h affected the differentiation gradients

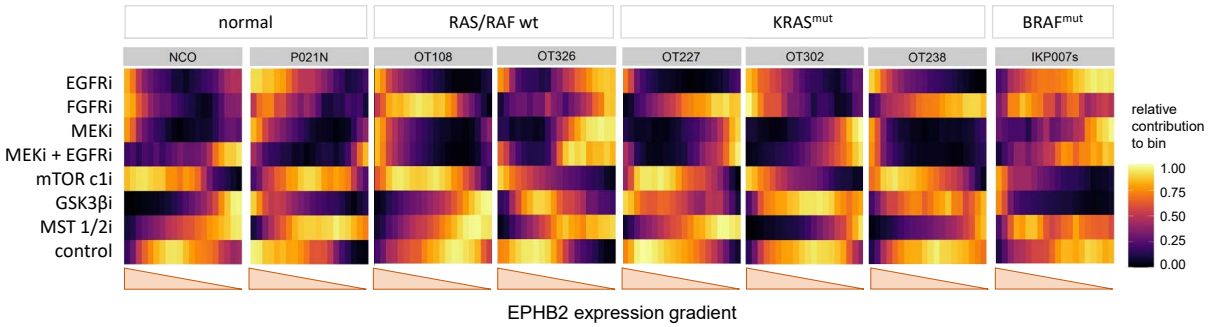

Figure 8: Inhibitors altered stem-cell factor EPHB2 expression. All cells of each organoid line were sorted by EPHB2 expression with high expression on the left side of each plot and expression decreasing towards the right side of the plots. Color code represents the relative contribution to the bin. Cells were binned into 20 groups containing the same amount of cells and then divided according to their perturbations to show the influence of selected perturbations on differentiation states.

of the organoid lines: looking firstly at MEKi and MEKi + EGFRi, there were two distinct reactions in the cancer lines. OT108 and OT238 reacted with a shift towards the undifferentiated state. The other four cancer lines had a reduction in EPHB2 expression and shifted toward the differentiated state. Only the normal organoid lines had a differential reaction towards MEKi and MEKi + EGFRi. MEKi alone induced an undifferentiated cell state, whereas MEKi + EGFRi caused cells to express less EPHB2. This was interesting because EGFRi alone did not have that effect. Overall MEKi and MEKi + EFGRi reduced the spread of cells along the differentiation axis. Upon EGFR inhibition most cells of six out of eight organoid lines shifted toward the undifferentiated cell state. Only in OT326

and BRAF^{mut} IKP007s more cells had low EPHB2 expression. The other RTK inhibitor, FGFRi, affected the two normal lines and OT302 in the same manner as EGFRi. In the other lines, a shift towards differentiated cells could be observed, whereas in IKP007s no clear shift was visible.
MST1/2 inhibition had a strong effect on all organoid lines: there were few cells with high EPHB2 expression in all but IKP007, meaning that the MST1/2i caused cells to differentiate. mTORi did not influence the differentiation state of cells in OT108, OT227, and OT238, induced dedifferentiation in OT302, OT326, IKP007s, and NCO, whereas P021N showed only a mild shift toward the differentiated cell state. GSK3βi should induce stemness in cells due to activation of the Wnt pathway, but only IKP007s and P021N showed the expected result. OT227, OT238, OT302, and OT326 showed barely a difference to the control treatment and NCO cells shifted towards the differentiated state. Noteworthy is that the organoid lines with the same driver mutations (KRAS^{wt}, KRAS^{mut}, BRAF^{mut} and normal WT) did not necessarily show the same response. Only the normal lines reacted similarly to five out of seven perturbations shown, with GSK3βi producing opposite results and mTORi non-congruent reactions.
Overall, these results showed that perturbations affect the differentiation state of cells and that certain perturbations restrict the differentiation space/spread. There was cellular heterogeneity within each organoid line, which can be altered by inhibitor addition for 48 hours causing induction or inhibition of differentiation.

3.4.4 Marker correlations in CyTOF data

Next, I performed a correlation analysis of all cells under all perturbations combined for the eight organoid lines to check for expected correlations and interesting pathway cross-talk.
Overall, I detected more positive correlations than negative ones, which suggests that the CyTOF data could be compromised by unwanted variation that is not related to specific signaling events or cell states. Indeed, as this type of data stems from antibody stainings, it is likely that larger cells generally bind more antibodies than smaller cells, either due to epitope-specific binding or due to non-specific background binding. Thus, all positive correlations have to be interpreted carefully, and independent validation would be required for all correlations that are being followed up in the future. There is also the possibility to remove unwanted variation from the CyTOF data, however, the development of a methodology to do so is still ongoing in the Blüthgen lab.
That said, some markers correlated significantly in all lines in an expected manner, like pMEK1/2 with pERK1/2, which are consecutive signaling molecules in the MAPK cascade, suggesting that consistent and strong correlations can be deduced from the CyTOF dataset without further accounting for unwanted variation. Also, cCasp3 and cPARP correlated

significantly in all organoid lines because they both mark apoptotic cells. Differentiation gradient marker EPHB2 correlated with translation initiation factor p4e-BP1 in all but NCO. Other markers correlated in all lines despite being from different pathways e.g. YAP with pSMAD2/3, pSMAD1/8, pMEK1/2, pAKT, and EPHB2. YAP correlating positively with EPHB2 might be due to YAP being able to reprogram cancer cells into stem cells. YAP and the SMADs might correlate since YAP can bind to SMAD complexes (Varelas et al., 2010). Furthermore, YAP is a part of the β-catenin destruction complex, which explains the strong positive correlation with Axin2 in all cancer lines and no significant correlation in the normal lines, which do not have the Wnt pathway constitutively activated and thus overall lower Axin2 levels. Checkpoint proteins pChk1 and 2 positively correlated with DNA damage marker pH2A.X in all but NCO, suggesting checkpoint activation upon DNA damage, which is common in most CRCs.

As possible artifacts, as discussed above would cause a general positivity in correlations across the dataset, negative correlations between markers are particularly noteworthy. I found that cCasp/cPARP and YAP were negatively correlated in six out of eight lines, but only significantly in the normal organoid lines. Furthermore, cPARP correlated negatively with EPHB2 significantly in P021N and non-significantly in three out of six cancer lines. This negative correlation was an expected response, since EPHB2 is a graded stem cell marker and cleaved PARP is an apoptosis marker. Only in the normal line P021N did the differentiation marker KRT20 correlate significantly negatively with Prom1, SMAD1/8, and PTK7.

Another noteworthy point is that all cancer lines showed significant negative correlation between CD8A and EPHB2, p-c-Jun, pP38, pAKT, pCDC25C, pChk1/2, pMEK1/2, SMAD1/8, SMAD 2/3 and YAP. CD8A is a surface marker for intraepithelial lymphocytes, whose role is to eliminate damaged epithelial cells to maintain barrier function (Jabri and Ebert, 2007), which might explain why it does not correlate with signaling molecules. Sadly CD8A was not measured in the normal colon organoid lines, which makes it impossible to tell whether this is an artifact or cancer-specific. However, looking at the density plots for this marker (c.f. fig. 24) it becomes evident that this antibody had a very low dynamic range/binding affinity. This is also true for other markers, where a positive correlation would be expected, but cannot be observed, like e.g. with LGR5 and pS6. In this case, both markers show a poor dynamic range of the antibody or low binding (c.f. fig. 24).

Overall, marker density, which depends on antibody binding, and cell size has to be considered when comparing marker correlations. Additionally, this analysis used bulk-CyTOF data, combining all perturbations, which might affect average marker expression. However, credibility is restored, if certain positive correlations can be found in eight independent non-batch corrected CyTOF runs, like the correlation between YAP and pSMAD2/3 or SMAD1/8, which is also biologically interesting, since active YAP in a high

cell-density setting sequesters SMAD2/3, which suppresses TGFβ signaling (Varelas et al., 2010).

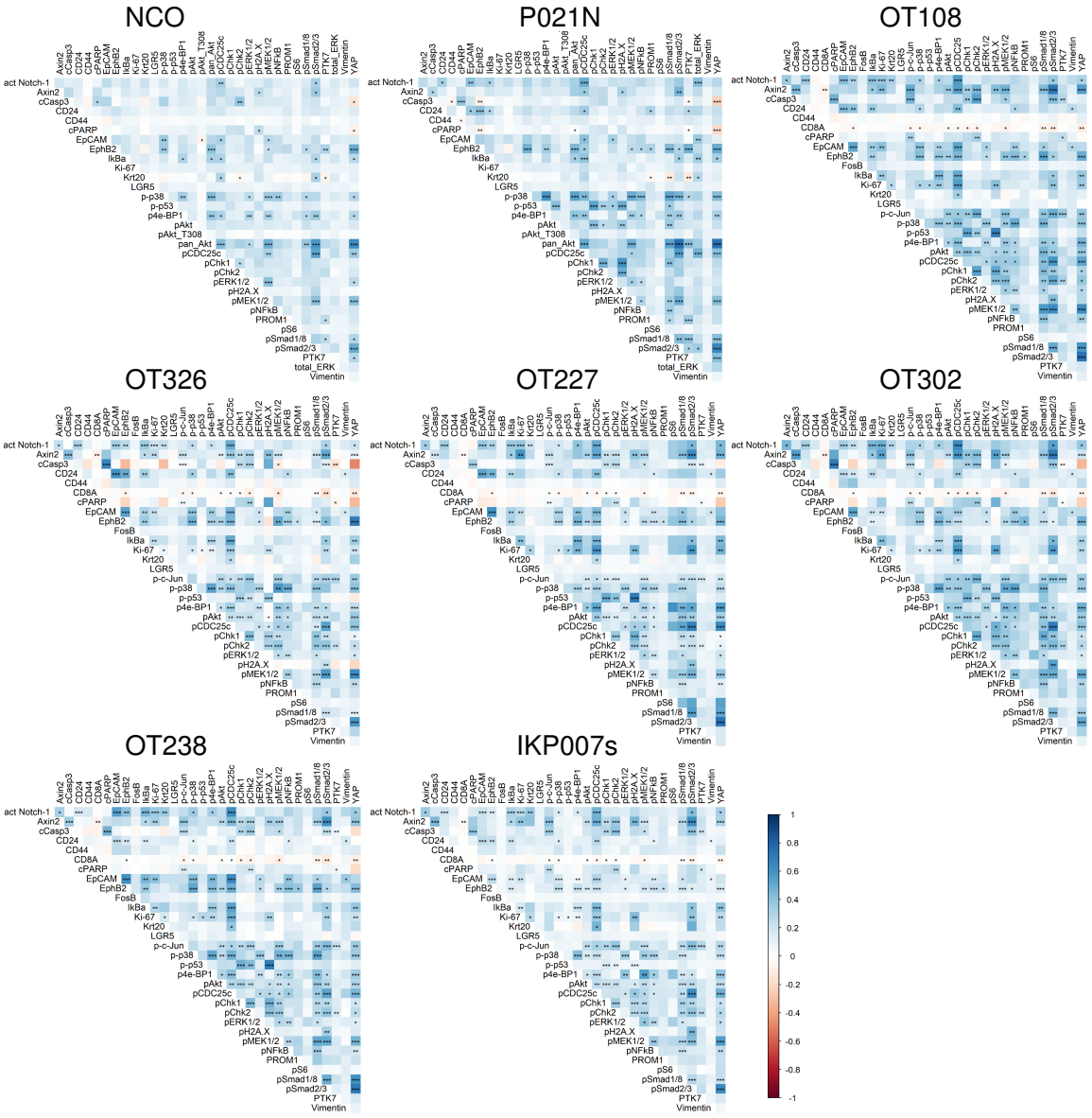

Figure 9: Spearman correlation matrices of all cells in the CyTOF runs, comparing all measured markers. Using significance levels: ns = $p > 0.05$; * = $p \leq 0.05$; ** = $p \leq 0.01$; *** = $p \leq 0.001$

3.5 Single cell RNA sequencing

3.5.1 scRNA seq demultiplexing and pre-processing

After the single-cell mass cytometry method was used to show heterogeneity between and within the organoid lines, I now come back to scRNA sequencing, which was done in parallel to the CyTOF sample acquisition, as shown previously in fig. 5. scRNA sequencing lets us analyze the transcriptome of single cells in a non-targeting and unbiased manner.

Thus, we can assess hundreds of features per cell in contrast to the limited number of marker measurements in CyTOF.
After two libraries per organoid line were sequenced, the sample tag information was used to unambiguously identify the organoid line. Figure 10A shows the sample tag (or hashtag) distribution according to the data (left) and how the sample tags were registered in a database called SODAR (right). SODAR is a non-public storage database for omics data and corresponding metadata (by the Core Unit Bioinformatics of the BIH). In the left panel of the figure, the yellow to green color means that the sample tag was present, whereas the purple color indicates that this tag was not found. Comparing experimental to theoretical data on the right panel, the organoid lines were positively identified. There is one disparity in the IKP007s-line where the database only shows one of the sample tags (#10) and #9 is missed, which is an entry mistake in the database. Normal organoid line P021N is not listed in figure 10A, because it was sequenced on its own so that it could not have been mixed up with any other organoid line (missing hashtag #3).
Next in pre-processing of the raw sequencing data was the removal of dead cells (figure 10B), which had a high percentage of mitochondrial genes ("percent.mt"). Exemplary data of the NCO line is shown, however, all organoids have been subjected to the same filtering settings. All cells which have more than 30% of mitochondrial genes were excluded. Cells with less than 100 or more than 6000 features were likewise excluded, which is the number of genes detected in each cell ("nFeature_RNA"). Cells with less than 1000 or more than 30000 RNA counts per cell ("nCount_RNA") indicating the number of molecules detected within a cell, were also excluded. A low feature count may indicate dying cells or empty droplets, whereas a high feature or RNA count may indicate doublets. The remaining cells are most likely singlets that were alive before fixing (Ilicic et al., 2016; Luecken and Theis, 2019).
Transcriptomes derived from single cells of all eight organoid lines were first depicted in one common UMAP (fig. 10D). Generally, transcriptomes formed clusters according to their developmental emergence. This means that the normal colon organoid lines NCO (dark yellow) and P021N (light green) form one overlapping cluster, the KRAS^{mut} and KRAS^{wt} lines form two interconnected clusters, whereas the BRAF^{mut} line IKP007s (purple) formed a separate cluster on its own (fig. 10D), with the largest distance to the normal cells on the UMAP component 1. This showed that the path of emergence of cancer was the strongest divisive feature between the transcriptomes of the organoid lines, while the normal cells from different donors were very similar and completely overlapping. The UMAP representation is in line with the hypothesis that cancer transcriptomes are primarily determined by their emergence path, which was determined by their mutational pattern.
To assess intra-line transcriptome heterogeneity in greater detail, figure 10C shows UMAP representations of each organoid line used in the perturbation screen, color-coded

according to the eleven sample tags (hashtags, abbreviated HT). This would reveal if any of the perturbations had a profound impact on the transcriptome within 48 hours of treatment. Most perturbations intermingled. However, there were two populations in KRAS^{mut} lines segregating a little from the other cells: In line OT227 hashtag 5 and 6, and in line OT238 hashtag 7 and 8, which corresponds to MEK and MEK + EGFR treatment. This could already indicate that MEK inhibition has a profound effect on KRAS^{mut} cells, altering transcriptomes in a manner that cannot be replicated by any other pathway node inhibition in the screen.

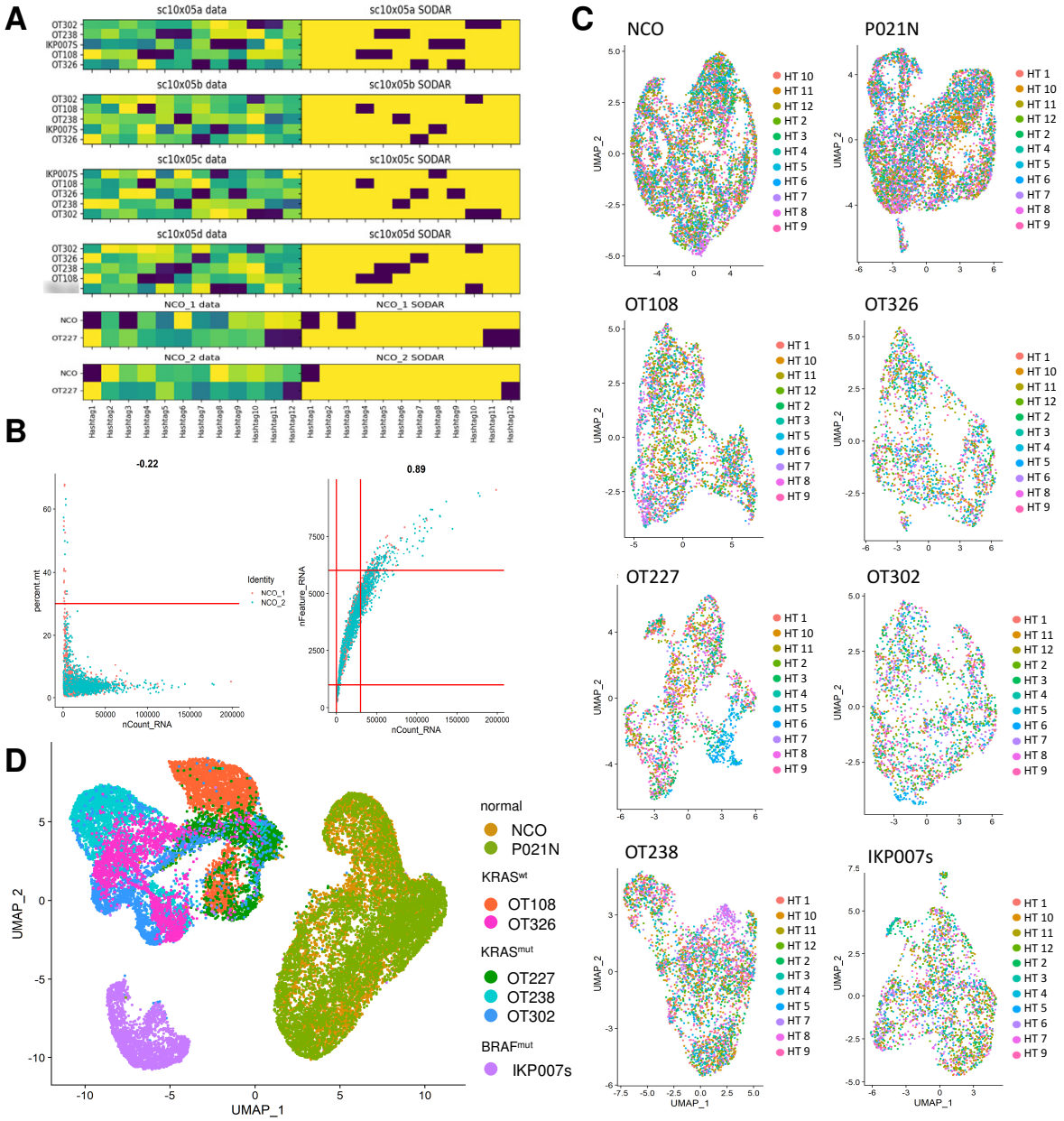

Figure 10: Demultiplexing and quality control for scRNA seq **A.** Organoid lines by sample tag according to data (left) and pipetting scheme (right) (analysis provided by Stefan Peidli) **B.** Pre-processing of raw sequencing data to filter out dead cells, empty droplets, and doublets **C.** UMAPs showing hashtag (HT or sample tag) distribution in each organoid line **D.** UMAP representation of all eight organoid lines showing contributions of emergence pathway/mutation pattern to the formation of three separate clusters.

3.5.2 Cellular heterogeneity not due to cell cycle phases

One main factor influencing changes in the transcriptome is the cell cycle (Schwabe2020). I had to exclude the possibility that some subpopulations only exist because of cell cycle states. The cell cycle phase of individual cells was determined with cell cycle-specific gene expression (fig. 11A). Most cells were in the growth G1-phase (reddish color in UMAPs). G2M- and S-phase cells (green and blue, respectively) formed a separate cluster,

with some of the S-phase cells interspersed in the G1 cluster. Different cell cycle phases may affect the response of cells to inhibitors due to changing/oscillating gene expression. Using the same UMAP representation in fig. 11B the heterogeneous MAPK pathway gene

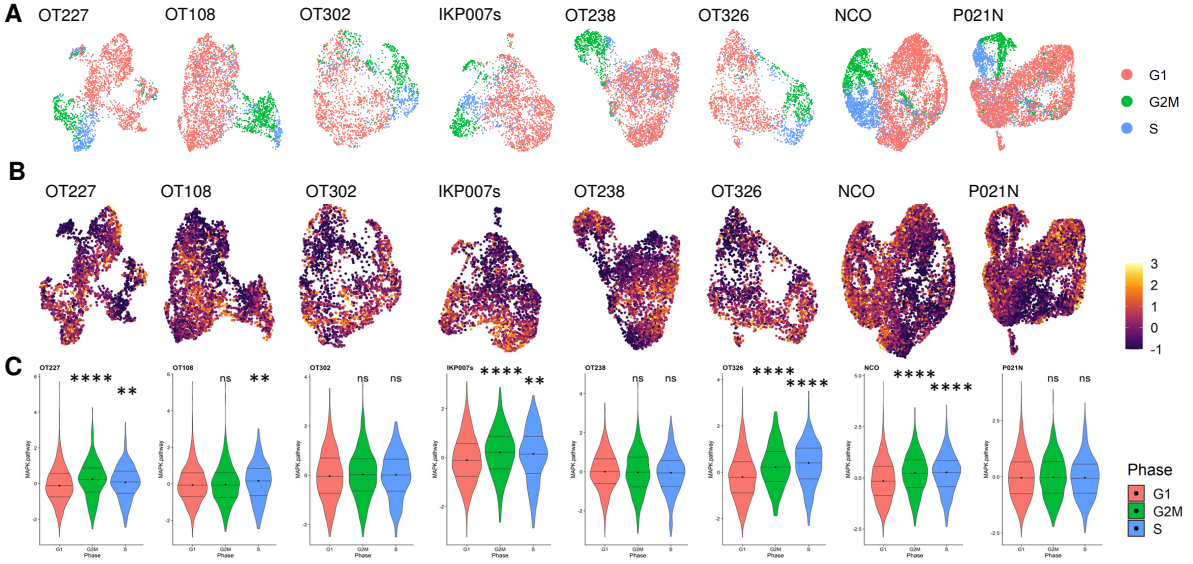

Figure 11: Heterogeneity within organoid lines **A.** scRNA seq data was used to visualize the cell cycle phases of organoid lines in UMAPs **B.** MAPK pathway gene signature expression scores color coded with light yellow color indicating a strong expression **C.** Violin plots showing MAPK activity per cell cycle phase. p-values show the difference to G1-phase. Significance was determined by Wilcoxon-Rank-Sum test, using ns = $p > 0.05$; * = $p \leq 0.05$; ** = $p \leq 0.01$; *** = $p \leq 0.001$; **** = $p \leq 0.0001$

signature expression is shown. MAPK pathway activation might act as a substitute for cell differentiation since MAPK activity decreases along the differentiation trajectory (Uhlitz et al., 2021). Comparing cell cycle and MAPK gene expression signatures, I could see that MAPK activity was not restricted to a specific cell cycle phase and each organoid line had an expression spectrum of MAPK activity across all cell cycle phases. Itemizing the MAPK pathway activity for each cell cycle phase (fig. 11C) there were three organoid lines with no significant difference between cell cycle phase and MAPK activity. Four organoid lines showed significantly higher MAPK activity in G2M compared to G1 and five lines upregulated MAPK activity in S phase compared to G1 phase. This showed heterogeneous MAPK activation which could not be attributed to an oncogenic mutation or absence thereof since the cancer lines and both normal lines had different MAPK activity patterns.

3.5.3 Perturbations affect cell distribution and cell cycle allocation

Next, the impact of inhibitors on changes in transcriptomes was analyzed. After cells were annotated with their respective perturbation, a UMAP algorithm was applied to visualize cell distribution. Figure 12 shows exemplary cell distribution for OT227. From visual inspection it became apparent that some inhibitor treatments affected transcriptomes, and thus transcriptome distribution in UMAP space. This effect was most pronounced in MEK, MEK+EGFR, and to a lesser extent other RTK inhibition treatments, which resulted in the selective depletion of cell populations.

To find out if this effect was only occurring in OT227 and which features defined

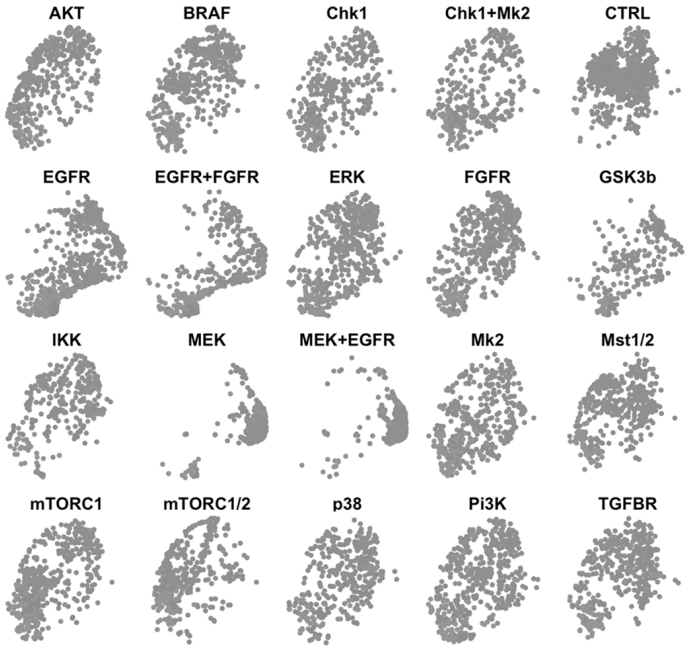

Figure 12: Effect of perturbations on cell distribution in organoid line OT227 shown as UMAP representations. Inhibitors affected the cell distribution in UMAP space.

transcriptomes of MEK and MEK+EGFR treated cells, percentages of cells in each cell cycle phase were compared (fig. 13). Most cells were in G1 phase, but some inhibitions altered the contributions of cell cycle phases. When looking at MEK inhibition, there were fewer cells in G2M and S phase in all but one cancer line compared to the control treatment. A more detailed look into the comparison between control and MEK inhibitor-treated cells (fig. 13 brackets from CTRL to MEK treatment) revealed that there was a significant increase of cells in G1 phase in half of the cancer organoid lines and a significant decrease in P021N, the normal colon organoid line. A significant decrease of cells in G2M phase was observed in four of six cancer lines and not in normal lines. Changes in S-phase were only found in three organoid lines, which constituted an increase in cell number in P021N and OT227 and a decrease in OT108. Only three organoid lines (NCO, OT326, OT302) did not have significant changes in any cell cycle phase between

control and MEK treatment.

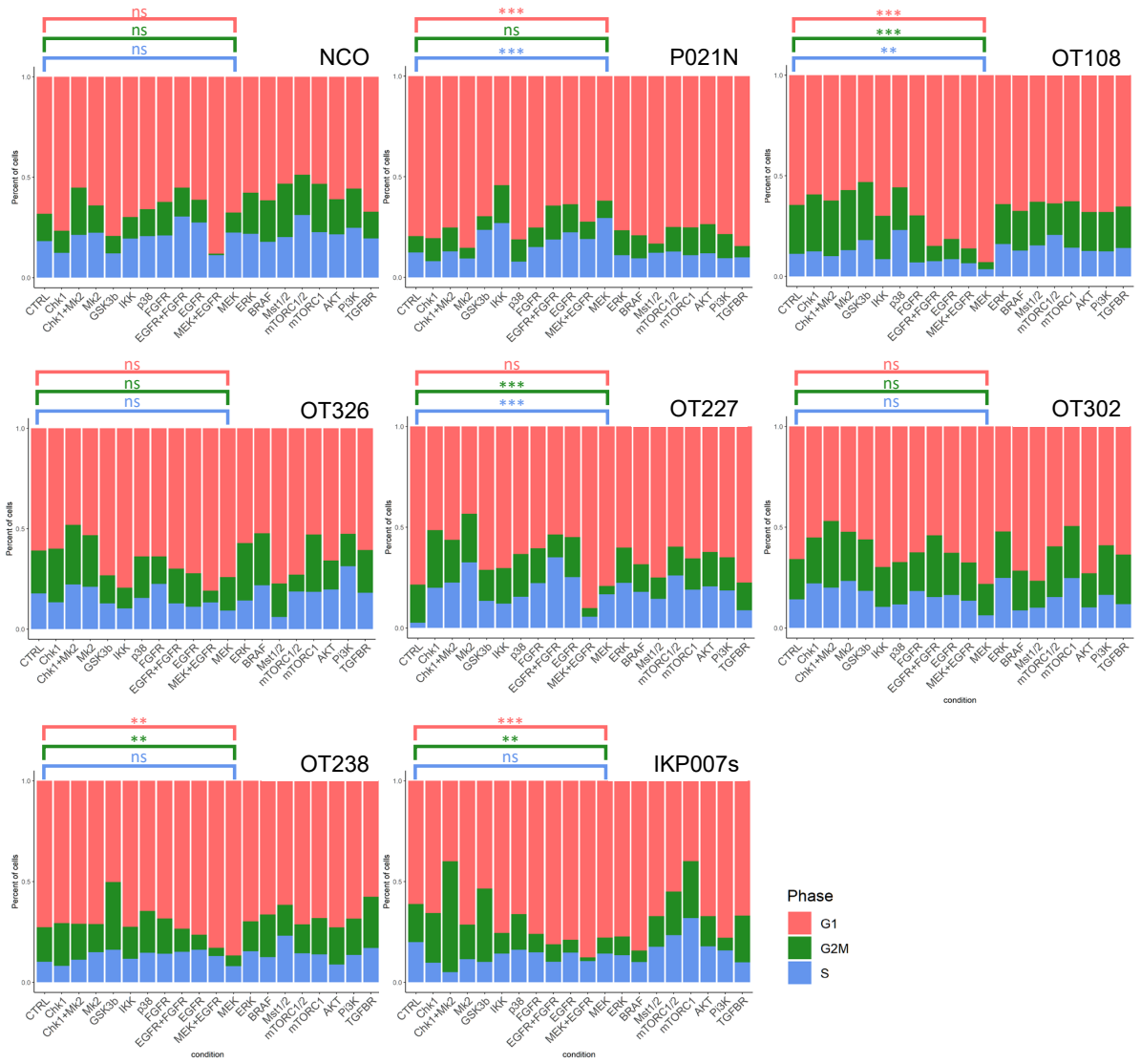

Figure 13: Effect of perturbations on cell cycle distribution. Bar graphs showing color-coded cell cycle phases depicting the percentage of cells in each phase. The brackets above each graph show significance levels of comparison between control and MEK inhibition per cell cycle phase. Significance was determined by Pearson's Chi-squared test with Yates' continuity correction, using ns = $p > 0.05$; * = $p \leq 0.05$; ** = $p \leq 0.01$; *** = $p \leq 0.001$

Overall MEK inhibition affected the cell distribution in UMAPs and the cell cycle distribution in many organoid lines. Cells of cancer organoid lines were arrested in G1, but in normal organoids, G1 contribution decreased, and cells attenuated in S-phase. In general, the number of cells surviving MEKi was reduced, with only a small subpopulation of cells surviving or resisting the inhibition.

3.6 Correlation between scRNA signatures and CyTOF readouts

After investigating the effects of perturbations in CyTOF data and scRNA seq separately, I wanted to see how the CyTOF and scRNA seq datasets come together. Therefore, I looked at the correlation between gene signature expressions from scRNA seq and single protein readout from CyTOF. For this, I used nine gene expression signatures that are related to pathway activities that were also assessed by specific CyTOF markers. Five of the nine signatures shown in figure 14 (MAPK, TGFβ, PI3K, WNT and P53) are from an R package called PROGENy by Schubert et al. (2018), which infers pathway activity from gene expression. For the MAPK signature, I expect to see a positive correlation with the phosphorylation of MEK and ERK, as these are positively acting downstream kinases of the MAPK cascade. For the TGFβ, PI3K, and P53 signatures, I did not expect all organoid lines to follow the same trend of either positive or negative correlations, since there is a lot of cross-talk and kinases from different pathways could phosphorylate receptors or other signaling molecules. "mTORc1 signaling" and "DNA repair" are HALLMARK signatures, which were curated from genes of the Molecular Signature Database, which collate results of many experiments to a single high-confidence signature (Liberzon et al., 2015). The "EGFR-YAP" signature was published by Gregorieff et al. (2015), which describes a YAP-induced regenerative program by activating EGFR - and suppressing WNT signaling. "LGR5-ISC stem cell" signature was published by Muñoz et al. (2012), who defined an $LGR5^{+}$ crypt base cell signature.

I now wanted to know whether it was possible to correlate the mean protein activity measured by CyTOF with related signatures used to quantify the transcriptional output of signaling pathways. For this, I produced correlation plots for the above-mentioned (phospho-)protein activities of the CyTOF dataset and transcriptional signatures for the same pathways across all lines and conditions (fig. 14), using pseudo-bulk values across all cells of each condition. Each dot represents one perturbation condition and the gray shading indicates a confidence interval for the regression line to easily see if signature and marker expression correlate in a positive or negative manner.

I found that only the MAPK pathway signature correlated positively with pERK1/2 in all organoid lines (fig. 14A), with OT227 and NCO showing a significant correlation between pERK1/2 and MAPK signature, which might be due to ERKs direct involvement in activating MAPK target gene transcription in the nucleus. However, I could not replicate this finding for the other pathways. TGFβ pathway signature (fig. 14B) did not show a significant positive correlation with pSMAD2/3, even though activated SMADs translocate to the nucleus and activate target gene transcription. However, SMAD2/3 could also be activated by other means than the TGFβ pathway, namely it could be phosphorylated by ERK (De Caestecker et al., 1998; Javelaud and Mauviel, 2005). A non-significant positive correlation was observed only in OT326 and P021N. AKT is downstream of PI3K and

pAKT decreases when PI3K was inhibited (c.f. fig. 15/16), but still there was a mostly negative correlation between pAKT and the PI3K pathway gene signature (fig. 14C). Only OT227, NCO, and OT325 showed a non-significant positive correlation. pAKT activates mTORc1, but only half of the organoid lines showed a positive correlation between pAKT and the HALLMARK mTORc1 signaling signature (fig. 14D). In fig. 14E correlation between YAP and the EGFR-YAP signature are depicted, with only half of the organoid lines showing a positive correlation, none of which were significant. Only the BRAF^{mut} organoid line IKP007s scored higher in EGFR-YAP signature expression, which could possibly be explained by the different emergence route of BRAF^{mut} cancers, which are not driven by Wnt mutations. When looking at the Axin2 expression in fig. 14F and G, two clusters, Axin2 low and high, can be observed. The two normal organoid lines, IKP007s, and OT227 had low and the two KRAS^{wt} and the other two KRAS^{mut} lines had higher Axin2 expression. However, it did not positively correlate significantly with the LGR5-ISC gene signature (fig. 14F). Axin2 levels correlated positively significantly with the WNT pathway gene signature in OT227 and P021N (fig. 14G). Otherwise, correlations were very heterogeneous, which might be because Axin2 is a negative regulator of the WNT pathway and also a target gene, which cannot be differentiated in the datasets (Lustig et al., 2002). Looking at the correlation between p-P53 and the P53 pathway gene signature, it becomes apparent that there was very little p-P53 measured in most lines (see fig. 24 in method section). OT238 and OT108 had measurable p-P53 levels, but no significant correlation with the signature (fig. 14H). Next, the DNA repair signature was correlated with the essential DNA repair protein pChk1 (fig. 14I). Only IKP007s correlated positively significantly ($p = 0.022$), whereas five of the eight lines showed a negative correlation.

Overall, the perturbations produced changes in RNA and protein expression, which lead to heterogeneous correlation, with positive and negative correlations even within one oncogenic driver mutation group (normal, KRAS$^{wt/mut}$, BRAF^{mut}). The finding underscores that protein signaling networks can be wired differently between organoid lines, and therefore, probably also between patient tumors. Furthermore, many of the protein signaling components quantified by CyTOF are not the most downstream signaling component of the pathway, giving room for further signal amplification or repression further downstream. Only pERK, which is a well-characterized direct regulator of transcription factors was well-correlated with the respective transcriptional signature. Analysis of downstream-most signaling components not covered by our CyTOF panel might identify more direct correlations.

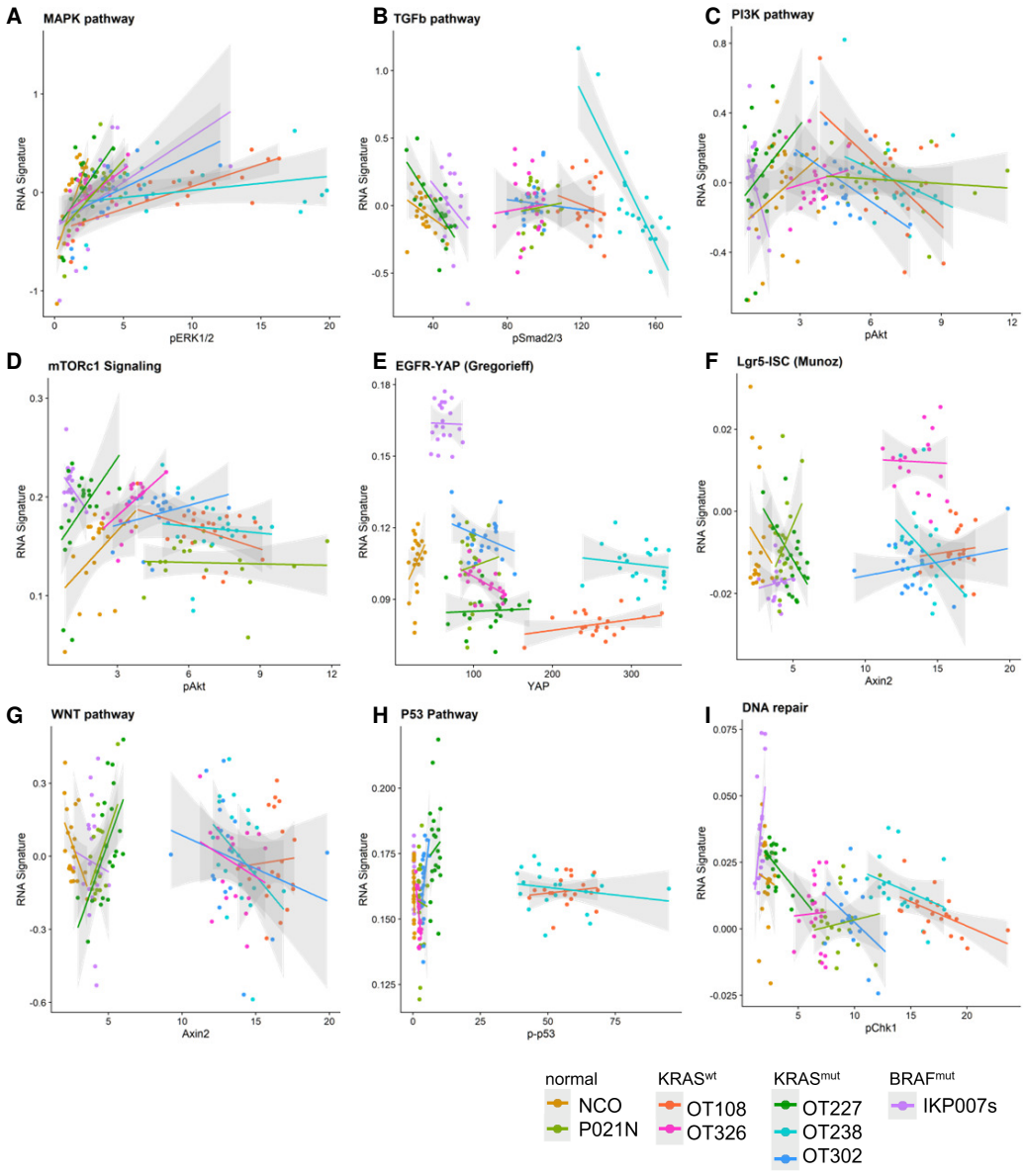

Figure 14: Heterogeneous correlation between RNA signatures and CyTOF readouts for all eight organoid lines. scRNA gene signature is shown on the y-axis and CyTOF protein readout is on the x-axis. Each dot represents one perturbation condition and the gray shading indicates a confidence interval for the regression line. **A.** MAPK pathway. OT227: p = 0.011; NCO: p = $7.4*10^{-5}$ **B.** TGFb pathway signature had no significant positive correlation with pSMAD2/3. OT326: p = 0.77; P021N: p = 0.65. **C.** PI3K pathway and pAKT. OT227: p = 0.25; NCO: p = 0.16 **D.** mTORc1 signaling. OT227: p = 0.059; NCO: p = 0.051 **E.** EGFR-YAP signaling. OT108: p = 0.12; NCO: p = 0.22 **F.** LGR5-ISC signature. OT108: p = 0.7; P021N: p = 0.11 **G.** WNT pathway. OT227: p = 0.0066; P021N: p = 0.016 **H.** P53 pathway. OT108: p = 0.53 **I.** DNA repair. IKP007s: p = 0.022; P021N: p = 0.53

3.7 Comparison between gene signature and single protein expression across perturbations

In the previous chapter, I showed that the CyTOF and scRNA seq datasets correlate heterogeneously for important pathways in cancer emergence and progression. However, only one CyTOF readout was shown per pathway.
Now, I wanted to look in detail at each perturbation and quantify transcriptional footprints of the different oncogenic signaling pathways targeted by our inhibitor panel, to assess the amount and specificity of the inhibition. For this task, I used pseudo-bulk transcriptional data like in the previous chapter, thus neglecting inter-cell heterogeneity, and compared the effects of all perturbations using gene expression signatures to condense effects on the transcriptomes. This task is complicated by the fact that target genes of the pathways are not unanimously defined. For each pathway, several target gene signatures exist that were defined in different studies with varying methodologies and in assorted cell lines. Whenever available, I preferred HALLMARK signatures, since these represent commonly regulated genes across many experimental conditions (Liberzon et al., 2015). In many cases, particularly when no HALLMARK signature was available, I decided to test several signatures per pathway and compare the results. I also compared the expression of the transcriptional signatures from the scRNA seq dataset to the inhibition on protein level, taking into account the respective (phospho-)protein data from the parallel CyTOF experiment. Ideally, inhibition of signal transduction on the protein level should correlate with the transcriptional output on the RNA level. However, in the previous chapter, we saw that the correlation was very heterogeneous (fig. 14). Here, I display the results as heatmaps, to show color-coded changes in expression strength in CyTOF data and in the scRNA seq data. All data were normalized to their respective control sample. The order of perturbations on the y-axis of the plots follows a pathway order: TGFβ, PI3K, Hippo, MAPK, NFκB, WNT, and DNA checkpoints.
Most inhibitors showed an effect in their respective pathway in some organoid lines. The TGFβ and PI3K HALLMARK signature expressions were downregulated upon TGFβR and PI3K inhibition respectively in more than half of the organoid lines. When considering mTOR signaling as well, all cancer lines downregulated signaling either upon inhibition of mTORc1, 2, or both in all cancer lines, only the normal colon organoid line P021N upregulated this signaling pathway. In the CyTOF data the effects were more refined with only the mTORc1/2 inhibitor downregulating p4EBP1 in all organoid lines, whereas mTORc1i upregulated this downstream target in most cancer lines, except OT326.
For the Hippo pathway, I tested three signatures from different publications (table 3). Upon MST1/2 inhibition two of the signatures were only expressed in maximum half of the cells with minimal impact in most organoid lines, whereas the third signature was only strongly downregulated in IKP007s and upregulated in P021N and OT326.

This signature follows EGFR activation and WNT suppression by YAP, which in IKP007s was downregulated upon MST1/2i and concomitantly the DNA repair signature was upregulated.
Most inhibitors targeted the MAPK pathway, which was read out on scRNA level by a MAPK and EGFR signature. Only a small number of cells expressed these signatures. MEK and MEK + EGFR inhibition lead to a downregulation of both signatures in all lines, whereas BRAFi upregulated those signatures in KRAS^{mut} lines, which is known as paradoxical activation (Poulikakos et al., 2010). Looking at the single readouts of CyTOF datasets, BRAF inhibition upregulated pMEK and pERK in all lines, except the BRAF^{mut} IKP007s. Furthermore, the characteristic upregulation of pMEK after MEK inhibition can be observed in all organoid lines. The cancer lines additionally upregulated pMEK upon MEK + EGFR inhibition, whereas in the normal colon organoid lines addition of EGFRi seemed to counteract the MEKi-induced effect. On the other hand, pERK was downregulated by MEKi and MEKi + EGFRi in all organoid lines.
The heterogeneity between organoid lines could be observed even between organoid lines with the same oncogenic driver mutation (cf. Mk2i, Chk1 and Mk2i + Chk1i strongly upregulate pERK in OT238, but have no effect on pERK in OT227). One normal line was hardly responsive (NCO) as could be seen by the shifted fold change in CyTOF data. Inhibitors that did not affect their target pathway directly may have affected different pathways. Most evident was the effect of MEKi and MEK + EGFRi on the apoptosis markers: KRAS^{mut} and KRAS^{wt} lines displayed a strong upregulation; the normal line only showed minimal upregulation, whereas the BRAF^{mut} line is the only line, downregulating these markers under MEK inhibition.
Here I compared both readouts to look for overarching trends or differences between the organoid lines. Comparing gene signature expression to single protein expression does not always concur, due to the fact that CyTOF is based on antibody binding. Antibodies could have a low dynamic range or simply not a very high binding affinity. On the other hand gene signature expression takes many genes into consideration, which might not all follow the same trend of being up- or downregulated by a certain inhibitor, which could downplay the specific effect the inhibitor might have.

Table 3: References for signatures used in dotplots

Signature name	**Reference**
TGFβ pw	PROGENy R package
Early TGFβ resp	Verrecchia et al. (2001)
Delayed TGFβ resp	Verrecchia et al. (2001)
TGFβ sig	HALLMARK
PI3K pw	PROGENy R package
PI3K-AKT-mTOR sig	HALLMARK
mTORc1 sig	HALLMARK
EGFR-YAP sig	Gregorieff et al. (2015)
WNT-YAP sig	Serra et al. (2019)
YAP sig	Cordenonsi et al. (2011)
MAPK pw	PROGENy R package
EGFR pw	PROGENy R package
NFκB pw	PROGENy R package
LGR5-ISC	Merlos-Suárez et al. (2011)
WNT pw	PROGENy R package
DNA repair	HALLMARK
G2M checkpoint	HALLMARK
EMT	HALLMARK
P53 pw	PROGENy R package
NOTCH sig	HALLMARK
MYC targets	HALLMARK

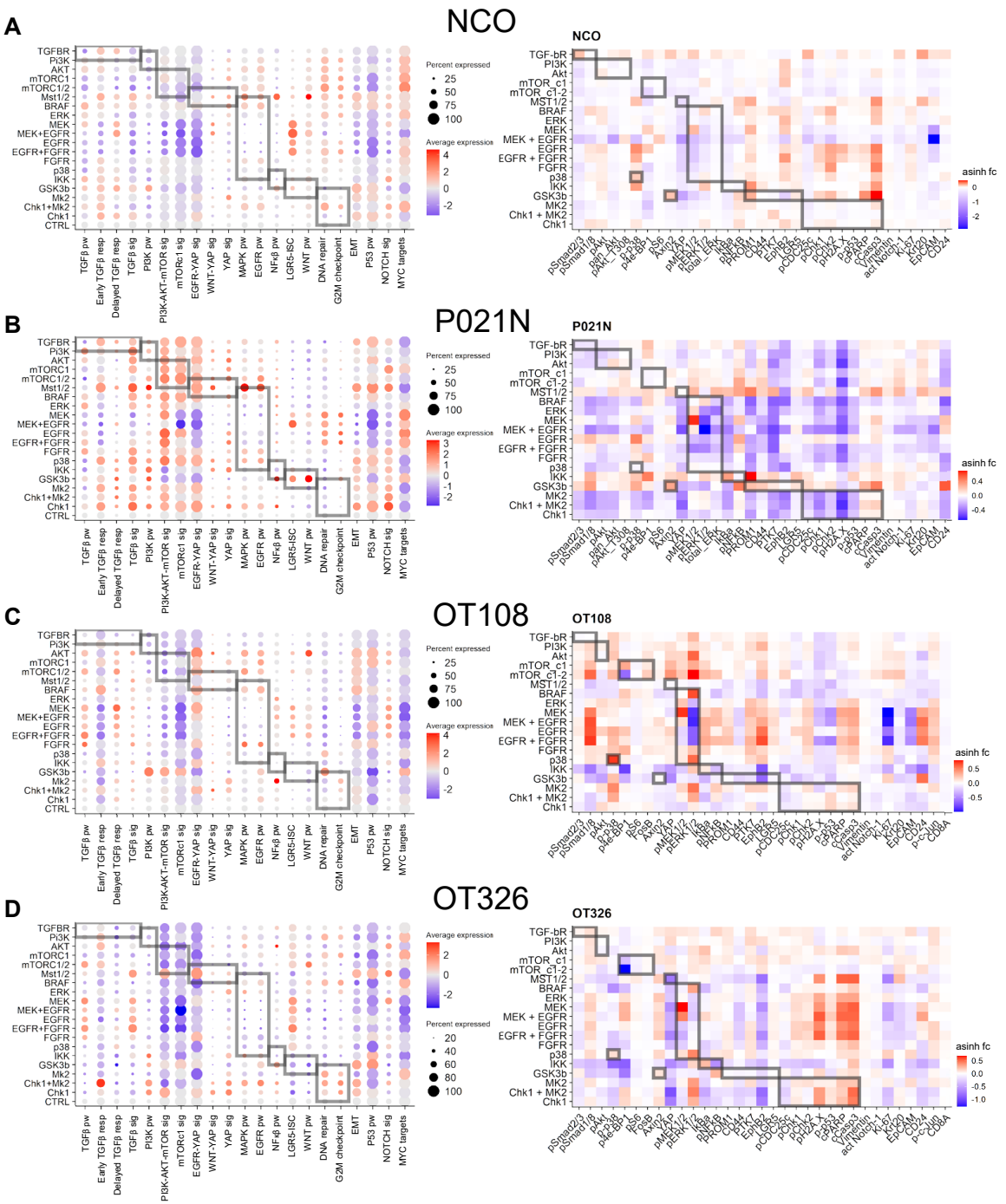

Figure 15: Comparison of perturbation screen results from CyTOF and scRNA seq. On the left side, scRNA seq data was used to produce dotplots showing gene signature expression scores. Plots on the right-hand side show CyTOF readouts (x-axis) for each perturbation (y-axis) as fold change compared to the control treatment. pw = pathway; sig = signaling

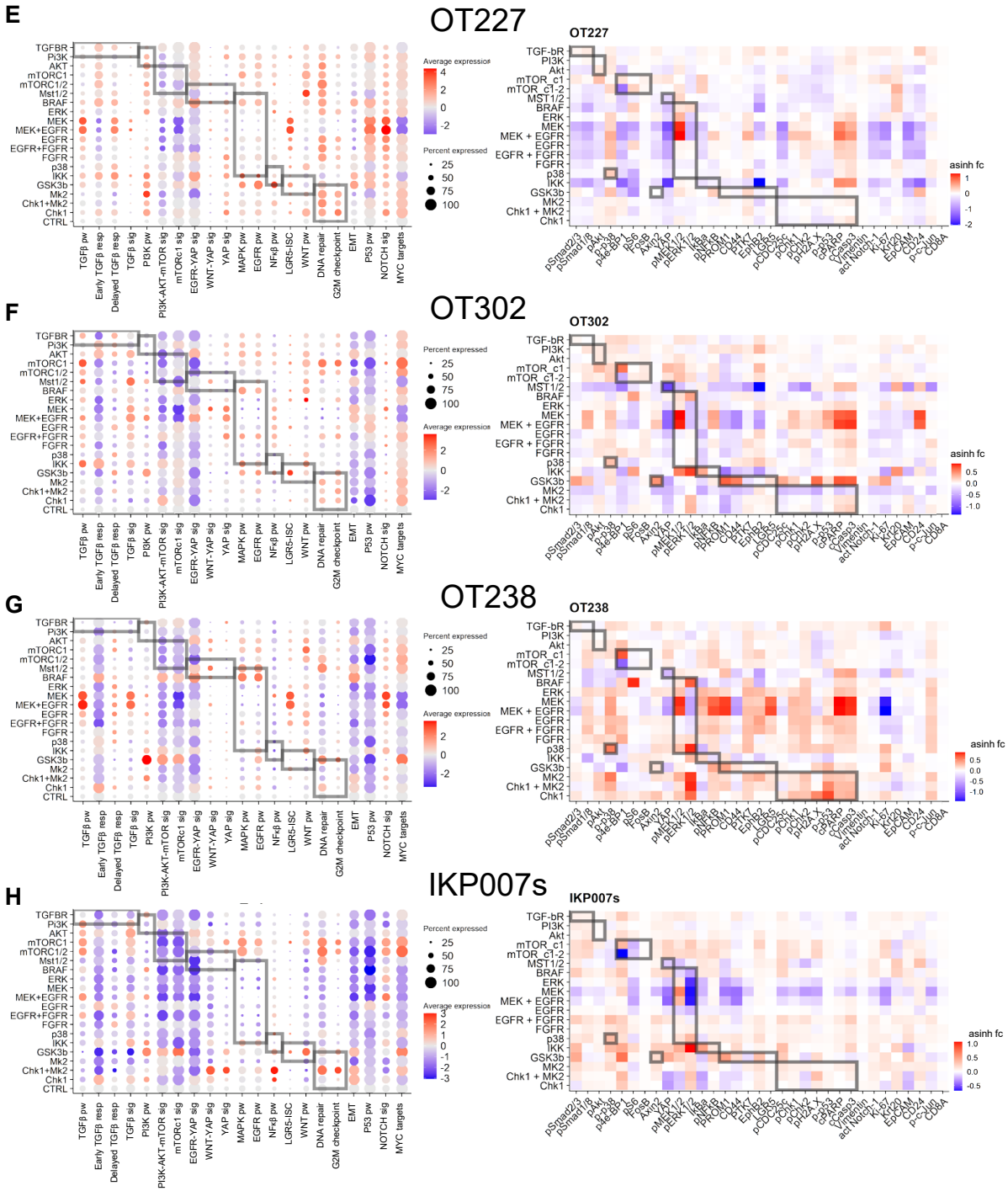

Figure 16: Comparison of perturbation screen results from CyTOF and scRNA seq. On the left side, scRNA seq data was used to produce dotplots showing gene signature expression scores. Plots on the right-hand side show CyTOF readouts (x-axis) for each perturbation (y-axis) as fold change compared to the control treatment. pw = pathway; sig = signaling

3.8 Combinations of inhibitors to reduce cell growth and increase apoptosis

Previously the direct effect of the inhibitors on their downstream targets in their respective or other pathways was investigated. In this chapter, I want to highlight the indirect effect inhibitors had on cells, namely apoptosis, which is a readout for effective therapy. In fig. 17A the CyTOF cCasp3 readout was assembled from eight individual datasets to visually highlight that MEK and MEK + EGFRi upregulated cCasp3 strongest in KRAS^{mut} cells, less in KRAS^{wt} and little to negative in BRAF^{mut} or normal organoid lines. Fig. 17B shows the HALLMARK apoptosis gene signature expression for all eight organoid lines. However, it did not become clear which perturbation affected apoptosis most. Next, I correlated both readouts (fig. 17C) and found that cCasp3 and the apoptosis signature correlate positively in six out of eight organoid lines. Only the normal line P021N and KRAS^{wt} line OT108 showed a negative correlation. This mediocre correlation emphasizes that apoptosis is a process best seen at a protein level since it does not need the involvement of transcriptional regulation.

We saw in fig. 13 that MEK inhibition restricts differentiation space to a small area of the UMAP by selectively depleting cell populations and here in fig. 17A we saw that MEK inhibitor involvement upregulated cCasp3 in most cancer lines. However, even with cell depletion and cCasp3 upregulation, cells were not completely eradicated. Thus, I wanted to explore if any of the other inhibitors in combination with MEK inhibition might result in cell death. This analysis was done *in silico* to investigate which inhibitor combinations had divergent effects on the cell distribution to maximize cell depletion. In figure 18 the idea is outlined: cells occupy specific areas of the UMAP under control conditions. When treated with inhibitors (Drug A or B) cell distributions shifted due to altered gene expression or selective killing of cells. When combining inhibitors that had an opposing effect on cell distribution in the UMAP, we hypothesized that this might increase cell depletion and result in cell death. Therefore, we looked for novel inhibitor combinations *in silico*. A Kullback-Leibler divergence (KLD) analysis was used to find the most contrasting inhibitor combinations. This analysis was done on both CyTOF and scRNA seq data. KLD measures the matching of two distributions (original mathematical publication Kullback and Leibler (1951)). In this case, it was applied to the distribution of cells under different inhibitor treatments. If the distribution of cells in the UMAP under inhibitor A was similar to the distribution under inhibitor B then the KLD value was low (close to 0), because the distributions were matching. However, we were looking for divergent distributions, meaning those inhibitor combinations that produced the highest KLD values (indicated by the orange to white color in fig. 19). Row 1 + 3 were made using scRNA seq data and row 2 + 4 depict CyTOF data. The diagonal line was made up of the lowest KLD values because that was the comparison between the same inhibitor.

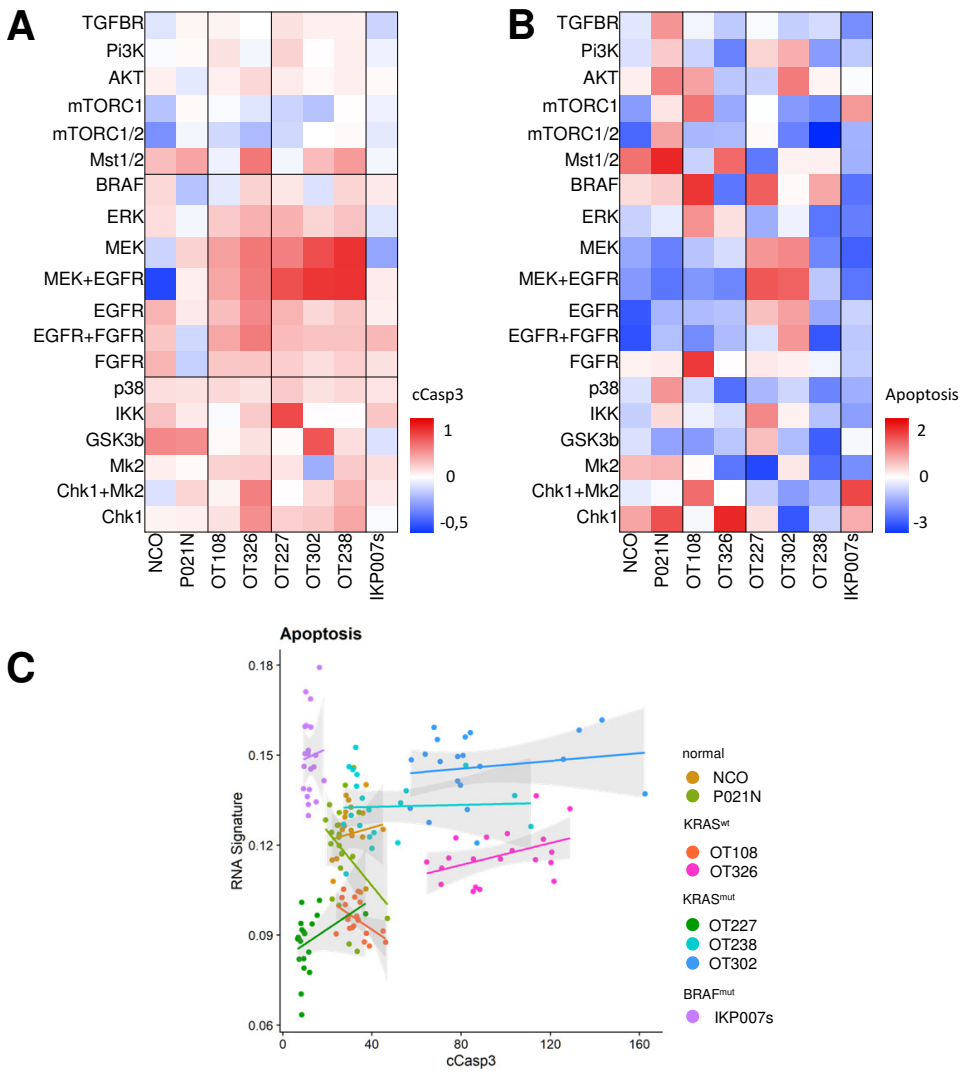

Figure 17: Apoptosis as an indirect effect of inhibitor treatment. **A.** cCasp3 expression from CyTOF data per perturbation for each organoid line. Normalized to control treatment per line. **B.** Expression of apoptosis HALLMARK gene signature comprised of genes mediating programmed cell death by activation of caspases. Cells of all eight organoid lines have been taken together and a bulk analysis was performed. Normalized to control treatment per line. **C.** Correlation plot between CyTOF readout cCasp3 and HALLMARK apoptosis signature expression.

Overall there was a high similarity between CyTOF and scRNA seq data. Six out of eight organoid lines show a clear bright cross pattern. This was made up of combinations with the MEK and MEK + EGFR inhibitors. Since MEKi had such a strong effect on the UMAP distribution, any other distribution compared to that produces a high KLD value. Only the BRAF^{mut} IKP007s and KRAS^{wt} OT326 did not produce this pattern. However, they also had the highest KLD value in inhibitor combinations containing MEK: either in combination with GSK3β and IKK (IKP007s) or with mTORc1/2 and Ch1 + Mk2 (OT326). The normal line NCO showed the highest disparity between CyTOF and scRNA data. In CyTOF only combinations with MEKi + EGFRi produced a high divergence value, whereas

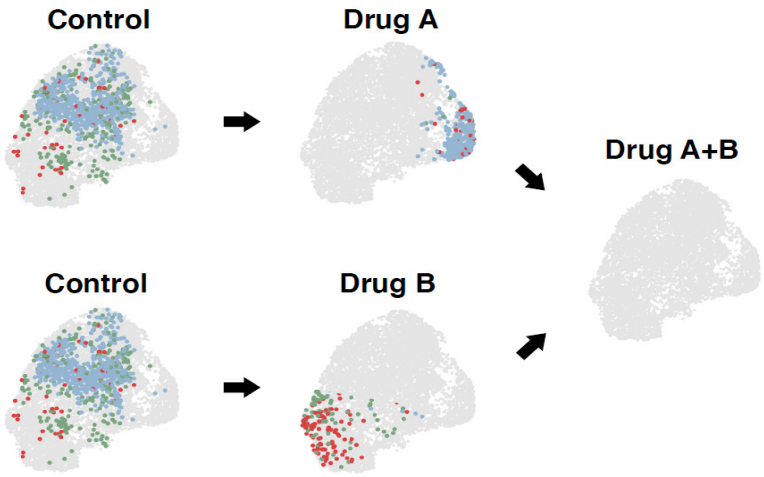

Figure 18: Scheme explaining the idea behind Kullback-Leibler divergence analysis. Finding contrasting/opposing inhibitor combinations which in combination might produce incompatible cell states and increase apoptosis. Image provided by Dr. Florian Uhlitz.

in scRNA data also combinations with only MEKi, EGFRi, EGFRi + FGFRi, and GSK3β indicated high KLD values. The other normal line P021N showed moderate responses to all combinations containing GSK3β, IKK, MEK and MEK + EGFR both in CyTOF and scRNA, whereas in CyTOF there is an additional moderate response to combinations containing MST1/2. The other KRAS^{wt} line OT108 showed in addition to the "MEK-cross" also a high reactivity towards combinations with EGFRi and EGFRi + FGFRi. The KRAS^{mut} lines OT227 and OT302 presented additional dissimilarity in combinations with GSK3β (scRNA seq) and IKK (CyTOF), whereas OT302 also showed a strong reaction to the MST1/2 inhibition.

To clarify which inhibitor combination affected the cell distribution most in CyTOF and scRNA data combined, the values were multiplied. Since low reactivity was indicated by low KLD values, the product of those values was close to 0, indicated by white or light purple color in fig. 19B. The darker the color the higher the value, meaning there were high KLD values in both CyTOF and scRNA seq data sets. Now it was more apparent that combinations with MEKi and MEKi + EGFRi were producing the most divergent UMAP distributions. Additionally some combinations with GSK3β, FGFR, mTORc1, and MST1/2 inhibition also produced strong effects. These combinations which indicated dissimilar UMAPs *in silico* were thought to produce incompatible cell states when tested *in vitro*, which might lead to apoptosis.

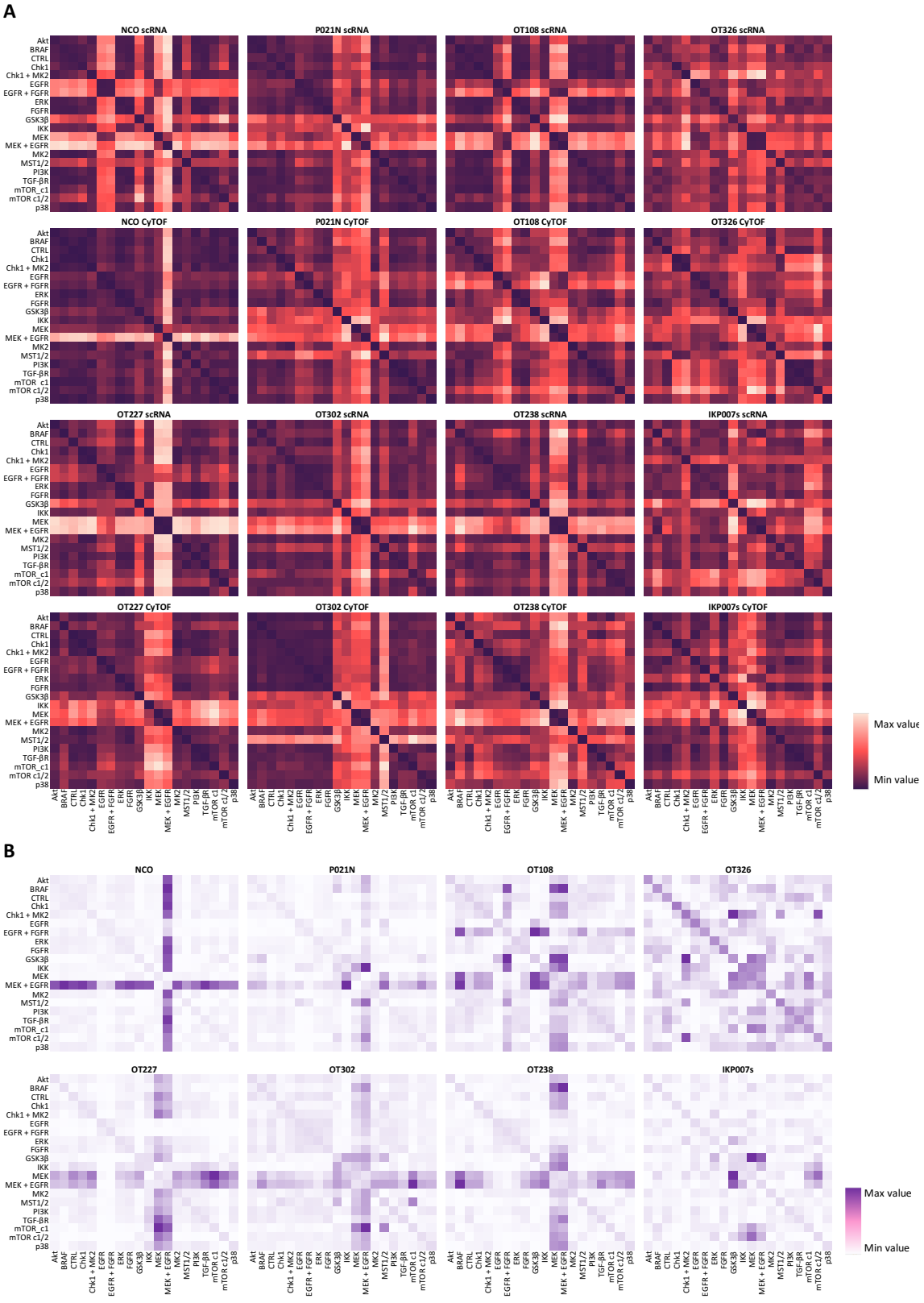

Figure 19: Kullback-Leibler divergence analysis (KLDs) predicting strong effects of inhibitor combinations containing MEKi. **A.** KLD analysis for the eight organoid lines shown for CyTOF and scRNA data individually. The color scale was min-max normalized per analysis with the darkest minimum value of 0 and the maximum value ranging from 0.28 to 0.83. The overall patterns show similarities between data sets. **B.** Product of CyTOF and scRNA seq matrices. The color gradient ranges from white (0) to dark purple (0.6). Analysis performed by Bettina Schmidt.

3.8.1 Testing of inhibitor combinations suggested by *in silico* analysis

In order to test if the *in silico* analysis predicted inhibitor combinations that lead to incompatible cell states and subsequently to apoptosis, I tested eight combinations *in vitro*. For each inhibitor, I tested three concentrations in triplicate, which were the concentrations previously described in table 2, plus 2/3 and 1/3 of that concentration. All eight organoid lines were cultured in 96-well plates and grown for three days before inhibitors were added in a controlled randomized manner using the TECAN pipetting robot. In fig. 20 measurements and pictures of only the maximum concentrations are shown to keep the figure overseeable. Fig. 20A, B, and C depict the metabolic activity of cells normalized to a DMSO-control treatment. The notion was that cells with low metabolic rates were dying or had stopped proliferating, which was indicated by low values (red color). High values (green) pointed towards healthy cells, which were metabolically more active than DMSO-treated control cells. In fig. 20A the values for single inhibition are depicted to have a point of comparison when looking at fig. 20B and C, which show the double inhibition treatments after 72 and 168 hours, respectively, with the upper half of the table showing combinations with MEKi and the lower half with MST1/2i. MEKi alone reduced the metabolic activity of cells drastically in all but the IKP007s line. GSK3β and MST1/2 inhibition alone also had a strong reduction effect in half of the lines. Now compared to the double inhibition treatment, the MEKi-combinations showed a strong metabolic activity reduction already after 72 h, except for IKP007s and two conditions of P021N. After 168h, however, all lines showed a strong reduction of at least 35.5% (IKP007s) to a maximum of 96.6% (OT227).
Combinations with MST1/2i did not affect the metabolic rate of IKP007s. The normal lines were only slightly affected in combinations that did not contain MEKi. $KRAS^{mut}$ lines were affected strongest, especially OT227, which had a residual metabolic rate of 5.3 to 10.1%.
In the same tissue culture plates membrane integrity was measured (fig. 20D). Once a cell membrane has been compromised the dye binds to intracellular DNA, increasing the measurable fluorescent signal. Again, all values were normalized to the DMSO-treated wells. The higher values (red) indicate stronger membrane impairment, indicative of cell death. In fig. 20D values for the double inhibition after 168 h are shown. Values below 1 hinted at fewer dying cells in those conditions compared to DMSO. This was due to the fact that cells under DMSO treatment had grown without inhibition for one week and naturally accumulated dead cells in the lumen of the organoid. When compared to inhibitor-treated wells, in which the organoids grew slower, there was less accumulation of dead or dying cells. The only time membrane impairment measurements were able to indicate an increase in dead cells was when organoids grew under treatment and DMSO at the same rate for some time and at some point the treated organoids cannot cope with

the inhibition any longer, start to break up and die, which can be observed for MST1/2i in three combinations in one KRAS^{wt} and one KRAS^{mut} line. Whenever MEKi was involved the cells did not grow visibly in most organoid lines and therefore did not accumulate dead cells.

For fig. 20E data from metabolic activity assays were used to calculate the Bliss score (Bliss, 1939): Bliss score = normalized value - expected value, where the expected value is the product of measured values for every single inhibition at different concentrations. If the score was 0, it indicated additivity, meaning that the measured effect mirrored the expected effect based on the effect of each drug alone. If the value was greater than 0, the effect was antagonistic, since the expected value was lower than the measured value, meaning the observed effect of the two drugs in combination was lower than expected. In synergy the two inhibitors together elicited a measured effect that was greater in diminishing the metabolic capabilities of the cells than the calculated expected value, leading to a negative outcome (indicated by the blue color). The strongest synergistic effect was observed in one normal colon organoid line in all combinations containing the MST1/2 inhibitor and the MST1/2i + MEKi combination in the BRAF^{mut} line. The KRAS^{mut} lines showed antagonistic results in the MST1/2i combinations and mostly additivity in the MEKi combinations. For the KRAS^{wt} lines MEKi combined with FGFRi, mTORc1i, and AKTi elicited a slight synergistic response, which was abrogated by the combination with GSK3βi.

In fig. 20F light microscopy pictures show the growth of exemplary organoid lines for each inhibitor combination tested. MEKi plus FGFRi showed a synergistic effect in OT326, which was not predicted by the metabolism measurement, where MEKi alone lead to a reduction of metabolic rate similar to the reduction in MEKi + FGFRi treatment (46.5% to 44.2% respectively). Also, the KLD analysis did not predict a synergistic effect in this line for this inhibitor combination. However, the Bliss score indicated a slight synergy between MEKi and FGFRi for this organoid line. The other three combinations with MEKi did not visibly show a strong synergistic effect, rather than just mirroring the effect seen in MEKi alone. In MST1/2i combinations with GSK3βi and MEKi, greater growth retardation can be observed than with MST1/2i alone.

When comparing the *in silico*, *in vitro*, Bliss score, and pictures, the data was mostly in accordance. For example, figure 19B showed a high KLD value in OT108 in the MEKi + GSK3βi combination, and the *in vitro* experiments showed a residual cell metabolic activity of 52.3% for MEKi and 74.0% for GSK3βi. With both inhibitors applied in combination, the residual metabolic rate drops to 44.3% after 168 hours, which would indicate a small synergistic effect, whereas the Bliss score indicated antagonism of the inhibitors, meaning that the effect was lessened by a combination compared to treatment with a single agent. Looking at the pictures of OT108, it seems like the calculated antagonism holds true since organoids seem bigger in MEKi + GSK3βi than in MEKi

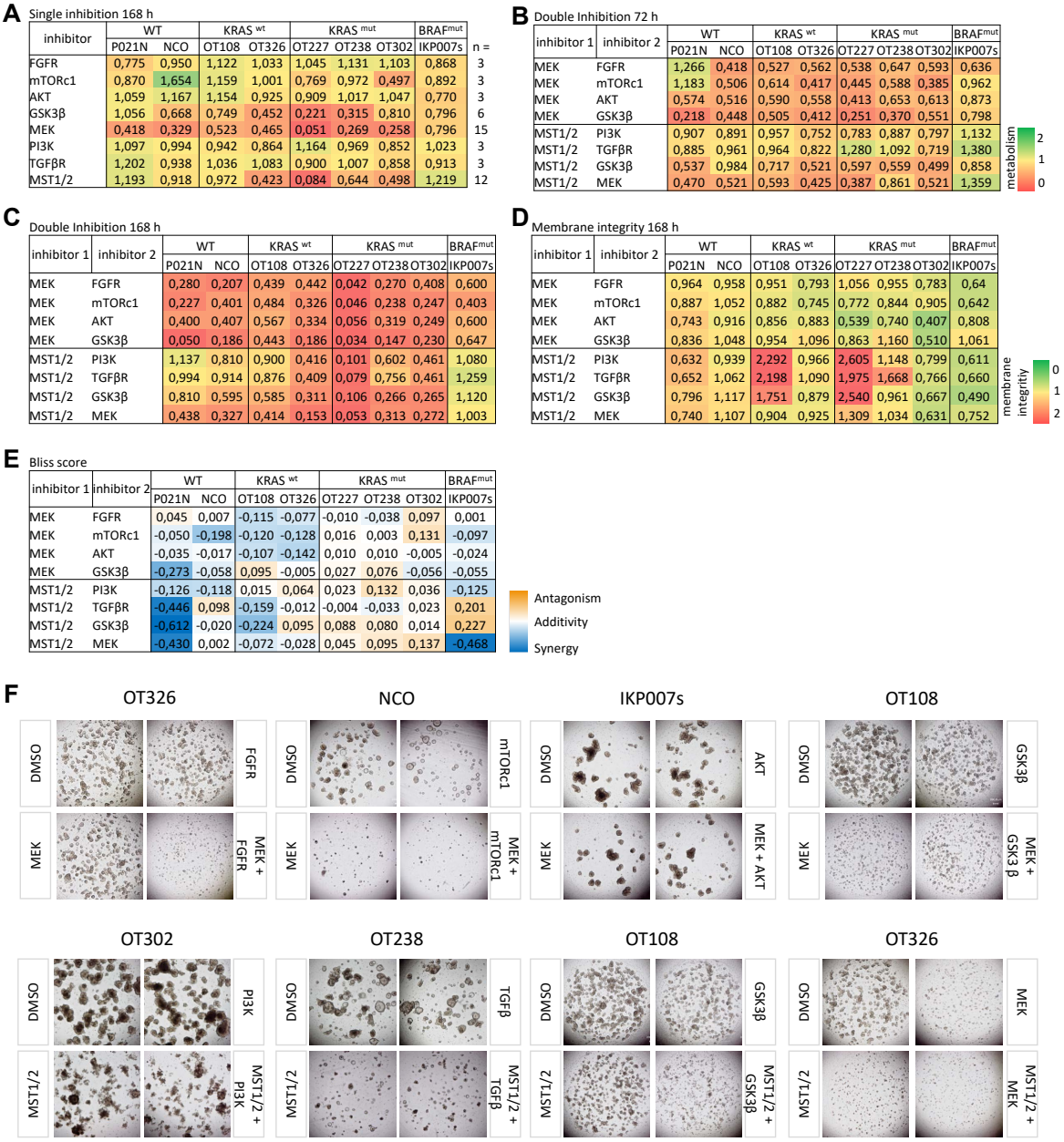

A Single inhibition 168 h

inhibitor	WT		KRAS wt		KRAS mut			BRAF mut	n =
	P021N	NCO	OT108	OT326	OT227	OT238	OT302	IKP007s	
FGFR	0,775	0,950	1,122	1,033	1,045	1,131	1,103	0,868	3
mTORc1	0,870	1,654	1,159	1,001	0,769	0,972	0,497	0,892	3
AKT	1,059	1,167	1,154	0,925	0,909	1,017	1,047	0,770	3
GSK3β	1,056	0,668	0,749	0,452	0,221	0,315	0,810	0,796	6
MEK	0,418	0,329	0,523	0,465	0,051	0,269	0,258	0,796	15
PI3K	1,097	0,994	0,942	0,864	1,164	0,969	0,852	1,023	3
TGFβR	1,202	0,938	1,036	1,083	0,900	1,007	0,858	0,913	3
MST1/2	1,193	0,918	0,972	0,423	0,084	0,644	0,498	1,219	12

B Double Inhibition 72 h

inhibitor 1	inhibitor 2	WT		KRAS wt		KRAS mut			BRAF mut
		P021N	NCO	OT108	OT326	OT227	OT238	OT302	IKP007s
MEK	FGFR	1,266	0,418	0,527	0,562	0,538	0,647	0,593	0,636
MEK	mTORc1	1,183	0,506	0,614	0,417	0,445	0,588	0,385	0,962
MEK	AKT	0,574	0,516	0,590	0,558	0,413	0,653	0,613	0,873
MEK	GSK3β	0,218	0,448	0,505	0,412	0,251	0,370	0,551	0,798
MST1/2	PI3K	0,907	0,891	0,957	0,752	0,783	0,887	0,797	1,132
MST1/2	TGFβR	0,885	0,961	0,964	0,822	1,280	1,092	0,719	1,380
MST1/2	GSK3β	0,537	0,984	0,717	0,521	0,597	0,559	0,499	0,858
MST1/2	MEK	0,470	0,521	0,593	0,425	0,387	0,861	0,521	1,359

metabolism 2 1 0

C Double Inhibition 168 h

inhibitor 1	inhibitor 2	WT		KRAS wt		KRAS mut			BRAF mut
		P021N	NCO	OT108	OT326	OT227	OT238	OT302	IKP007s
MEK	FGFR	0,280	0,207	0,439	0,442	0,042	0,270	0,408	0,600
MEK	mTORc1	0,227	0,401	0,484	0,326	0,046	0,238	0,247	0,403
MEK	AKT	0,400	0,407	0,567	0,334	0,056	0,319	0,249	0,600
MEK	GSK3β	0,050	0,186	0,443	0,186	0,034	0,147	0,230	0,647
MST1/2	PI3K	1,137	0,810	0,900	0,416	0,101	0,602	0,461	1,080
MST1/2	TGFβR	0,994	0,914	0,876	0,409	0,079	0,756	0,461	1,259
MST1/2	GSK3β	0,810	0,595	0,585	0,311	0,106	0,266	0,265	1,120
MST1/2	MEK	0,438	0,327	0,414	0,153	0,053	0,313	0,272	1,003

D Membrane integrity 168 h

inhibitor 1	inhibitor 2	WT		KRAS wt		KRAS mut			BRAF mut
		P021N	NCO	OT108	OT326	OT227	OT238	OT302	IKP007s
MEK	FGFR	0,964	0,958	0,951	0,793	1,056	0,955	0,783	0,64
MEK	mTORc1	0,887	1,052	0,882	0,745	0,772	0,844	0,905	0,642
MEK	AKT	0,743	0,916	0,856	0,883	0,539	0,740	0,407	0,808
MEK	GSK3β	0,836	1,048	0,954	1,096	0,863	1,160	0,510	1,061
MST1/2	PI3K	0,632	0,939	2,292	0,966	2,605	1,148	0,799	0,611
MST1/2	TGFβR	0,652	1,062	2,198	1,090	1,975	1,668	0,766	0,660
MST1/2	GSK3β	0,796	1,117	1,751	0,879	2,540	0,961	0,667	0,490
MST1/2	MEK	0,740	1,107	0,904	0,925	1,309	1,034	0,631	0,752

membrane integrity 0 1 2

E Bliss score

inhibitor 1	inhibitor 2	WT		KRAS wt		KRAS mut			BRAF mut
		P021N	NCO	OT108	OT326	OT227	OT238	OT302	IKP007s
MEK	FGFR	0,045	0,007	-0,115	-0,077	-0,010	-0,038	0,097	0,001
MEK	mTORc1	-0,050	-0,198	-0,120	-0,128	0,016	0,003	0,131	-0,097
MEK	AKT	-0,035	-0,017	-0,107	-0,142	0,010	0,010	-0,005	-0,024
MEK	GSK3β	-0,273	-0,058	0,095	-0,005	0,027	0,076	-0,056	-0,055
MST1/2	PI3K	-0,126	-0,118	0,015	0,064	0,023	0,132	0,036	-0,125
MST1/2	TGFβR	-0,446	0,098	-0,159	-0,012	-0,004	-0,033	0,023	0,201
MST1/2	GSK3β	-0,612	-0,020	-0,224	0,095	0,088	0,080	0,014	0,227
MST1/2	MEK	-0,430	0,002	-0,072	-0,028	0,045	0,095	0,137	-0,468

Antagonism
Additivity
Synergy

F OT326 NCO IKP007s OT108 OT302 OT238 OT108 OT326

DMSO FGFR MEK MEK + FGFR
DMSO mTORc1 MEK MEK + mTORc1
DMSO AKT MEK MEK + AKT
DMSO GSK3β MEK MEK + GSK3 β
DMSO PI3K MST1/2 MST1/2 + PI3K
DMSO TGFβ MST1/2 MST1/2 + TGFβ
DMSO GSK3β MST1/2 MST1/2 + GSK3β
DMSO MEK MST1/2 MST1/2 + MEK

Figure 20: Synergy testing of eight inhibitor combinations showing growth reduction driven by MEK inhibition alone **A.** Metabolic activity of organoids after one week (168 h) under indicated inhibition. Measured with RealTime Glo (Promega). **B.** Metabolic activity of double inhibition after 72 h. **C.** Metabolic activity of double drug treatment after 168 h. **D.** Membrane integrity was measured by CellTox Green (Promega) in the same wells treated with inhibitor combinations for 168 h. **E.** Bliss score to calculate if the inhibitor combinations had a synergistic (blue) or antagonistic (orange) effect. Calculations based on data obtained after 168 h inhibition. **F.** Light microscopy pictures of the highest single and double inhibitor concentrations. Top row combinations with MEKi and bottom row with MST1/2 inhibitor.

alone.

Some organoid lines display a disconnect between the metabolic measurements and the pictures, which most likely stems from the RealTime Glo agent used to measure metabolic

activity. If cells were active, then the reagent was used up more quickly, which happened faster in the control wells. Thus, the medium with reagents and inhibitors had to be renewed every two to three days.
Overall these experiments confirmed the expected outcome of decreased cell metabolism and growth when treated with the MEK inhibitor, however, the results did not show consistent synergistic effects with other inhibitors, meaning that most of the reduction of metabolism stemmed from the MEK inhibition alone.

3.9 CRC differentiation follows MAPK drive

Previously, I have shown that MEK inhibition affected cell differentiation and proliferative capacity. Since MAPK signaling has important clinical relevance I widened the inhibitor testing to not only MEK but additional MAPK pathway inhibition to see which MAPK inhibition deregulated cellular differentiation most. Additionally, other organoid lines were used which were established in the scope of Uhlitz et al. (2021): two organoid lines each with either KRAS^{mut}, RAS/RAF^{wt} or BRAF^{mut}, which were treated with DMSO, BRAFi, EGFRi, EGFRi + BRAFi, EGFRi + MEKi or MEKi (fig. 21A). scRNA seq revealed that MAPK-targeted therapy-induced transcriptomic changes led to distinct UMAP distributions. Transcriptomes of DMSO-treated control cells (gray in UMAP) did not overlap with MEKi or MEKi + EGFRi treated cells (blue or purple, respectively) in KRAS^{mut} lines. In RAS/RAF^{wt} lines transcriptomes of DMSO-treated cells formed a distinct cluster compared to EGFRi, EGFRi + BRAFi or EGFRi + MEKi treated cells (red, orange, purple, respectively). Albeit more intermingled, the BRAF^{mut} lines showed less overlap between DMSO and EGFRi + MEKi (purple). These treatments which produced the highest plastic change in UMAP cell allocation were further analyzed in cell viability assays. Fig. 21B shows growth retardation in inhibitor-treated organoids, in accordance with a gradual reduction in metabolic activity (right panels of fig. 21B).
Next, I focused on P013T since the EGFRi treatment produced a very pronounced reaction which lead to cluster separation (gray vs. red in fig. 21A). It is noteworthy that this response to EGFR inhibition could be therapeutically meaningful, as the P013T line is RAS/RAF^{wt} and thus EGFR inhibition is the first-line therapy for such cancers, at least when progressed. To investigate if the EGFRi-treated cells were actually dying or entering a senescent-like cell state (c.f. pictures in 21B), a scSLAM seq experiment was performed to visualize cellular differentiation trajectories (fig. 21C). SLAM seq enables time-resolved measurements of newly synthesized RNA by incorporation of 4sU into nascent RNA, which leads to the incorporation of a G instead of an A during reverse transcription, leading to a T to C substitution in the final library. This information can be used to distinguish existing from newly formed RNA (Herzog et al., 2017), which reveals a transcriptomic differentiation trajectory.

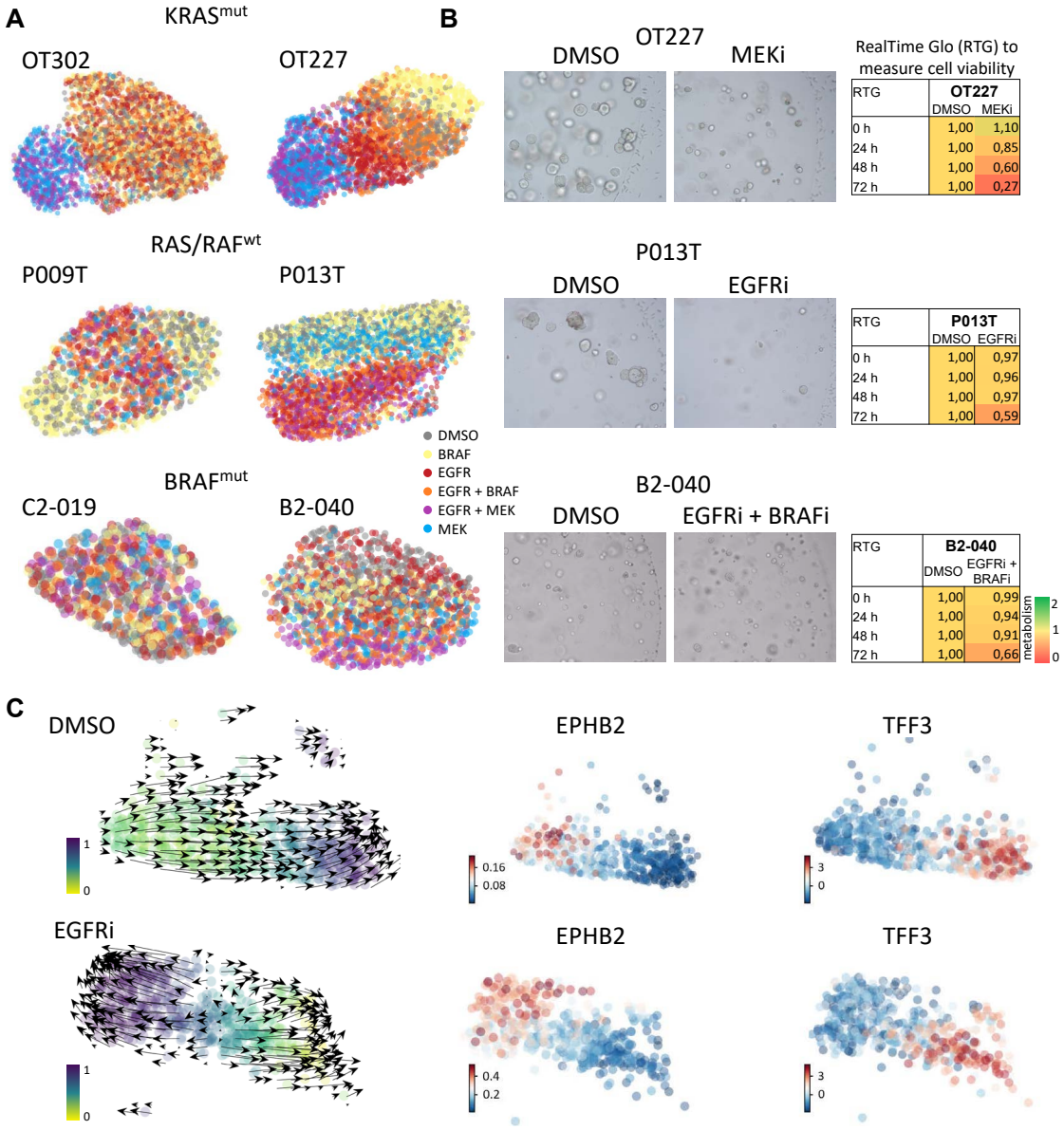

Figure 21: MAPK inhibition induces cellular plasticity **A.** Six organoid lines treated with three MAPK inhibitors and their combinations. UMAPs show color-coded cell distribution for each perturbation. **B.** Pictures of control cells and one selected treatment after 72 hours and accompanying measurements of cell metabolic activity (RealTime Glo). **C.** P013T SLAM seq trajectories after 48 hours of inhibition for DMSO and EGFRi treatment.

In this case, two hours prior to harvesting, P013T organoids were treated with 4SU for subsequent SLAM seq data analysis. In fig. 21C the DMSO treatment produced a clear trajectory of all cells moving from one corner of the UMAP, high in EPHB2 expression, into one direction, which was dominated by secretory lineage marker TFF3 expression, meaning cells follow the typical gradient from stem-cell like to differentiated cells. In the EGFRi-treated condition, the trajectory split into two developmental endpoints. One was defined by TFF3 expression in differentiated cells, but other cells were reverting into more stem-like cells, high in EPHB2 expression, meaning that EGFRi induced plasticity overriding the normal developmental trajectory and producing a new cell population,

which might form a therapy-resistant cell population.

3.9.1 Epigenetic reprogramming to induce differentiation

After seeing that MAPK inhibition induced plasticity, which had overridden normal developmental trajectories, Iwanted to test if Ican induce differentiation in the stem-like cell population to prohibit the outgrowth of that cell population and prevent therapy resistance. Therefore, I combined MAPK inhibition with two different inhibitors of epigenetic regulator MLL1, which is naturally expressed in cells with high Wnt activity and lost upon differentiation (Grinat et al., 2020). The upper panel of fig. 22A shows metabolic activity after two days of treating the six organoid lines, described in the previous chapter. KRAS^{mut} organoid lines were more sensitive to MLL1 inhibition, specifically more sensitive to MI-503 as compared to MI-2 inhibition (upper half vs. lower half of that panel). After 96 hours this trend was more pronounced, with both MLL1 inhibitors reducing metabolic activity in both KRAS^{mut} lines drastically. It is of note that the BRAF^{mut} line C2-019 has an additional rare KRAS mutation at M189L, which is considered "likely benign" according to the Human Variome Project. This may be the reason for the sensitivity of these three lines to either MLL1 inhibition alone and to their combination with MAPK inhibition. However, one KRAS^{wt} line (P009T) also shows a reduction in metabolic rate upon MLL1 inhibition. The remaining KRAS^{wt} and BRAF^{mut} line (P013T and B2-040) showed little effect to MLL1 inhibition alone, but the reduction of metabolic activity largely stemmed from the MAPK inhibition.

Accompanying measurements of cell membrane integrity (fig. 22B) showed little apoptosis onset after 48 h of inhibitor treatments. Only P009T showed an increase in apoptosis when combining MLL1 inhibition with BRAFi + EGFRi. After 96 hours the other KRAS^{wt} line increased the onset of apoptosis in the combination treatment. Most striking was that MI-2 alone had increased apoptosis in all lines, but B2-040. MAPK inhibition had a mild effect and reduced the severity of MI-2 in the combination (antagonism). In panel C of fig. 22 microscopy pictures show that MI-503 alone did not prohibit growth or induce apoptosis. However, organoid size and color in MI-2i pictures of P013T and OT227 after 96 h indicated that organoids were first growing and then dying, substantiating measurements in fig. 22B.

Overall the MI-2 inhibitor takes longer to act, however, when it elicited a cellular response, it was coupled to a loss of membrane integrity and therefore lead to apoptosis of cells in all, but B2-040. The addition of MAPK inhibition antagonized this effect.

A

Inhibition 48 h

inhibitor	KRAS wt		KRAS mut		BRAF mut	
	P013T	P009T	OT227	OT302	B2-040	C2-019
DMSO	1,00	1,00	1,00	1,00	1,00	1,00
MI-503 (3 µM)	0,98	0,88	0,64	0,87	0,92	0,37
MAPK	0,73	0,89	0,77	0,77	0,69	0,88
combination	0,84	0,78	0,42	0,56	0,75	0,37
DMSO	1,00	1,00	1,00	1,00	1,00	1,00
MI-2 (1,5 µM)	0,91	0,90	0,99	0,82	0,98	0,70
MAPK	0,92	0,83	0,93	0,70	0,91	0,81
combination	0,88	0,75	0,85	0,61	0,90	0,68
	BRAFi + EGFRi (0,1 µM)		EGFRi (0,1 µM)		MEKi (8 µM)	

Inhibition 96 h

inhibitor	KRAS wt		KRAS mut		BRAF mut	
	P013T	P009T	OT227	OT302	B2-040	C2-019
DMSO	1,00	1,00	1,00	1,00	1,00	1,00
MI-503 (3 µM)	0,99	0,78	0,33	0,67	0,91	0,27
MAPK	0,54	0,99	0,17	0,37	0,59	0,95
combination	0,53	0,70	0,07	0,21	0,53	0,40
DMSO	1,00	1,00	1,00	1,00	1,00	1,00
MI-2 (1,5 µM)	0,97	0,69	0,16	0,24	1,07	0,14
MAPK	0,69	0,89	0,22	0,40	0,77	0,82
combination	0,57	0,62	0,18	0,29	0,68	0,43
	BRAFi + EGFRi (0,1 µM)		EGFRi (0,1 µM)		MEKi (8 µM)	

metabolism 2 1 0

B

Inhibition 48 h

inhibitor	KRAS wt		KRAS mut		BRAF mut	
	P013T	P009T	OT227	OT302	B2-040	C2-019
DMSO	1,00	1,00	1,00	1,00	1,00	1,00
MI-503 (3 µM)	1,06	1,10	1,04	1,05	1,01	1,11
MAPK	1,06	1,04	1,02	1,18	1,00	1,04
combination	1,10	1,23	1,11	1,18	1,01	1,08
DMSO	1,00	1,00	1,00	1,00	1,00	1,00
MI-2 (1,5 µM)	1,07	1,21	1,14	1,10	1,01	1,20
MAPK	1,04	1,05	1,02	1,02	1,00	1,01
combination	1,10	1,29	1,01	1,03	1,02	1,07
	BRAFi + EGFRi (0,1 µM)		EGFRi (0,1 µM)		MEKi (8 µM)	

Inhibition 96 h

inhibitor	KRAS wt		KRAS mut		BRAF mut	
	P013T	P009T	OT227	OT302	B2-040	C2-019
DMSO	1,00	1,00	1,00	1,00	1,00	1,00
MI-503 (3 µM)	1,06	1,06	1,05	1,03	1,00	1,31
MAPK	1,03	1,07	1,01	1,07	1,02	1,00
combination	1,30	1,57	1,24	1,11	1,01	1,13
DMSO	1,00	1,00	1,00	1,00	1,00	1,00
MI-2 (1,5 µM)	1,97	3,20	2,62	2,01	1,00	2,80
MAPK	1,03	1,27	1,04	1,16	1,04	1,14
combination	1,17	1,81	1,10	1,24	1,04	2,04
	BRAFi + EGFRi (0,1 µM)		EGFRi (0,1 µM)		MEKi (8 µM)	

membrane integritiy 0 1 2

C

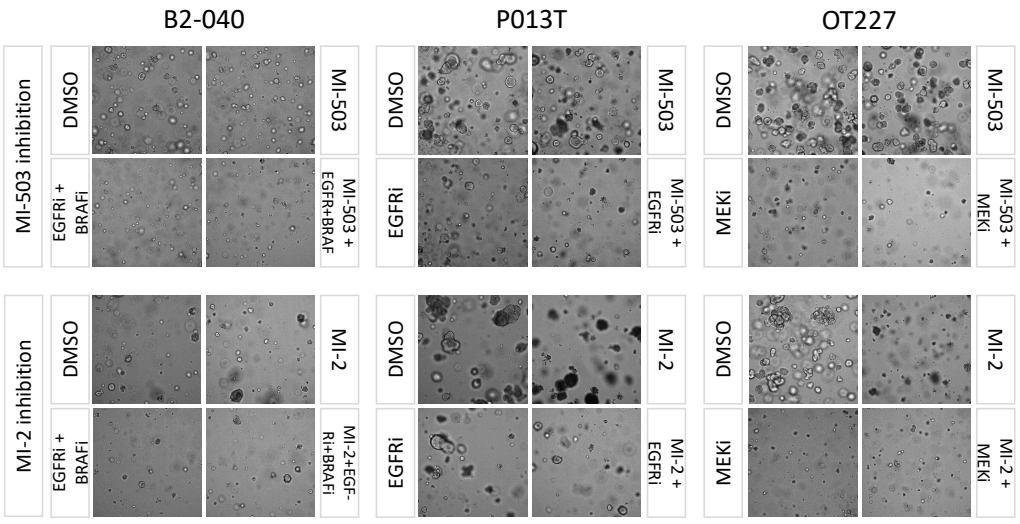

Figure 22: MLL inhibition affects organoid lines with KRAS^{mut} **A.** Metabolic activity of organoids after 48 and 96 hours under indicated inhibition (RealTime Glo, Promega). The red color indicates decreased metabolic activity normalized to DMSO. **B.** Membrane integrity of cells after 48 and 96 h (CellTox Green, Promega), displayed as the difference to 0h time point measurement. Increased values indicate loss of membrane integrity (red infill in table). **C.** Pictures were taken after 96 hours of inhibition.

3.9.2 Cells recovered after EGFRi removal

The fact that EGFRi produced a new developmental trajectory towards dedifferentiation as shown in fig. 21C prompted the question if these stem-like cells would be able to grow out again during treatment or only if the treatment was stopped. Therefore, I performed a scRNA seq time course experiment, treating P013T organoids for six days either with DMSO or EGFRi, then removing EGFRi from the organoids and taking three additional samples (fig. 23).
When treating P013T organoids with DMSO they grew as expected which was corroborated by the rising number of single cells per well (red line in fig. 23A). However, when treated with EGFRi cells stopped proliferating as indicated by the stagnating number of cells per well in subsequent days (blue line in fig. 23A). After six days of treatment the inhibitor was washed out of the remaining wells, organoids recovered their growth potential and were able to proliferate again as seen by the rising number of cells per well from 24 to 96 hours after inhibitor removal (green line). In fig. 23C light microscopy pictures depict organoid growth after 96 and 144 h, showing the stalled growth under EGFRi. However, the blue arrows point to a phenotypic switch, showing a spheroidal growth of a limited number of cells that were able to grow under inhibitor treatment. These spheroids seem to be therapy resistant and most likely the pool of cells, which quickly grew after inhibitor removal.
scRNA seq data of the three conditions was used to generate a cell phase composition plot of the combined time points per treatment (fig. 23B). It demonstrated that EGFRi lead to a cell arrest in G1, but after removal of inhibition, the cell cycle composition reverted back to a DMSO-like distribution. Looking more closely at the distribution of transcriptomes per cell in a UMAP, which was color coded for the time points of each condition (fig. 23D), depicted a clear overlap between the 24 h DMSO and 240 h EGFRi to DMSO time point (light red and dark green, respectively). Following the treatment and time points from DMSO, EGFRi to removal, there was a circular development visible, with only the EGFRi-treated cells forming a separate cluster, whereas the other two conditions intermingled. It becomes evident that cells that were treated with EGFRi and then the inhibitor was removed (three shades of green color), were moving towards the DMSO-treatment area of the UMAP (orange-red color). These developmental trajectories confirmed the recuperation of cells after EGFRi treatment suspension.
Overall anti-MAPK therapy-induced changes in developmental trajectories could cause the formation of therapy-resistance stem-like cell populations, which do not proliferate under inhibitor treatment. However, if treatment was suspended these resistant cell populations were able to grow quickly, recover the full spectrum of cell cycle distribution, and approximate DMSO-like transcriptomes.

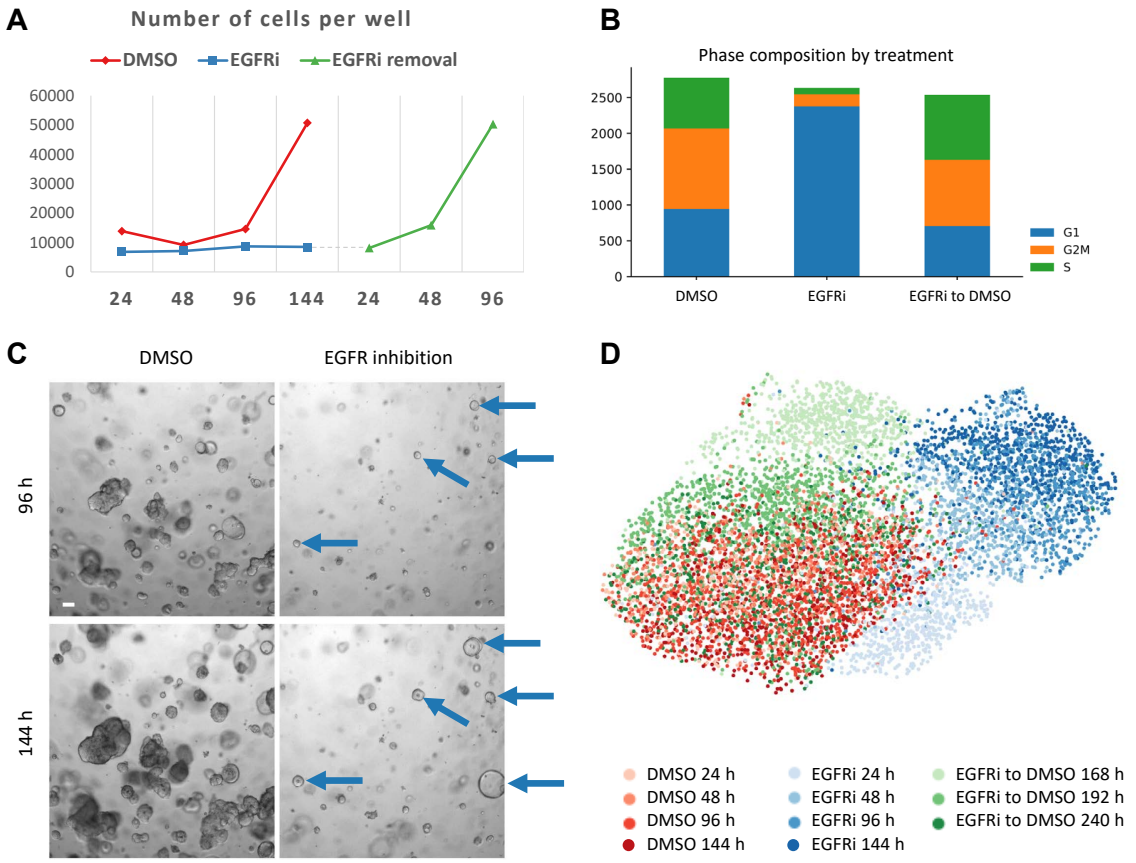

Figure 23: Organoids recover after EGFRi removal **A.** Cell number per well harvested for scRNA seq time course experiment of P013T. **B.** Cell cycle distribution of the combined time points of each treatment group, showing cell arrest in G1 under EGFRi. **C.** Light microscopy pictures of DMSO control and EGFRi treated P013T organoids at indicated time points revealing EGFRi resistant subpopulation. Scale bar 100 µm. **D.** Cell distribution color-coded for time points per treatment showing the overlap between DMSO and EGFRi to DMSO treatment.

4 Discussion

Cell heterogeneity hampers curative treatment of cancers such as colorectal cancer by driving acquired resistance and thus, is a major issue for diagnosis, prognostic prediction, and therapeutic response (Lim and Ma, 2019). Not only genetic cellular heterogeneity affects treatment and outcome (Misale et al., 2012), but also non-genetic mechanisms have been described, such as microenvironmental cues like reactive oxygen species (Woolston et al., 2019; Oren et al., 2021). Additionally, the differentiation state of cells influences metastasis and therapy resistance (Fumagalli et al., 2020).
One of the approaches to investigate cell heterogeneity is using patient-derived CRC organoids since they recapitulate the structure and function of the primary tissue (Corrò et al., 2020). Using organoids enabled me to investigate the response of cells to perturbations and study non-genetic mechanisms, such as the interactions between oncogenic drivers, cell differentiation, signal transduction, and cell plasticity at single-cell resolution. Here, I provided experiments and analyses of a perturbation screen to assess the signaling network on transcriptional and protein levels. I confirmed that patient-derived organoid lines with different mutational patterns consist of heterogeneous cell types. Subsequently, I found that cellular hierarchies correlate with MAPK pathway activation, both can be altered by perturbations. Inhibitors also affect cell distribution in UMAPs and cell cycle allocation. However, no inhibitor alone lead to the eradication of cancer lines, thus combinations and epigenetic reprogramming were tested to maximize apoptosis. Additionally, I found that EGFR inhibition alters the differentiation trajectory of some cells, leading to a therapy-resistant stem-cell-like phenotype. Those cells are able to resume growth after EGFRi removal.

4.1 Organoids are heterogeneous

An organoid is a stem cell-driven 3D cell culture that can reconstitute the different tissue-specific cell types from a stem cell (Sato et al., 2009). Originally, Sato and coworkers cultured intestinal epithelial stem cells and defined conditions under which stem cells grew into different cell types, such as absorptive enterocytes and secretory cells, including Paneth cells and goblet cells. Later the culture conditions were improved to also allow for a broader spectrum of differentiated cells (Fujii et al., 2018). They also found out that malignant tissue, such as colon cancer or metaplastic Barrett's esophagus tissue could be cultured in the form of organoids (Sato et al., 2011a). Normal tissue has well-defined cell type markers, however, in the case of cancer tissue, this is not the case. My thesis aimed at contributing to the question of intra-cancer organoid cell heterogeneity. To confirm that organoids are heterogeneous and suitable for further investigation, I performed an immunohistochemistry experiment, staining cell type and signaling markers (fig. 2),

which showed differential expression between organoid lines but also within organoids. Performing similar experiments on a single-cell basis, using CyTOF to assess proteins and scRNA seq to assess transcriptomes, allowed for marker quantification while still showing heterogeneity between and within organoid lines (fig. 3 + fig. 7). Within organoids of different lines, I detected heterogeneity of known differentiation markers, such as KRT20, and apoptosis markers such as cCasp3. Furthermore, I found broad gradients of EPHB2, which is a graded marker for differentiation in the normal intestine and also marks a subpopulation of CRC cells in patients (Merlos-Suárez et al., 2011; Batlle et al., 2002). My findings, therefore, suggest that organoid cultures contain heterogeneous types of cancer cells.

Additionally, I found that cell heterogeneity extended to signaling molecules. To arrive at this conclusion, I ordered cells according to their EPHB2 expression, since EPHB2 is a graded stem cell marker, expressed highest in stem cells and decreasing intensity with differentiation. Inspecting marker expression along this gradient reveals heterogeneity of signaling activity, such as ERK and MEK phosphorylation. Part of this thesis was published in Uhlitz et al. (2021) where we showed that this MEK and ERK gradient drives cell development in colon cancer organoids. Thus, graded heterogeneity of the signaling network is intrinsically linked to the differentiation state that we can read out in the form of marker expression, e.g. KRT20 and cCasp3.

Organoids are not only heterogeneous in the cell types they contain, but they are also heterogeneous due to their origin. The former level of heterogeneity is termed intra-organoid heterogeneity, whereas the latter is commonly termed inter-patient or inter-organoid line heterogeneity. I found heterogeneity between organoid lines of different patient origins on protein and RNA levels (fig. 7 and fig. 10D). Marker expression strength differed between organoid lines, such as KRT20 and cCasp3 expression. Also at the level of MARK signaling different activity strengths can be observed. Using CyTOF I found that the different lines had different levels of signaling molecule phosphorylation, in the case of MAPK signaling, phosphorylation of MEK and ERK. The same pathway activities could also be observed using sets of pathway-specific target genes. In the case of MAPK signaling, protein phosphorylation, and pathway activity correlated positively, because the phosphorylation is direct e.g. from MEK to ERK, and then ERK activated transcription (Zheng and Guan, 1993; Zhao et al., 2003). However, in other pathways, this might not be the case, since signal transduction might be more indirectly linked to transcription.

Looking at inter-line heterogeneity on a transcriptome level in a UMAP, organoid lines were divided according to their expected path of origin, i.e. whether they were normal tissue, or likely arose via the conventional adenoma-carcinoma or the serrated pathway (fig. 10D). It is likely that the differences in protein markers and transcriptomes between the lines stem from genetic mutations in the tumors and probably also epigenetic differences that were carried over from their cell of origin or selected during tumor progression. How-

ever, while the UMAP clustered normal and BRAF^{mut} organoid cells separately, KRAS^{wt} and KRAS^{mut} lines intermingled. Also on protein level, no unambiguous marker for KRAS^{mut} cancers was observed. This is in line with previous findings, that not even a KRAS mutation reliably activates MARK pathway (Schumacher et al., 2019). However, broad assumptions cannot be made, since I only had a limited number of organoid lines, e.g. only one line with a BRAF^{mut}.
This poses the question of whether the transcriptome could be used as a classifier for meaningful subdivision of CRCs with a clinical or translational impact. Previously other groups have developed classifiers to group colorectal cancers not only according to their genetic differences but also other differences, such as microsatellite stability status, immune infiltration, or transcriptome features conforming consensus subtypes (Guinney et al., 2015). Recently, this classification system was updated based on single-cell findings (Joanito et al., 2022), grouping colorectal cancers into either iCMS2 or iCMS3 epithelial subtypes. Work performed on my organoid lines showed that the BRAF^{mut} line belongs to iCMS3 and the KRAS$^{mut/wt}$ lines belong to the iCMS2 subtypes (data not shown). This means that the separate clusters for the BRAF^{mut} and shared cluster for the KRAS$^{mut/wt}$ organoid lines also mirror the iCMS3 versus iCMS2 division. This classification system highlights that there are more organizing features in CRC than mutational patterns. Overall, I showed that organoids are heterogeneous within and between lines on protein and transcriptome levels.

4.2 Inhibition of MAPK activity limits heterogeneity

MAPK is a frequently aberrated pathway in CRC, with clinical relevance as it is also a therapy target. 40% of the patient's tumors have KRAS mutations, approx. 10% contain activated BRAF mutations, and smaller groups contain activating NRAS or inactivating NF-1 mutations (Morkel et al., 2015). These mutations are predictive for therapy (Karapetis et al., 2008; Pietrantonio et al., 2015). First-line treatment of metastatic CRC is EGFR-targeted antibodies like Cetuximab or Panitumumab, in case the tumor is RAS/RAF^{wt}. Patients with BRAF^{mut} cancers can profit from EGFR/BRAF inhibitor combination therapy. However, no targeted treatment has been shown to improve the course of disease for patients with KRAS^{mut} cancers.
I found that CRC organoids are composed of a range of cells, from stem-like to differentiated (fig. 7). When cells were sorted according to their EPHB2 expression, I also saw a gradient in MAPK signaling activity following the same gradient (pERK and pMEK in fig. 7). The observed heterogeneity of cells within an organoid line leads to the question of whether all cell states are similarly sensitive to clinical MAPK inhibition. Furthermore, I asked the question of whether interference with MAPK signaling, as it is used clinically, changes the differentiation states of cells. This could conceivably result in resistant cell

populations. To answer these questions, I treated eight organoid lines with targeted inhibition to investigate differential responses to the treatments. Regarding the question of sensitivity to MAPK inhibition, I found that the KRAS^{mut} lines were most sensitive to MEK inhibition, whereas the BRAF^{mut} line was most resistant to MEK inhibition. This might be due to transcriptomic differences, which were shown in the clustering where BRAF^{mut} and KRAS$^{wt/mut}$ cells formed separate clusters. In the clinic mutational patterns are relevant. According to my limited data, only parts of these mutational patterns reflect the grouping of cells in the UMAP as KRAS^{mut} and KRAS^{wt} lines overlapped in UMAP space. This means that the transcriptome might not be an adequate readout for clinical use since it did not differentiate between KRA^{mut} and KRAS^{wt}.
In regard to the question of whether MAPK could change differentiation states, I found plastic change of differentiation states under inhibitor treatment (fig. 8). In general inhibitor addition induced or inhibited differentiation and notably, MEKi and other inhibitors and combinations targeting the MAPK pathway were able to restrict the differentiation spread of cells (fig. 8). As a striking example, single-cell transcriptomes of the KRAS^{mut} line OT227 inhabited only a small area of the original UMAP space after MEK or combined MEK + EGFR inhibition (fig. 12). This indicates that the heterogeneity of cells is reduced after MAPK inhibition.
All the above-mentioned results, MAPK follows the EPHB2 differentiation gradient, sensitivity to MEKi differs according to the mutational pattern and MAPKi restricts the differentiation space, highlight the importance of the MAPK pathway. Thus, I have focused on MAPK signaling and inhibition in subsequent experiments, since MAPK inhibition is able to reduce differences in differentiation states, making cells more homogeneous, which might reduce resistance or improve following treatments.
This is an important aspect, as heterogeneous cell populations in cancer are associated with poor outcomes and poor relapse-free survival in many different cancer types implying that genetic and non-genetic heterogeneity of cell populations increase the odds of some cells surviving the efforts of curative treatment leading to resistant cell populations (Lee et al., 2014; Almendro et al., 2014; Morris et al., 2016). My findings could be relevant in a clinical context as it has been shown previously that clinically used MAPK inhibition has side effects that can be traced back to cellular differentiation states (Schmidt et al., 2018). In this paper lineage tracing was used to follow cell plasticity after MAPK or NOTCH inhibition. Targeting each pathway alone resulted in outgrowth of a resistant cell population. However, targeting both at the same time eradicated cancer in the mouse model used. In conjunction with my own results, namely that cellular heterogeneity is diminished by MAPK inhibitor treatments, this opens the possibility of treating cancers first with MAPK inhibitors to homogenize cells, potentially reducing resistance and making it easier to drive cells towards apoptosis to improve therapy outcomes.

4.3 MAPKi elicits a stem cell phenotype, which is reversible

I observed that MAPK inhibition induces cellular plasticity and influences differentiation states. To understand how cells are able to survive MAPK inhibition I performed a time course experiment where I inhibited EGFR in the RAS/RAF^{wt} line P013T. Under inhibitor treatment, most cells stopped growing with just a small fraction of cells surviving the treatment (fig 21B + 23B). Cells under DMSO treatment show an expected differentiation course moving from EPHB2 expressing stem-like cells towards TFF3 expressing differentiated cells. However, under EGFRi treatment this normal development was overridden and a new developmental endpoint appeared with cells expressing stem cell markers (fig. 21C). Upon removing the EGFR inhibitor, P013T cells were able to quickly recover their growth potential and resume cycling through all cell cycle phases (fig. 23B). The transcriptome of cells where the inhibitor was removed for four days was similar to the transcriptome of DMSO-treated control cells and thus both samples overlap in a UMAP representation (dark green overlapping with orange/red in fig. 23D). This is an important finding since therapy in patients could similarly lead to a resistant stem-like subpopulation, which can lead to a relapse in tumor growth after the conclusion of therapy (Lupo et al., 2020). Additionally, these slow-growing cells could gain a mutation and become a founder cell for a genetically resistant clone. Relevant in this context, Russo et al. (2019) found a survival strategy of CRC cells, namely the induction of mutability and microsatellite instability. In order to evade EGFR antibody and BRAF inhibitor treatment CRC cells are able to reduce their growth rate, while downregulating mismatch repair DNA genes and upregulating error-prone polymerases to increase mutation rates Russo et al. (2019).

The finding that cancer cells can modify their transcriptome, inducing cell states to overcome drug stress, as mentioned above, adds a non-genetic layer to heterogeneity. It is conceivable that the modification of the transcriptome imposing a stem-like cell state also includes epigenetic modifications to DNA or histone methylation (Brock et al., 2009). This could be further researched on a single cell level in organoids using ATAC seq, which was done for the P013T organoid model in the lab, however, the data has not been analyzed yet.

Blaj et al. (2017) stated that cells high in MAPK activity ceased to proliferate and underwent EMT. They also show that MAPK-high cells display increased WNT signaling and express stem cell markers. This paper showed that MAPK activity is highly heterogeneous and not only serves to enable proliferation but in cancer it balances stem cell populations and tumor growth (Blaj et al., 2017) together with Wnt and YAP activities (Uhlitz et al., 2021). In my experiments, MAPK-inhibited cells revert to a stem cell-like phenotype. This might hint at different potential ways to induce a stem-like cell state, some with a high and some with low MAPK activity.

Overall, I showed that EGFRi is able to override differentiation trajectories and induce a new developmental endpoint of stem-like resilient cells. As soon as the inhibitor is removed, cells resume proliferating at a speed comparable to control cells.

4.4 Inhibition of MAPK activity is not sufficient to cause complete apoptosis

Cancer therapies aim at killing all cancer cells. Even though MAPK inhibition restricts the differentiation space of cells, MAPK inhibition alone did not result in apoptosis of all cancer cells in the assays I performed. In fact, none of the inhibitors in the panel drove all tested cancer organoid lines into apoptosis and left the normal colon organoid lines proliferating. The apoptosis marker expression of cCasp3 in fig. 17 indicates that MEK inhibition leads to an upregulation of cCasp3, which is most prominent in KRAS^{mut} lines. The BRAF^{mut} line even downregulated the apoptosis marker under MEKi. In line with this, the cell survival assays based on metabolism showed a reduction of metabolism in organoid lines under MEKi, but again the BRAF^{mut} line is least affected (fig. 20A). In all cases, subpopulations of cells survived the short-term treatment in the perturbation screen. Even in the long-term experiment, where I treated line P013T with EGFRi for 144 hours (fig. 23) the resistant subpopulation was not eradicated. However, the cells that survived were largely quiescent.
It has been frequently observed that, besides induction of apoptosis, cancer treatment can also induce a quiescent cell state. When cancer cells are in a quiescent state, they are typically more resistant to the effects of targeted treatments, because they have reduced metabolic activity and are less likely to be killed by drugs that target actively dividing cells. As a result, quiescent cells can serve as a reservoir of drug-resistant cells that can eventually give rise to a drug-resistant tumor. Oren et al. (2021) found so-called cancer persister cells, which are a small population of cells that are resistant to therapy and can give rise to tumor recurrence. This study found that cancer persister cells arise from two distinct lineages: a quiescent lineage that is resistant to therapy but does not proliferate, and a cycling lineage that proliferates but is sensitive to therapy. Both lineages have distinct programs that control cell proliferation and cell death (Oren et al., 2021). Additionally, EGFR inhibition alone can lead to a quiescent subpopulation, with Paneth cell characteristics, which are EGFR independent and mainly signal via the PI3K pathway. Combination therapy of EGFRi and PI3Ki increases apoptosis and prevents regrowth after inhibitor removal (Lupo et al., 2020). Furthermore, resistance to Cetuximab in RAS^{wt} CRC samples can be driven by a switch from a sensitive TA-subtype to a stem-like subtype, which is high in fibroblasts and growth factors (Woolston et al., 2019).
Zhan et al. (2019) reported that MEK inhibition activates WNT signaling *in vitro* and *in vivo*, and induces stem cell plasticity, which would explain, why MEKi did not lead to

apoptosis of all cells. Instead, elevated WNT signaling in KRAS^{mut} cells can dedifferentiate epithelial cells to reacquire stem cell properties and initiate tumorigenesis (Schwitalla et al., 2013).
There are some attempts to overcome resistance to cancer treatments. One way is to use a different treatment approach, such as targeted therapy or immunotherapy. Another way is to use a combination of different treatments. One approach to prevent resistance from developing is to use treatments that target multiple pathways simultaneously. This makes it more difficult for the cancer cell to develop resistance.

4.5 Combination therapy is one possibility to achieve apoptosis

To minimize the emergence of resistant cell populations, combinatorial treatments can be employed. Combining MAPK inhibition with other inhibitors should not only reduce cellular heterogeneity and proliferation but also drive cells into apoptosis. Therefore, I analyzed my screen to identify potential drug combinations boosting apoptosis in an additive or synergistic manner. In fig. 17 I analyzed the effect of the inhibitor panel on the organoid lines, seeing that MEK inhibition upregulates the apoptosis marker cCasp3 in most cancer lines. However, as mentioned above, MEK inhibition alone does not cause complete apoptosis. Thus, we have performed an *in silico* analysis on the divergence of gene expression and phospho-protein distributions under inhibition with the aim to determine which novel inhibitor combinations might produce incompatible cell states to increase apoptosis. The analysis revealed that six out of eight organoid lines had strong divergent distributions of gene expression and phospho-protein patterns of multiple inhibitors in the panel when compared to the effects of the MEK inhibitor (fig. 19). Thus, combinations of MEK with other inhibitors were tested as potential synergistic drug combinations. The most striking synergistic effect with inhibitor combinations could be observed for MEKi + FGFRi in OT326 (fig. 20F). While our *in silico* approach predicted the combination of FGFR and MEK inhibitors as a potential drug combination, the line OT326 was not predicted to have this synergy, highlighting the limitations of our approach. OT326 is a RAS/RAF^{wt} line. It is noteworthy that the FGFR is an RTK that can activate MAPK and also other downstream pathways (Hadari et al., 2001). The observed synergy might hint at non-overlapping functions of FGFR and the downstream MEK kinase. Experiments with further inhibitors and phospho-protein analysis would be required to unravel the mechanistic basis for the finding.
In my screen for potential synergy, responses were best seen in microscopy, and the metabolic cell survival assays were not adequate to assess synergism. This was probably because MEKi alone was already reducing the metabolic rate of cells drastically (fig. 20A). In my experiments, I did not test whether cells were irrevocably pushed towards apoptosis or just quiescence, which would allow them to continue proliferating after inhibitor

removal, similar to EGFRi-treated P013T cells mentioned in the previous chapter.
In the case of BRAF^{mut} organoid lines there is an expected synergism between BRAF and EGFR inhibition to overcome BRAF inhibitor-induced reactivation of EGFR signaling, as this is used in the clinic as a first-line therapy (Corcoran et al., 2012, 2018). However, in my double inhibitor screen, this combination was not tested since I only had one BRAF^{mut} line in the screen.
Beyond assessing drugs used in my initial screen, how can we prevent the emergence of this stem cell-like subpopulation? As written above, stem cell-like states might be defined by a specific epigenetic make-up of the emerging resistant cell populations after MAPK inhibition. Gunnarsson et al. (2020) use a mathematical model to investigate non-genetic drug resistance. They report that epigenetic modifications can drive long-term resistance, which can be overcome by epigenetic drugs or combinations with conventional therapy in a specific order. To concomitantly target the cells epigenome, I treated organoids with a specific MLL1 inhibitor, MI-2, which has been shown to drive intestinal stem cells into differentiation (Grinat et al., 2020). In my experiments, Cell tox green assays, which assess membrane integrity, indicated that organoid cells died after 96 hours of MI-2 inhibitor, and no synergy with MAPK inhibitors was found. Grinat et al. (2020) modified MLL levels genetically using a tamoxifen-inducible floxed MLL. Their research shows that MLL1 is controlled by Wnt signaling, but MLL1 is needed to sustain CRC stemness, without affecting WNT signaling activity. Thus, ablation of MLL leads to differentiation of stem cells. To see whether my experiments reflect these published results, a more in-depth analysis would be needed, not only metabolism and membrane integrity measurements. A SLAM-seq experiment would indicate, whether stem cell marker expression decreases over time, whereas goblet cell markers increase. Also, a wash-out step after one week of inhibition would have been informative to see if cells are able to recover or are irrecoverably pushed towards differentiation.
Combining inhibitors to combat cancer growth and prevent tumor relapse is a focus of many studies: Theoretical work by Raatz et al. (2021) suggests sequential application of growth rate-dependent and growth rate-independent treatment types to diminish cellular heterogeneity and prolong relapse times. This would also impact slow-growing subpopulations, which otherwise are a pool for relapse.

4.6 Organoids as predictive tools

The challenge of accurately predicting the success of a treatment or treatment combination for each individual patient is complex. To address this, predictive tools are needed to provide insight into the biological characteristics of each patient's tumor. One such cutting-edge tool is the use of organoids, which can be used to study various aspects of human physiology and disease. Through organoid technology, researchers can gain a greater

understanding of the underlying biology of a tumor and can develop new treatments and screen drugs for efficacy in a general or patient-specific manner.
In recent years, organoids are being used to predict whether a patient with hereditary cystic fibrosis will benefit from drug treatment or not by treating patient-derived rectal organoids with the available drugs and assessing organoid response (Dekkers et al., 2016). Another research area that benefits from organoid cultures is influenza research, where airway organoids consisting of four different epithelial airway cell types are grown in culture and infected with different virus strains to quickly assess the infectivity of new influenza strains to humans (Zhou et al., 2018).
Additionally, organoids can be used in toxicological research. Instead of using mice to test the toxicity of a new drug, it could be tested on panels of human organoid lines from different organs, e.g. gastrointestinal organoids recapitulate drug response of patients with 90% accuracy (Belair et al., 2020).
Also in colorectal cancer research, organoids have been shown to be predictive tools, since they can recapitulate the heterogeneity of colorectal tumor cell composition (Fujii et al., 2018). As such, organoids can be used in personalized medicine approaches to tailor treatment to the individual patient (van de Wetering et al., 2015; Vlachogiannis et al., 2018). For example, patient-derived organoids are able to predict response to chemotherapy for patients with rectal cancer or metastatic CRC (Ganesh et al., 2019; Ooft et al., 2019).
Organoids as predictive tools further the understanding of how drugs affect cancer cells, which is important for determining drug combinations that can drive cancer cells into apoptosis. This begs the question of whether my experiments are useful as a predictive tool, as they could provide insight into the effects of certain drug combinations on cancer cells. In my experiments, I initially used metabolic readouts to screen for inhibitor combination synergy (fig. 20). Cells that had been affected by inhibitor addition and stopped proliferating showed a reduction in metabolic activity, which was most prominent when treated with MEKi. However, subsequent experiments revealed the presence of a quiescent stem cell-like subpopulation in organoid line P013T after EGFRi addition, indicating that the metabolic readout alone would most likely not be sufficient to accurately assess whether an organoid line had stopped proliferating. This is because the readout could not distinguish between cells that had stopped proliferating to undergo apoptosis and those that had entered a quiescent state and could resume growth in more favorable conditions. If the inhibitor leads to a quiescent stem cell-like subpopulation it might be growing very slowly (Hirata et al., 2013) and thus not be picked up by the metabolic assays. This means that for patient-specific prediction the assays used were not suitable and for broader mutation-related response prediction my cohort of eight organoid lines was too small.
There are also other limitations to the use of organoids besides types of assays or the

number of samples. While organoids have been used to study chemotherapy responses, their utility in predicting immunotherapy outcomes for CRC has yet to be determined. This is because the interplay between cancer cells and other cells in the microenvironment, such as stromal cells, is missing in organoids (Schütte et al., 2017). As a result, stand-alone organoid experiments may not be able to accurately recapitulate the complex interactions that occur in the tumor microenvironment and may not be able to predict immunotherapy response in CRC patients.
However, in a recent study, researchers used organoids created from the patient's own tumor tissue to test the effectiveness of chimeric antigen receptor (CAR) immunotherapy (Schnalzger et al., 2019). CARs are generated proteins that can recognize and bind to specific targets on the surface of cancer cells. This allows the CAR-bearing immune cells to specifically target and kill cancer cells while sparing normal cells. Schnalzger et al. (2019) developed a system to assess CAR-mediated cytotoxicity against tumor-associated antigens, which could be used for patient-specific therapy testing. They achieved tumor cell eradication without impacting co-cultured antigen-negative cells. However, tumor-specific antigens need to be identified first to prevent toxicity in patients, but the work by Schnalzger et al. (2019) shows promise for their use in the development of new and effective immunotherapy treatments for colorectal cancer.
The use of organoids has the potential to revolutionize the way we treat and manage cancer, providing more personalized and effective treatments tailored to each individual patient. However, their use as predictive tools is still capable of further improvement, which would allow the use of organoids in other research fields such as transplantation and regenerative medicine.

4.7 Technical aspects and advancements

Single cells used to be analyzed by fluorescent-activated cell sorting (FACS) to group cells into subgroups based on antigen expression (Herzenberg et al., 2002). For this technique to work, a single-cell suspension is labeled with fluorophore-conjugated monoclonal antibodies for specific surface markers and measured in a flow cytometer, allowing for quantitative analysis of the fluorescent labels. The maximum number of labels is constrained by the overlapping of light emission from the fluorescent tags.
Even though the first single-cell mass cytometry paper was published in 2007 (Tanner et al., 2007), this technique was more commonly used as of 2011, when Bendall et al. (2011) described CyTOF and its use in immunophenotyping of hematopoiesis. The biggest advantage of mass cytometry in contrast to flow cytometry is the absence of fluorescently labeled antibodies. Instead of fluorophores, the antibodies are conjugated to isotopes of rare metals, which allows for simultaneous measurement of at least 45 parameters (Bendall et al., 2012).

At first, I could only use fresh cells for antibody staining and measurement, which complicated cell culture handling due to the different growth rates of the organoid lines. To overcome these technical issues I employed Proteomic Stabilizer (Fernández-Zapata et al., 2020), allowing me to unify sample preparation and storage. This novel workflow allowed us to publish a paper using single-cell CRC organoids in a CyTOF experiment (Brandt et al., 2019).

Recently it has become overt that the shape of organoids is influenced by genetic interactions and can be altered by drugs (Lukonin et al., 2020; Betge et al., 2022). Both papers used image-based assays for the evaluation of organoid survival, proliferation, migration, and differentiation in response to drugs and other treatments. Imaging also allows for the detection of the effects of genetic and epigenetic modifications on the organoid phenotype, providing valuable insights into the mechanisms underlying organoid behavior (Lukonin et al., 2020; Betge et al., 2022).

Combining the advantages of image-based organoid assessment with gene expression data provides a powerful tool for understanding organoid function. Since 2018, when I began my project, technological advancements have enabled simple spatial transcriptomics, such as 10X's "Visium Spatial Gene Expression" assay for the assessment of fixed tissue. This would allow us to visualize the expression of any gene of interest on a spatial map, helping us to identify if there is a graduated expression or not. Seeing cell-to-cell variability after inhibitor addition would be useful to understand evasion mechanisms because it provides insight into how different cells can respond to the same inhibitor stimulus in different ways. However, this method would be more informative if we could visualize the influence of the microenvironment, which I do not have in my organoid culture system.

When I started working on this project, there was no method that combined scRNA sequencing with multiple protein measurements. Measuring both proteins and RNA of one single cell alleviates the need for any batch correction or data integration. Recently, methods have emerged to overcome the limitation of performing multiple laborious experiments and combining scRNA and protein measurements commonly termed CITE-seq (cellular indexing of transcriptomes and epitopes by sequencing). Since mRNA abundance does not reflect protein expression (Raj et al., 2006), measuring both translational stages improves the analysis of cell states. E.g. Reimegård et al. (2021) presented their method "SPARC", which measures global mRNA and 89 intracellular proteins at cellular resolution. Mair et al. (2020) and Shum et al. (2019) have developed targeted approaches to measure 400 transcripts and 40 proteins to analyze immune cell or PBMC heterogeneity, respectively.

In the future single-cell multi-omics will further the understanding of gene regulation and cellular heterogeneity to aid in the development of new clinical approaches.

4.8 Limitations of my work

All experiments were focused on intracellular signaling and changes due to perturbations. However, there is also paracrine signaling between cells, which leads to heterogeneous cell types in organoids (Serra et al., 2019). It is known that the WNT pathway is active in cancer stem cells, however, this stemness does not solely depend on WNT activity but is orchestrated by the cues from the microenvironment. Vermeulen et al. (2010) showed that fibroblasts release growth factors, which activate stemness and self-renewal. The microenvironment is the integral part influencing cancer stem cell marker expression (Lenos et al., 2018). Initiation of CRC also depends on mesenchymal niche factors from fibroblasts, which influence tumor-initiating stem cells by activating YAP-signaling (Roulis et al., 2020). However, in my *in vitro* experiments, I did not co-culture with fibroblasts or other influencing cells but focused on cell-intrinsic responses to perturbations. Thus, even if an inhibitor combination is found to kill CRC organoids, responses could be modified by the microenvironment *in vivo*.
Inhibitor concentrations for experiments were taken from previously published papers (see table 2) and no dose-response experiments were conducted on the organoid lines, which were used. Some inhibitor concentrations may seem very high, e.g. MEK inhibitor selumetinib. This concentration was taken from Riemer et al. (2017) and also because KRAS^{mut} colorectal cancer cell lines are unresponsive to low concentrations of selumetinib (Sun et al., 2014).
A limitation of most single-cell experiments is the absence of replicates since sequencing is still a costly endeavor. There may be thousands of cells, but all in one biological replicate. To ensure reproducibility, experiments would need to be repeated. However, as multiplexing options become more versatile and methods advance to measure RNA and protein in one experiment, this might soon be a problem of the past. Five of my eight organoid lines were sequenced together to abolish batch effects, but there are batch effects when compared to the other lines, which were sequenced in different runs. In CyTOF every organoid line was processed individually and measured on its own since every batch contained 20 palladium-based isotope barcodes. Nowadays, there are other barcodes, which are amine- or thiol-reactive, which makes them suitable to barcode cells while they are still embedded in matrigel (Qian et al., 2020). Those barcodes could be combined with the palladium barcodes to extend the number of samples in one run. Additionally, Cisplatin is naturally occurring in six isoforms, meaning that the current CyTOF barcoding system could be expanded six times (McCarthy et al., 2017). When combining cisplatin and additional monoisotopic tellurium maleimide (TeMal) (Qin et al., 2020), enough unique combinations could be produced to run all my eight organoid lines together in one run, albeit a long overnight run. Since I still have backup samples, this could be performed for further in-depth analysis circumventing the need for

batch correction. The antibody I used to detect MEK, detects MEK1 and MEK2 without distinction, which fits the inhibitor which specifically inhibits MEK1/2. However, the ERK feedback regulation regulates MEK 1 and 2 levels differently. MEK1 increases on a transcriptional level, whereas MEK2 regulation happens on a protein level (Hong et al., 2015). This might explain differences in MEK reactivation between scRNA seq data and CyTOF data.
scRNA seq data analysis was limited by the use of signatures to collate the effects seen on transcriptome changes, which may come at the cost of specificity, since signaling networks are highly context-specific and what is considered a "canonical" pathway depends on the database, where components and interactions vary (Kirouac et al., 2012). Thus, colorectal cancer-specific expression signatures might have produced slightly different results.
Overall, I used eight organoid lines for my perturbation screen and an additional four lines in later experiments. This cohort size is too small to make patient-relevant predictions, but it serves to further unravel the intrinsic wiring of CRC organoids.

4.9 Outlook

My perturbation screen with eight human-derived organoid lines and further MAPK inhibition experiments with six organoid lines provides insight into the heterogeneity of the cellular composition of organoids and differential responses to inhibitors. The analyses I provided could be expanded and the data interrogated from different viewpoints or analyses could be further elaborated, such as modeling of the perturbation data in order to find novel interactions or feedback loops. *De novo* network generation could produce predictive context-specific networks (Molinelli et al., 2013). Or specifically for this task, STASNet could be used to perform modular response analysis to model pathway activities and dependencies (Dorel et al., 2018). Certain inhibitors in the panel were chosen with modeling in mind, e.g. the type and concentration of the MEK, PI3K, AKT, mTOR, and GSK3β inhibitors, which were used in Riemer et al. (2017) to investigate network states in CRC organoids. New ways of data processing are constantly developed. One of these is CellBox by Yuan et al. (2021), which is able to predict responses to untested perturbations.
In order to see if cancer driver mutations are responsible for specific responses to inhibitors, more organoid lines or even cell lines need to be tested. The best would be to use an isogenic organoid line and insert specific mutations with CRISPR, then observe e.g. upregulation of cCasp3 under e.g. MEK inhibition and then perform a rescue experiment, supplementing wildtype KRAS and restoring the wildtype signaling network. Additionally, CRISPRi or CRISP KO screens could be performed to find synthetic lethal interactions between signaling pathways in CRC. e.g. MAPK inhibitors could be screened against major nodes in other pathways to find suitable drug combinations for effective therapy.

Once suitable inhibitor combinations are found that drive cancer organoids into apoptosis, without harming normal colon organoids, these combinations could be tested *in vivo*. However, keeping previous research and my findings in mind, these inhibitor combinations might be cell-line dependent. This is precision medicine, where a biopsy from a cancer patient is used to generate an organoid line, which can be tested for its response to therapy. Since organoids have the same genetic mutations and recapitulate the pathophysiology of the original tumors, their responses mimic the clinical responses of patient tumors. However, engrafted tumors in mice display heterogeneous responses to chemotherapy, but coupling organoid and mice experiments will help to choose the best mix of chemotherapy, radiation, resection, and inhibitors to optimize treatment outcomes for individual patients (van de Wetering et al., 2015; Ganesh et al., 2019; Yao et al., 2020).
On the other hand, new inhibitors have been developed, such as a $KRAS^{G12C}$ inhibitor (Canon et al., 2019), Sotorasib, which is an approved treatment for non-small cell lung cancer as of 2022 in EU, which could be tested in the colorectal context. Recently, Cercek et al. (2022) published results of a phase 2 trial: 12 patients with MMR deficient colorectal cancer received PD-1 (programmed death 1) antibodies and all patients showed complete response with no detectable cancer after 6 months of treatment, underlining the importance of immunotherapy in the fight of cancer. Even though this is a promising result for this type of localized tumors, their testing cohort was too small to draw serious conclusions.
Besides common strategies for cancer treatment, there is also the attempt to activate apoptosis in cancer cells directly by inducing tumor necrosis factor-related apoptosis-inducing ligand (TRAIL). Since most cancers are primarily resistant to TRAIL-monotherapy, tumors can be sensitized by combination with a CDK9 inhibitor. Both agents work synergistically to kill tumor cells *in vivo*, chemo- and targeted therapy-resistant cells and CRC organoids (Montinaro et al., 2022). This combination might be effective in a variety of solid cancers but need to be evaluated clinically.

In conclusion, even though my work might not be translated into a treatment for CRC patients directly, it furthers the understanding of cell-intrinsic signaling, plastic responses to inhibitors, and the emergence of therapy-resistant subpopulations. Further studies will be needed to elucidate which combination therapies work best in which cancer subtypes to improve targeted cancer therapy in the future.

5 Material and Methods

5.1 Organoid cell culture

Patient-derived organoids (PD3Ds) were obtained from the Oncotrack biobank ("OT" = OncoTrack consortium, Schütte et al. (2017)). They were handled under sterile conditions in a laminar flow hood.
Crypt culture medium (CCM) for organoid culture was prepared according to table 4 and frozen in 40 ml aliquots. These aliquots were supplemented with additives depending on the organoid line (table 4).
Organoids were stored in liquid nitrogen and for reviving, the cryo-vials were rapidly warmed in a 37°C-water bath. 500 µl of medium was added and the suspension was transferred to a BSA-coated low-binding tube for centrifugation. Afterwards, the medium with a freezing agent was removed and the organoids were resuspended in 20% medium, shortly chilled on ice before adding 80% Matrigel. 20 µl droplets of this suspension were plated in a 24-well plate in the appropriate number of wells. After the matrigel polymerized ($\sim$ 5 min under the hood or $\sim$3 min in the incubator) 500 µl CCM medium (composition see table 4 below) were added per well and the plates kept in an incubator with 5% CO_2 at 37°C. Medium was exchanged every two to three days.
For passaging/splitting, the matrigel containing organoids was washed out of the wells with 500 µl PBS (more wells could be pooled). Matrigel and PBS were removed after centrifuging the suspension. The organoid pellet was washed once in PBS and then resuspended in 300 µl TrypLE and put in the incubator for organoid disintegration/digestion. To corroborate that organoids were digested, they were pipetted up and down and checked under the microscope every 3 minutes. If sufficient digestion was visible, then $\sim$1 ml PBS or CCM was used to dilute the TrypLE before centrifuging. The supernatant was discarded and the pellet was resuspended in 20% medium, mixed with 80% matrigel, and plated in at least double the number of wells (ratio 1:2).
When freezing organoids, they were harvested three to four days after splitting them. After the second washing step in PBS, the organoid pellet was resuspended in "Recovery Cell Culture Freezing Medium" (Life Technologies, see table 12). The amount of freezing medium depended on how many organoid wells were harvested. It was calculated so that the number of organoids corresponding to two or three wells could be distributed into each cryo-vial containing 1 ml freezing medium, respectively. Vials were put overnight in a cryo-storage container into a -80°C freezer. For long-term storage, vials were transferred to liquid nitrogen tanks.

Table 4: Media composition: basis is crypt culture medium (CCM)

CCM (basic)	**Company**	**Cat. No.**	**Stock**	**Final**	**Add**
Advanced DMEM/F12	Gibco	12634-010	1x	1x	500 ml
B-27 Supplement	Gibco	12587-010	50x	1x	10 ml
N-2 Supplement	Gibco	17502-048	100x	1x	5 ml
1xP/S	Invitrogen	15140-122	100x	1x	5 ml
GlutaMAX	Invitrogen	35050	100x	1x	5 ml
Hepes	Invitrogen	15630-056	1 M	10 mM	5 ml
N-Acetyl-L-cysteine	Sigma Aldrich	A9165	500mM	1mM	500 µl
For OT lines: added fresh to CCM					in 40 ml
bFGF	Sigma-Aldrich	SRP3043	100 µg/ml	20 ng/ml	8 µl
EGF	Invitrogen	PMG8043	1000 µg/ml	50 ng/ml	2 µl
WERN Medium for NCO and P021N					for 50 ml
CCM					30-40 ml
Wnt-CM				see 5.6	10-20 ml
R-SPO-CM				see 5.6	2,5 ml
B27	Gibco	12587-010	50x	1x	1 ml
NIC	Sigma-Aldrich	N0636	1 M	10 mM	500 µl
NAC	Sigma-Aldrich	A9165-5G	500 mM	1.25 mM	125 µl
Primocin	Invivogen	ant-pm-1	50 mg/ml	100 µg/ml	100 µl
EGF	Invitrogen	PMG8043	500 µg/ml	50 ng/ml	5 µl
P38i (SB202190)	Sigma-Aldrich	S7067	30 mM	3 µM	5 µl
TGFβi (A83-01)	Tocris	2939	5 mM	500 nM	5 µl
Noggin	PeproTech	250-38-250		100 ng/ml	
TNEPP Medium for C2-019, P013T and P009T					for 50 ml
CCM					50 ml
EGF	Invitrogen	PMG8043	250 µg/ml	25 ng/ml	2.5 µl
P38i (SB202190)	Sigma-Aldrich	S7067	30 mM	3 µM	5 µl
TGFβi (A83-01)	Tocris	2939	5 mM	500 nM	5 µl
NIC	Sigma-Aldrich	N0636	1 M	10 mM	500 µl
Primocin	Invivogen	ant-pm-1	50 mg/ml	100 µg/ml	100 µl

Table 5: Human organoid lines and their most relevant oncogenic mutations

Sample	Gene	Codon change	AA change
OT108	APC	c.4280delC	p.(P1427Lfs*46)
OT108	TP53	c.817C>T	p.R273C
OT108	TP53	c.215C>G	p.P72R
OT326	APC	c.3924_3925delAG	p.(E1309Lfs*5)
OT326	ATM	c.2572T>C	p.F858L
OT326	TP53	c.272G>A	p.W91*
OT326	TP53	c.215C>G	p.P72R
P009T	APC	c.3856G>T (het)	p.E1286*
P009T	FBXW7	c. 1438G>C	p.D480H
P009T	TP53	c.743G>A	p.R248Q
P013T	APC	c.3856G>T	p.E1286*
P013T	NOTCH1	c.4802A>T	p.H1601L
OT227	APC	c.4737delT	p.(I1580Ffs*70)
OT227	KIT	c.1621A>C	p.M541L
OT227	KRAS	c.38G>A	p.G13D
OT227	TP53	c.814G>T	p.V272L
OT227	TP53	c.215C>G	p.P72R
OT302	FLT3	c.2541+1G>A	splice don. var.
OT302	KDR	c.1416A>T	p.Q472H
OT302	KRAS	c.35G>A	p.G12D
OT302	TP53	c.215C>G	p.P72R
OT238	KDR	c.1416A>T	p.Q472H
OT238	KIT	c.1621A>C	p.M541L
OT238	KRAS	c.35G>A	p.G12D
OT238	SMAD4	c.1496G>A	p.C499Y
OT238	TP53	c.818G>A	p.R273H
OT209	APC	c.3926-3930delAAAAG	p.(E1309Dfs*4)
OT209	FBXW7	c.1780C>T	p.L594F
OT209	KRAS	c.35G>T	p.G12V
OT209	TP53	c.524G>A	p.R175H
OT209	TP53	c.215C>G	p.P72R
IKP007s	BRAF	c.1799T>A	V600E
IKP007s	KDR	c.2146A>T	p.K716*
IKP007s	DLC1	c.762AA>CG	p.QN254HD
IKP007s	PRKD1	c.2696A>G	p.H899R

IKP007s	NOTCH3	c.4480G>T	p.G1494C
IKP007s	TP53	c.215C>G	p.P72R
B2-040	MLH1	c.655A>G	p.I219V
B2-040	PIK3CA	c.1173A>G	p.I391M
B2-040	BRAF	c.1799T>A	p.V600E
B2-040	DLC1	c.762AA>CG	p.QN254HD
B2-040	TP53	c.644G>T	p.S215I
B2-040	SMAD4	c.1015T>C	p.F339L
B2-040	SMAD4	c.1248A>T	p.R416S
C2-019	TGFBR2	c.1657C>T	p.R553C
C2-019	PIK3CA	c.3140A>T	p.H1047L
C2-019	BRAF	c.1799T>A	p.V600E
C2-019	DLC1	c.762AA>CG	p.QN254HD
C2-019	KRAS	c.565A>C	p.M189L
C2-019	POLE	c.6494G>A	p.R2165H
C2-019	TIAM1	c.739GG>AT	p.G247M
NCO	no oncogenic driver mutations		
P021N	no oncogenic driver mutations		

5.2 Immunohistochemistry (IHC)

Organoids were grown and treated as described in the method or result section (sections 5.1 and 3.2) respectively. Histogel was heated to 70°C to liquify and then kept at 60°C until used. Organoids were harvested and washed in PBS to remove matrigel and then resuspended in 50 µl PBS. This suspension was mixed with 150 µl warm histogel and pipetted into small labeled disposable base molds. To harden the gel, molds were cooled in a fridge for one hour.

Afterward, the tiny pink gel blocks were removed from the molds and put into white histology cassettes, which were labeled with a pencil. In the routine pathology laboratory the blocks were embedded in paraffin and either stored in the fridge or cut the next day on a microtome with a water slide. Slices were captured on Superfrost Micro Slides (VWR).

To remove paraffin and rehydrate the slices, the slides were incubated for 1 h at 65°C. Afterwards they underwent a rehydration series: 3 x 5 min Xylene, 2 x 5 min 100 % EtOH, 1 x 3 min 95% EtOH, 1 x 3 min 80% EtOH, 1 x 3 min 70% EtOH, 1 x 5 min H_2O.

To quench endogenous peroxidase activity and retrieve antigens, slides were washed for 10 min in 3% H_2O_2 solution, 3 x 5 min PBS and then for 20 min in a steamer in pre-heated retrieval buffer (0,01 M Na-Citrate, pH 6, 0,05% Tween-20). Cool down buffer and slides slowly for at least 20 min. Slides were then washed in 2 x 3 min PBS. Organoid sections

on slides were outlined with a Pap pen. For blocking slides were placed in a wet chamber and covered with heat-inactivated horse serum (∼150 µl per slide) for 30 min at RT. For primary antibody incubation, slides were also placed in a wet chamber and covered in antibodies diluted in horse serum as required, covered with hybrislips, and incubated for 2 h at RT or overnight at 4°C.
Hybrislips were removed by washing them off gently with PBS. Slides were washed 3 x 3 min in PBS on a rocking platform. Afterward, slides were placed back in the wet chamber and covered with ImmPRESS secondary antibody solution, covered with hybrislips, and incubated for 1 h at RT. To remove excess, slides were washed 3 x 3 min in TBS while gently moving on a rocking platform. To visualize the signal, slides were stained with NovaRed substrate for peroxidase. Substrate solution contained destilled water plut 12% reagent 1 and 8% reagent 2, 3 and H_2O_2 respectively. Substrate solution was put on each slide individually while observing under the microscope. After 20 to 50 seconds the slide was washed in tap water to stop the reaction. For counterstaining, slides were covered in hematoxylin for 5 min, washed in water, rinsed in 70% EtOH and HCl, and washed in water again.
For dehydration, all slides were washed in increasing EtOH concentrations for 10 seconds (70%, 80%, 90%, 100%, 100%), then twice in Xylene. For mounting Vitro Clud was mixed 1:1 with Xylene, put on the sections, and covered with a coverslip. Slides were dried under a fume hood overnight.

Table 6: Immunohistochemistry antibodies and their dilution

Antibody	Cat. No.	Buffer	Dilution	Duration	Counterstain
Cleaved Caspase 3	AB9661	Citrat buffer	1:200	50 seconds	yes
Cleaved Caspase 3	AB9664	Citrat buffer	1:1000	50 seconds	no
KI67		Tris-EDTA	1:400	20 seconds	no
pERK	AB4370	Citrat buffer	1:400	50 seconds	no
pMEK	CS9121	Citrat buffer	1:800	50 seconds	no
KRT20	13063	Citrat buffer	1:1000	20 seconds	no

5.3 CyTOF

As I described in Brandt et al. (2019), the organoids were harvested in PBS and digested to a single cell solution in 1:1 Accutase (Biolegend) and TrypLE (Gibco) with the addition of 100 U/ml Universal Nuclease (Thermo Scientific) at 37°C. Cells were counted and a maximum of 500.000 cells were stained with 5 µM Cisplatin in PBS for 5 min at 37°C. After washing, cells were resuspended in their respective growth medium and allowed to rest for 30 min at 37°C. Subsequently, cells were resuspended in 10%BSA-PBS solution, mixed 1:1,4 with Proteomics Stabilizer (Smart Tube Inc.), and incubated for 10 min. at room temperature. Afterwards, cells were frozen in -80°C for storage.

One day prior to analysis, cells were thawed in 37°C water bath and mixed with Maxpar PBS. Cells were washed again in Maxpar Cell Staining Buffer (CSB), then in Barcode Perm Buffer (all three Fluidigm). Resuspended in 200 µl Barcode Perm Buffer, 25 µl of Barcode Labels (Fluidigm) were added to each appropriate sample and incubated for 30 min. at room temperature, which is a downscaled version of the manufacturer's protocol. Afterwards, cells were washed twice in CSB, pooled into one tube, and counted. 3 x 10^6 cells were then stained with surface antibody cocktail for 30 min. at room temperature. After washing in CSB, cells were refixed in 2% water-free formaldehyde solution (Pierce, diluted in MaxPar PBS) for 10 min. at room temperature. Cells were washed in CSB and put on ice for 10 min. Permeabilizing was done by adding 1 ml of 4°C methanol for 15 min. on ice. Afterwards, cells were washed twice in CSB and incubated with a phospho-protein antibody cocktail for 30 min. at room temperature. Cells were washed twice in CSB and incubated with 1 ml 62.5 nM Cell-ID Intercalator-Ir in Maxpar PBS (Fluidigm) for 20 min. at room temperature. Cells were washed in Maxpar PBS, and fixed in 2% formaldehyde overnight at 4°C.
The next day, cells were washed with CSB and twice with Milli-Q water. Cell number was adjusted to 2.5 – 5 $\times$ 10^5/ml with Milli-Q water and filtered through 20 µm cell strainers (CellTrics, Sysmex) and supplemented 1:10 with EQ Four Element Calibration Beads (Fluidigm), which was done by CyTOF core facility staff. Data was acquired on a Helios CyTOF system (BCRT, Chrité Virchow). Mass cytometry data was normalized using the Helios software, removing bead-related events. Data was filtered to remove doublets (DNA content (191Ir and 193Ir) vs. event length) and apoptotic debris (platin channel, 195Pt). Afterwards, the barcoded sample was deconvoluted using the CATALYST R package version 1.5.363 (Chevrier et al., 2018).
Antibodies which were bought from Fluidigm directly, were already pre-conjugated. The other antibodies were labeled using the Maxpar Antibody Labeling Kit (Fluidigm) according to the manufacturer's instructions.
Figure 24 depicts the CyTOF readouts of all eight organoid lines as density plots in alphabetical order. All antibodies had been tested and worked in other cell lines or organoid lines, but in the perturbation screen, some inhibitors were not detectable and could thus not be used for assessment of signaling activity. For example, CD8A, FosB, LGR5, p-p53, pS6, and Vimentin showed no noticeable expression in any line. A marker was considered "expressed" when the signal strength was above 10 or when a clear peak was visible, cf. act-Notch and PTK7.

5.3.1 IDU staining

In case of cell cycle analysis in CyTOF data, cells were treated with Cell-ID IDU (Fluidigm) at 25 µM for 30 min before harvest by adding IDU directly to the cell media.

Table 7: CyTOF antibodies

Marker	Target	Company	Clone	Label	Cat. No.
Cell type	CD133 (PROM1)	MACS	AC133	154Sm	130-108-062
Cell type	CD326 (EpCAM)	BioLegend	9C4	167Er	324229
Cell type	EPHB2	BD	2H9	158Gd	564698
Cell type	Krt20	CST	D9Z1Z	176Yb	13063BF
Cell type	PTK7 (CCK-4)	MACS	188B.12.45	146Nd	130-095-212
Cell type	Vimentin	CST	D21H3	165Ho	5741BF
Signalling	Axin 2	Abcam	poly	145Nd	ab32197
Signalling	FosB	CST	5G4	174Yb	2251BF
Signalling	Notch-1	R&D Sys	527425	173Yb	MAB5317
Signalling	p-c-Jun [S73]	CST	D47G9	144Nd	3270BF
Signalling	p-p53 [S15]	CST	16G8	172Yb	9286BF
Signalling	p4e-BP1 [T37/46]	CST	236B4	170Er	2855BF
Signalling	pCDC25c [S216]	CST	63F9	159Tb	4901BF
Signalling	pChk1 [S345]	CST	133D3	148Nd	2348BF
Signalling	pChk2 [T68]	CST	C13C1	141Pr	2197BF
Signalling	pMEK1/2 [S217/221]	CST	41G9	151Eu	9154BF
Signalling	pNF-kB p65 [S536]	CST	93H1	155Gd	3033BF
Signalling	pSmad1 [S463/S465] pSmad8 [S465/S467]	BD	N6-1233	149Sm	562508
Signalling	pSmad2 [S465/467] pSmad3 [S423/425]	CST	D27F4	153Eu	8828BF
Signalling	YAP	CST	D8H1X	150Nd	14074BF
Cell type	CD24	Fluidigm	ML5	169Tm	3169004B
Cell type	CD44	Fluidigm	BJ18	166Er	3166001B
Cell type	CD8A	Fluidigm	SK1	168Er	3168002B
Cell type	LGR5	Fluidigm	4D11F8	161Dy	3161025B
Phenotype	cCASP3	Fluidigm	D3E9	142Nd	3142004A
Phenotype	cPARP	Fluidigm	F21-852	143Nd	3143011A
Phenotype	Ki-67	Fluidigm	B56	162Dy	3162012B
Phenotype	pH2A.X [S139]	Fluidigm	JBW301	147Sm	3147016A
Signalling	IκBα	Fluidigm	L35A5	164Dy	3164004A
Signalling	p-p38 [T180/Y182]	Fluidigm	D3F9	156Gd	3156002A
Signalling	pAKT [S473]	Fluidigm	D9E	152Sm	3152005A
Signalling	pERK1/2 [T202/Y204]	Fluidigm	D13.14.4E	171Yb	3171010A
Signalling	pS6 [S235/236]	Fluidigm	N7-548	175Lu	3175009A

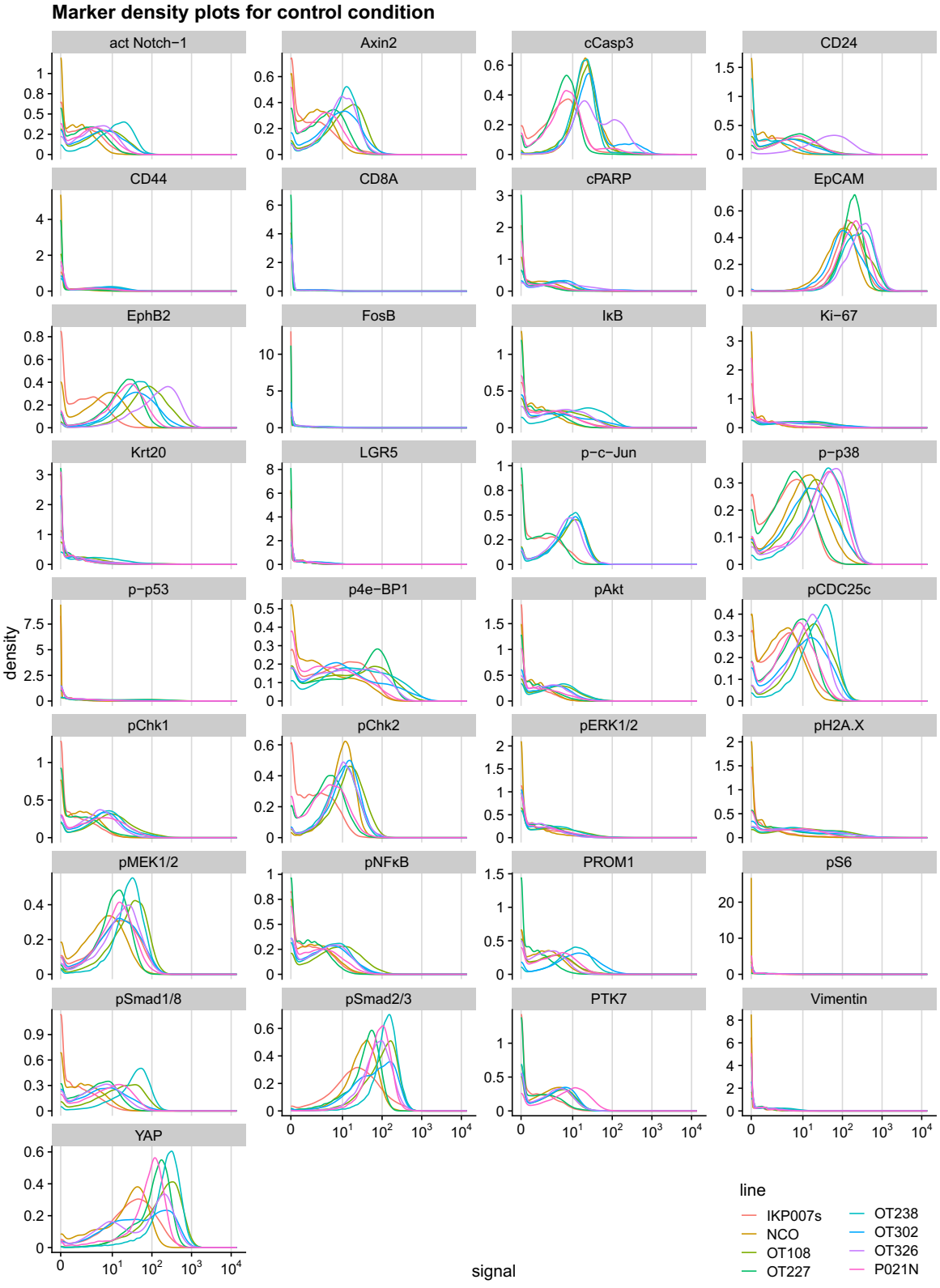

Figure 24: CyTOF density plots for all eight organoid lines in control (DMSO) condition to compare which antibody worked well and had a high dynamic range and which antibodies were not detectable, because cells did not express the target. Organoid lines color coded. y-axis = marker density; x-axis= signal strength per cell

5.4 scRNA sequencing

One perturbation sample in the scRNA seq experiments originated from two wells of a 24-well plate to have sufficient single cells for the downstream experiment. After 48 hours of inhibition treatment (see table 11), the organoids were harvested by washing with PBS and collecting in BSA-coated low-binding tubes. The suspension was washed twice in PBS to remove residual matrigel and debris. Organoids were then resuspended in 200 µl Accutase, complemented with 12 µl DNAse I (100 U/µl), and incubated for 15 min. at 37°C. In case of visible free genomic DNA (i.e. formation of sticky strings and cell aggregates) more DNAse I was added. After 15 min. 200 µl TrypLE Express was added and cells were put back at 37°C. Every 5 min. the cell suspension was resuspended and checked under the microscope to see if proper digestion was achieved. Once ∼90% of the cells were single cells, 1 ml of CCM (see table 4)+ 0.5% BSA was added and mixed with the cells. After centrifuging the cells shortly, medium was removed to keep cells from being digested further. Then the cells were resuspended in 1 ml CCM and filtered through a 30 µm filter and then counted in an automatic counting chamber. Cell number was adjusted to the lowest cell number in that experimental batch to keep a 1:1 ratio between perturbations for sequencing.
The single-cell suspensions were then barcoded with Sample Tags according to the "BD Single-Cell Multiplexing Kit-Human" protocol (Doc ID: 179682 Rev.1.0, pages 11 and 12), which was just downscaled 50%. Briefly, the cells were spun down and resuspended in 100 µl BD Stain Buffer (FBS). 10 µl of Sample Tags were added to each tube respectively and carefully mixed by pipetting. After 20 min of incubation at room temperature, 200 µl BD Stain Buffer (FBS) was added and mixed. Cells were centrifuged at 300 x g for 5 min and the supernatant was removed. 500 µl of RNAse-free PBS was used to resuspend and collect all samples as a pool in one tube, which was put on ice. Another 300 µl of RNAse-free PBS was used to rinse the tubes again and added to the existing pool.
To prepare the fixation in methanol (MeOH) cell number in the pools was determined in an automatic counting machine. Cells were then centrifuged at 300 x g for 3 min and the supernatant was removed. The pellet was resuspended in 20% RNAse free PBS (amount depending on cell number). While mildly vortexing, 80% pre-chilled MeOH was added dropwise. This suspension was kept on ice for 15 min before aliquoting $1*10^6$ cells into Eppendorf tubes. These were labeled and sealed with parafilm to be stored at -80°C.
Once enough samples were collected, the cells needed to be rehydrated to continue the experiment: Cell pools were put on ice until they reached 4°C and then pelleted at 1000 x g for 5 min in a pre-cooled centrifuge. MeOH-PBS supernatant was removed and cells were resuspended in 1 ml rehydration buffer (DBPS + 1% BSA + 0.5 U/µl RNAse inhibitor). Cells were pelleted again, resuspended in 500 µl rehydration buffer, and passed through a 40 µm cell strainer. Cells were counted to prepare loading of the

10X Chromium chip.
The "Chromium Single Cell 3' Reagents Kits v3"-protocol (Document Number CG000183 - Rev A) was followed exactly to prepare single-cell libraries for sequencing. Since Sample Tags from the BD Multiplexing-Kit were used for pooling samples, at step "2.3 cDNA Cleanup - SPRIselect" the supernatant was transferred to a new tube strip and not discarded (comparable to Feature Barcoding protocol CG000185 - Rev A). This supernatant was used to prepare the Sample Tag library according to the "BD Single Cell Multiplexing Kit-Human" protocol mentioned above (pages 13 to 22 of the protocol).

Table 8: 10X Genomics Chromium and BD kits

10X Genomics Kits	**Cat. No.**	**Content**
Chromium Single Cell 3'GEM	PN-1000075	Single Cell 3'GEM, Library, Gel Bead Kit
Chromium Single Cell B Chip Kit	PN-1000074	Partitioning oil, recovery agent, Chip B, gaskets
Chromium i7 Multiplex Kit	PN-120262	96-well plate with indices
BD Kit		
BD Single Cell Multiplexing Kit	PN 633780	Human Sample Tag (12) Component and Single-Cell Multiplexing Kit Library Amplification Component (*no longer available)

Ready libraries were run on an Agilent TapeStation for quality control. To determine the concentration precisely qPCR-based "KAPA Library Quantification" was performed in addition. Subsequent sequencing was done using a NextSeq or a HiSeq sequencer.

5.4.1 4sU staining and alkylation for SLAM-seq

In order to visualize cell development trajectories, the base analog 4-thiouridine (4sU, Sigma Aldrich, T4509) was added directly to the medium two hours prior to cell harvest at a concentration of 250 µM. Then cell handling as described above until storage at -80°C. Here, the alkylation will be inserted as follows: Cells were warmed to room temperature and then divided into two samples. To one sample 1 M Iodacetamid (IAA, Sigma Aldrich, I1149-5G) was added for the alkylation reaction, the other half of the sample did not receive IAA as a negative control. Samples were incubated for 16 hours at room temperature in the dark with mild rotation. Afterwards, samples were spun down at 300xg for 3 min at 4°C and washed with 1ml freshly prepared fixation buffer (20% PBS + 80% Methanol). Cells were spun again and the buffer was removed. To quench IAA, cells were rehydrated in 1 ml PBS + 0.01% BSA + 100 mM DTT + RNase inhibitors for 10min. Cells were pelleted again, the buffer removed and pellets resuspended in 500 µl rehydration buffer. Before counting, cells were filtered through a 40 µm FlowMi filter.

The number was adjusted to 700 - 1200 cells/µl either fixed in methanol again or directly loaded into the Chromium according to the manufacturer's protocol.

5.5 Synergy testing

Synergy testing was performed to assess whether the effect of two inhibitors is greater than the sum of both inhibitors individually (synergistic effect). The experimental setup started with plating 1500 filtered single cells in 5 µl matrigel droplets in a black 96-well plate with clear bottom. 150 µl of medium was added and the cells were allowed to grow for 96 hours without inhibitors. In order to spot human error, three technical replicates were prepared and the TECAN dispenser (hp) was used to administer the inhibitor combinations into the wells after a medium exchange.

Table 9: Inhibitor combinations (1, $\frac{1}{3}$, $\frac{1}{9}$ and 0 of concentration shown in table 11)

Inhibitor 1	Inhibitor 2
MEK	FGFR
MEK	mTORc1
MEK	AKT
MEK	GSK3b
MST	Pi3K
MST	TGFb
MST	GSK3b
MST	MEK

There were two inhibitor combinations per plate: Fig. 25 shows the example of MEKi + FGFRi and MEKi + mTROc1i first in a non-randomized manner how the experiment was conceptualized (left panel). Using the TECAN software these wells were randomized (middle panel) and normalized to the highest DMSO concentration on the plate (indicated by the gray color present in each well, except the highest double-concentration wells). After 72 and 168 hours medium was removed to assess cell health.

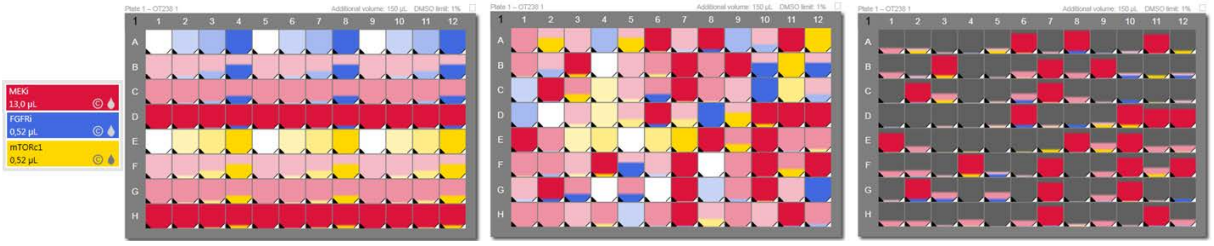

Figure 25: Visualization of randomized plate layout using the TECAN for inhibitor application

5.5.1 Metabolic activity and cytotoxicity measurements

In order to test cell viability the metabolic activity was measured using RealTime Glo reagent (Promega) 72 and 168 hours after inhibitor treatments. At the same time, CellTox Green Cytotoxicity Assay (Promega) was performed to detect changes in cell membrane integrity. Since the green dye binds to DNA, but is not readily taken up by the cells, higher fluorescent readout indicates a compromised cell membrane. When RealTime Glo and CellTox Green were used together in one experiment, the medium containing

inhibitors was removed and 50 µl CCM containing 1:1000 MT Cell Viability Substrate and NanoLuc Luciferase enzyme (RealTime Glo) and 1:1000 CellTox Green (Cytotoxicity Assay) were added to each well for two hours at 37°C. Afterwards, luminescence and fluorescence (485–500 nm excitation and 520–530 nm emission range) were measured in a plate reader (Synergy 2).
Then 100 µl CCM was added per well and the same TECAN program was used to add the inhibitors again until the second measurement (endpoint) at 168 hours.

5.6 Conditioned media production

Since the non-caner organoid lines (NCO, P021N) do not have oncogenic driver mutations, they need exogenous Wnt and R-Spondin-1 supplied in their medium to keep the stem cell pool and continue to proliferate. Two genetically engineered fibroblast lines excreted one of the proteins (either Wnt or R-Spo) into their respective growth medium, which is then called "conditioned medium".

5.6.1 2D-cell culture

Cells were frozen in cryo vials in liquid nitrogen. For revival, they were warmed in a 37°C water bath and then transferred to a 15 ml falcon containing 10 ml of warm D10 medium (see table 13). After centrifugation for 3 min at 1000 x g, the supernatant was removed and cells were resuspended in 10 ml D10 again and transferred to a T75 vented flask. Medium was exchanged the next day to remove dead cells, which did not attach to the plastic bottom of the flask. When cells became confluent (covering 80 to 95% of the flask surface) they were split: first, medium was removed and the flask was washed with 9 ml PBS. Then 1,5 ml TrypLE was added for 3 to 5 min at 37°C (incubator). To check if cells detached, the side of the flask was tapped lightly. If detachment could be observed, 9 ml D10 medium was added to the flask, cells were washed off the bottom of the flask and then collected in a 15 ml falcon tube. They were spun down and the supernatant was exchanged for 10 ml D10 medium. For seeding dilutions of 1:2 to 1:20 were used.

5.6.2 R-Spondin-1 conditioned medium production

To produce R-Spo, HA-F-R-Spo-293T cells were thawed onto two 10 cm dishes. When cells became confluent, the two dishes were split onto 10 15 cm dishes. After cells reached 80% confluence, D10 medium was removed and 15 ml CCM was added per plate. After 10 days of incubation, the medium was harvested: medium was collected in 50 ml-falcon tubes and centrifuged for 3 min at 1000 x g so dead cells were collected at the bottom. The clear medium was filtered first through 0.45 µm and then through 0.22 µm syringe filters and aliquotted into 2 ml Eppendorf tubes.

For testing which concentration of R-Spo should be used, mouse colon organoids were thawed and cultured in 48-well plates with 300 µl medium per well (CCM + REN using previously produced and tested R-Spo, see table 13). Organoids were expanded and for testing a dilution series of new R-Spo was prepared: two wells each with R-Spo at 0, 1:200, 1:100, 1:50, and 1:20. Since mouse colon organoids need R-Spo for their survival, it was obvious by visual inspection after three days which least concentration was needed for organoid survival. This concentration was then also used for normal colon organoid culture.

5.6.3 Wnt conditioned medium production

For Wnt-conditioned medium production, L-Wnt3A cells were thawed and cultured in a T75 flask. When cells were 50% confluent, Zeocin was added at 125 µg/ml. Once cells are 80% confluent, they were split into five T175 culture flasks and 20 ml growth medium was added. Only one flask received Zeocin again. When flasks without Zeocin are confluent, they were trypsinized, pooled, and plated onto 25 15 cm dishes with 20 ml medium in total.
After seven days the first batch of medium was harvested (like in R-Spo CM production): collected in falcons, spun, pre-filtered through 0.45 µm, and then sterile filtered using a 0.22 µm-filter bottle UltraCruz. New medium was added to the dishes for another harvest the week after. Three batches of medium were obtained like this. Wnt concentrations in batches four and five were too low to be used for cell culture.

5.6.4 Dual Luciferase Assay

To determine the Wnt concentration in the conditioned medium, HEK293T cells were used for a TOP/FOP assay. This reporter assay worked with a Wnt-sensitive luciferase reporter (TOP plasmid) and a negative control FOP plasmid. Firefly luciferase was measured and an increase in relative Firefly luciferase activity was observed when Wnt was present in the medium. A second luciferase "Renilla" was used to normalize each sample for transfection efficiency.
It was determined how many wells were needed by calculating three wells for each Wnt-batch (triplicate measurements), duplicating because of a 1:1 and a 1:3 dilution of Wnt-CM in D10 and doubling that number for transfection with the TOP and FOP plasmid. For example: if three batched of medium were tested, thirty-six wells need to be used (3 batches *3 replicates *2 dilutions *2 transfections). To that the positive and negative control were added in undiluted form (six wells each).
Transfection mixes were prepared according to table 10 for the number of wells calculated. 40.000 HEK293T cells were seeded per well of a black 96-well plate in 90 µl medium. 20 min. after seeding the cells 10 µl of transfection mix was added to each well and the plate(s) were incubated for 48 hours. Afterwards, the medium was removed and 100 µl

of 1:1 Wnt in D10 or 1:3 Wnt in D10 (diluted) were added to the respective wells and incubated for 24 hours.
For the dual luciferase assay, the wells were washed carefully with PBS (cells could detach). 25 µl of 1x Lysis buffer in H_2O were added per well and the plate was put on an orbital shaker for 30 min. at room temperature. Cell lysate was pipetted up and down and 20 µl was transferred to a new black 96-well plate. In order to run the Dual luciferase protocol, 20 µl per sample plus 1.1 ml LARII and Stop/Glo reagent were prepared according to the protocol (Promega) and used to prime the two injectors of the Synergy 2. The synergy program automatically added 20 µl LARII, shook the plate for 2 seconds, and read firefly luciferase luminosity. Directly afterwards, 20 µl of Stop/Glo were added to the same well, the plate was shaken for 2 seconds, and renilla luciferase luminosity was read. This process was repeated for all selected wells.
Using the renilla luminosity values for normalization and the values of the Wnt-CM from a previous batch, the obtained relative values were used to calculate how much Wnt-CM is necessary for continued long-term organoid culture.

Table 10: Transfecting HEK293T cells with TOP or FOP plasmid for DLA

Mix	Reagent	c (ng/µl)	per sample	50 wells TOP	50 wells FOP
DNA mix	TOPflash	10	0,1 µl	5 µl	
	FOPflash	10	0,1 µl		5 µl
	Renilla-Luc	1	0,1	5 µl	5 µl
	pcDNA/4TO (stuffer DNA)	100	0,1 µl	5 µl	5 µl
	P3000		0,2 µl	10 µl	10 µl
	Opti-MEM		5 µl	250 µl	250 µl
Lipo mix	Lipofectamine-3000		0,3 µl	15 µl	15 µl
	Opti-MEM		5 µl	250 µl	250 µl
		Total		540 µl	540 µl

5.7 Data Analysis

Initial scRNA seq data analysis was done by Dr. Florian Uhlitz. After all data sets were collected, extensive data analysis was done by other collaborators of AG Blüthgen: Thomas Sell analyzed CyTOF data, Bettina Schmidt performed the Kullback-Leibler divergence analyses. Stefan Peidli analyzed the SLAM-seq data and produced new Seurat files for me for further analysis.
I analyzed the data using R version 3.6.3 and RStudio Version 1.2.5033. For CyTOF analysis the libraries magrittr, tidyverse, viridisLite, viridis, ggplot2, corrplot and cowplot

were used to produce boxplots, correlation matrices and heatmaps. For scRNA sequencing data analysis tidyverse, magrittr, Seurat, ggplot2, viridisLite, viridis, readxl, dplyr, progeny and cowplot were used to produce heatmaps, violin plots and gene signature plots.
The code I used to produce the plots can be found on in the HU-Box link or the USB stick provided with this copy of the thesis.

6 Appendix

6.1 Network perturbation inhibitor panel

Table 11: Perturbation inhibitor panel

No.	Cat. No.	Target	Final Concentration
1	AZD8931	EGFR	50 nM
2	CH5183284	FGFR	200 nM
3	/	EGFR + FGFR	/
4	PLX4032	BRAF	3 µM
5	AZD6244	MEk	8 µM
6	/	MEk + EGFR	/
7	SCH772984	ERK	100 nM
8	LY2228820	P38	200 nM
9	PF3644022	Mk2	2,5 µM
10	PF477736	Chk1	1 µM
11	/	Chk1 + Mk2	/
12	GDC0941	PI3K	500 nM
13	MK2206	AKT	250 nM
14	AZD8055	mTOR (both complexes)	100 nM
15	Rapamycin	mTOR –> S6	100 nM
16	Chir99021	GSK3b	6 µM
17	SB525334	TGFb receptor	1 µM
18	IKK-16	Ikk	10 µM
19	S8334	Mst1/2	1 µM
20	/	DMSO Control	1:1000

6.2 Consumables, kits and devices

Table 12: Other material, consumables and machines used for cell culture

Other Cell Culture Material	Company	Cat. No.
Matrigel Basement Membrane Matrix	Corning	356231
TrypLE Express	Gibco	12604-013
Accutase	Biolegend	A6964-100ML
Dimethyl Sulfoxide for Cell Culture	PanReac AppliChem	A3672,0056
DPBS (10X)	Gibco	14200-067
Rho-Kinase Inhibitor (StemMACS Y27632)	Miltenyi Biotec	130-103-922
Recovery Cell Culture Freezing Medium	Life Technologies	12648010

BSA		
Proteomics Stabilizer	Smart Tube Inc.	PROT1
Desoxyribonuclease I	Sigma Aldrich	D4263-1VL
RealTime Glo	Promega	G9712
CellTox Green	Promega	G8742
RNasin Plus	Promega	N2615
Mouse Wnt3a	Time Bioscience	rmW3aH-010
Consumables		
100 - 1000 Biosphere Filter Tips	Sarstedt	70.762.211
20 - 300 Biosphere Filter Tips	Sarstedt	70.765.210
2 - 100 Biosphere Filter Tips	Sarstedt	70.760.212
0.5 - 20 Biosphere Filter Tips	Sarstedt	701.116.210
6-well plates	falcon	353046
24-well plates	falcon	353047
48-well plates	falcon	353078
50 ml cell star tubes	Greiner bio-one	227261
15 ml falcon	Corning	352097
T8+ Dispensehead cassettes	hp	FOL59A
D4+ Dispensehead cassettes	hp	FOL60A
Cell Counting Slides for TC10(tm)/TC20	Bio-Rad Laboratories	1450016
Low binding tubes	Corning (costar)	3207
CellTrics, 30 µm filter	sysmex	04-004-2326
KAPA Library Quantification Kit	Roche	07960140001
Hardware		
Centrifuge for tubes	eppendorf	5415C
Centrifuge for falcons	eppendorf	5810R
waterbath	GFL	1004
Pipetting robot	TECAN	D300e
Chromium Controller	10X Genomics	1000202
TapeStation	Agilent	4200
Synergy 2	BioTek	12592357

Table 13: Media composition for production of conditioned medium and testing

Wnt-CM	**Company**	**Cat. No.**	**Final**	**Add**
Dulbecco's MEM: 3.7g/L $NaHCO_3$, 4.5g/L d-Glucose, stable Glutamin, w/o NaPyruvate, low Endotoxin	Merck	FG0435		500ml

OR: DMEM, w: 4.5 g/L Glucose, stable Glutamine, w/o: Sodium pyruvate, w: 3.7 g/L $NaHCO_3$	PAN Biotech	P04-04500		500 ml
1% Pen/Strep	Invitrogen	15140-122	1x	5 ml
12% FCS				60 ml
Rspon1-CM: D10 medium				
DMEM low glucose (1g/L)	Sigma	D5546-500ml		500ml
1x GlutaMAX	Invitrogen	35050	1x	5ml
1% P/S	Invitrogen	15140-122	1x	5ml
10% FCS				5ml
Mouse colon organoids (CCM + REN)				40 ml
CCM				
R-Spo				1:50
EGF	Invitrogen	PMG8043	50 ng/ml	2 µl
Noggin	PeproTech	250-38-250		

6.3 Abbreviations

Abbreviation	Meaning
3D	three dimensional
4EBP1	Eukaryotic translation initiation factor 4E-binding protein 1
AKT	Protein kinase B
APC	Adenomatous polyposis coli
ATP	Adenosine triphosphate
BRAF	v-Raf murine sarcoma viral oncogene homolog B1
BSA	Bovine serum albumin
CCM	crypt culture medium
CIMP	CpG island methylator phenotype
CIN	Chromosomal instability
CM	conditioned medium
CRC	Colorectal cancer
CyTOF	Cytometry by time of flight
DMSO	Dimethyl sulfoxide
DNA	Deoxyribonucleic acid
EGF	Epidermal growth factor
EGFR	Epidermal Growth Factor Receptor
ERBB	Erythroblastic oncogene B
ERK	Extracellular signal-regulated kinase

FGF	fibroblast growth factor
GSK-3β	Glycogen synthase kinase-3 beta
KRAS	Kirsten Rat Sarcoma virus
MAPK	Mitogen-activated protein kinase
MEK (MAPKK)	MAPK kinase
MSI	Microsatellite instability
MSS	Microsatellite stable
mTOR	Mammalian target of rapamycin
mTORC	Mammalian target of rapamycin complex
mut	mutant
nM	nanomolar
nl	nanoliter
OT-	onco track
p-	phospho-protein
PBS	Phosphate buffered saline
RAF	rapidly accelerated fibrosarcoma
RAS	Rat sarcoma
RNA	Ribonucleic acid
RTK	Receptor tyrosine kinase
scRNA seq	single-cell RNA sequencing
SLAMseq	Thiol (SH)-Linked Alkylation for Metabolic sequencing
UMAP	Uniform Manifold Approximation and Projection for Dimension Reduction
wt	wildtype
µl	microliter
µM	micromolar

6.4 Statement of independent work

Herewith I confirm that I wrote this dissertation in its entirety and that no additional assistance was provided, other than from the sources listed. I expressly declare that I have not previously submitted or published this thesis in this or a similar form elsewhere as a dissertation.

Date, Signature

7 References

Alberts, B., Johnson, A., Lewis, J., Morgan, D., Raff, M., Roberts, K., and Walter, P. (2014). *Molecular Biology of the Cell*. Garland Science, New York, 6th editio edition.

Almendro, V., Cheng, Y. K., Randles, A., Itzkovitz, S., Marusyk, A., Ametller, E., Gonzalez-Farre, X., Muñoz, M., Russnes, H. G., Helland, Å., Rye, I. H., Borresen-Dale, A. L., Maruyama, R., VanOudenaarden, A., Dowsett, M., Jones, R. L., Reis-Filho, J., Gascon, P., Gönen, M., Michor, F., and Polyak, K. (2014). Inference of tumor evolution during chemotherapy by computational modeling and in situ analysis of genetic and phenotypic cellular diversity. *Cell Reports*, 6(3):514–527.

Arena, S., Bellosillo, B., Siravegna, G., Martínez, A., Cañadas, I., Lazzari, L., Ferruz, N., Russo, M., Misale, S., González, I., Iglesias, M., Gavilan, E., Corti, G., Hobor, S., Crisafulli, G., Salido, M., Sánchez, J., Dalmases, A., Bellmunt, J., De Fabritiis, G., Rovira, A., Di Nicolantonio, F., Albanell, J., Bardelli, A., and Montagut, C. (2015). Emergence of multiple EGFR extracellular mutations during cetuximab treatment in colorectal cancer. *Clinical Cancer Research*, 21(9):2157–2166.

Bakhoum, S. F., Ngo, B., Laughney, A. M., Cavallo, J. A., Murphy, C. J., Ly, P., Shah, P., Sriram, R. K., Watkins, T. B., Taunk, N. K., Duran, M., Pauli, C., Shaw, C., Chadalavada, K., Rajasekhar, V. K., Genovese, G., Venkatesan, S., Birkbak, N. J., McGranahan, N., Lundquist, M., LaPlant, Q., Healey, J. H., Elemento, O., Chung, C. H., Lee, N. Y., Imielenski, M., Nanjangud, G., Pe'er, D., Cleveland, D. W., Powell, S. N., Lammerding, J., Swanton, C., and Cantley, L. C. (2018). Chromosomal instability drives metastasis through a cytosolic DNA response. *Nature*, 553(7689):467–472.

Barker, N., Ridgway, R. A., Van Es, J. H., Van De Wetering, M., Begthel, H., Van Den Born, M., Danenberg, E., Clarke, A. R., Sansom, O. J., and Clevers, H. (2009). Crypt stem cells as the cells-of-origin of intestinal cancer. *Nature*, 457(7229):608–611.

Barker, N., Van Es, J. H., Kuipers, J., Kujala, P., Van Den Born, M., Cozijnsen, M., Haegebarth, A., Korving, J., Begthel, H., Peters, P. J., and Clevers, H. (2007). Identification of stem cells in small intestine and colon by marker gene Lgr5. *Nature*, 449(7165):1003–1007.

Batlle, E., Henderson, J. T., Beghtel, H., Van den Born, M. M., Sancho, E., Huls, G., Meeldijk, J., Robertson, J., Van de Wetering, M., Pawson, T., and Clevers, H. (2002). β-catenin and TCF mediate cell positioning in the intestinal epithelium by controlling the expression of EphB/EphrinB. *Cell*, 111(2):251–263.

Behrens, J., Von Kries, J. P., Kühl, M., Bruhn, L., Wedlich, D., Grosschedl, R., and Birchmeier, W. (1996). Functional interaction of β-catenin with the transcription factor LEF- 1.

Belair, D. G., Visconti, R. J., Hong, M., Marella, M., Peters, M. F., Scott, C. W., and Kolaja, K. L. (2020). Human ileal organoid model recapitulates clinical incidence of diarrhea associated with small molecule drugs. *Toxicology in Vitro*, 68(April):104928.

Bendall, S. C., Nolan, G. P., Roederer, M., and Chattopadhyay, P. K. (2012). A deep profiler ' s guide to cytometry. *Trends in Immunology*, 33(7):323–332.

Bendall, S. C., Simonds, E. F., Qiu, P., Amir, E. A. D., Krutzik, P. O., Finck, R., Bruggner, R. V., Melamed, R., Trejo, A., Ornatsky, O. I., Balderas, R. S., Plevritis, S. K., Sachs, K., Pe'er, D., Tanner, S. D., and Nolan, G. P. (2011). Single-cell mass cytometry of differential immune and drug responses across a human hematopoietic continuum. *Science*, 332(6030):687–696.

Betge, J., Rindtorff, N., Sauer, J., Rauscher, B., Dingert, C., Gaitantzi, H., Herweck, F., Srour-Mhanna, K., Miersch, T., Valentini, E., Boonekamp, K. E., Hauber, V., Gutting, T., Frank, L., Belle, S., Gaiser, T., Buchholz, I., Jesenofsky, R., Härtel, N., Zhan, T., Fischer, B., Breitkopf-Heinlein, K., Burgermeister, E., Ebert, M. P., and Boutros, M. (2022). The drug-induced phenotypic landscape of colorectal cancer organoids. *Nature Communications*, 13(1).

Billin, A. N., Thirlwell, H., and Ayer, D. E. (2000). β-Catenin–Histone Deacetylase Interactions Regulate the Transition of LEF1 from a Transcriptional Repressor to an Activator. *Molecular and Cellular Biology*, 20(18):6882–6890.

Blaj, C., Schmidt, E. M., Lamprecht, S., Hermeking, H., Jung, A., Kirchner, T., and Horst, D. (2017). Oncogenic effects of high MAPK activity in colorectal cancer mark progenitor cells and persist irrespective of RAS mutations. *Cancer Research*, 77(7):1763–1774.

Bliss, C. I. (1939). The Toxicity of Poisons Applied Jointly. *Annals of Applied Biology*, 26(3):585–615.

Brandt, R., Sell, T., Lüthen, M., Uhlitz, F., Klinger, B., Riemer, P., Giesecke-Thiel, C., Schulze, S., El-shimy, I. A., Kunkel, D., Fauler, B., Mielke, T., Mages, N., Herrmann, B. G., Sers, C., Blüthgen, N., and Morkel, M. (2019). Cell type-dependent differential activation of ERK by oncogenic KRAS in colon cancer and intestinal epithelium. *Nature Communications*, 10(1):2919.

Brock, A., Chang, H., and Huang, S. (2009). Non-genetic heterogeneity a mutation-independent driving force for the somatic evolution of tumours. *Nature Reviews Genetics*, 10(5):336–342.

Calon, A., Espinet, E., Palomo-Ponce, S., Tauriello, D. V., Iglesias, M., Céspedes, M. V., Sevillano, M., Nadal, C., Jung, P., Zhang, X. H., Byrom, D., Riera, A., Rossell, D., Mangues, R., Massagué, J., Sancho, E., and Batlle, E. (2012). Dependency of Colorectal Cancer on a TGF-β-Driven Program in Stromal Cells for Metastasis Initiation. *Cancer Cell*, 22(5):571–584.

Calon, A., Lonardo, E., Berenguer-Llergo, A., Espinet, E., Hernando-Momblona, X., Iglesias, M., Sevillano, M., Palomo-Ponce, S., Tauriello, D. V., Byrom, D., Cortina, C., Morral, C., Barceló, C., Tosi, S., Riera, A., Attolini, C. S. O., Rossell, D., Sancho, E., and Batlle, E. (2015). Stromal gene expression defines poor-prognosis subtypes in colorectal cancer. *Nature Genetics*, 47(4):320–329.

Canon, J., Rex, K., Saiki, A. Y., Mohr, C., Cooke, K., Bagal, D., Gaida, K., Holt, T., Knutson, C. G., Koppada, N., Lanman, B. A., Werner, J., Rapaport, A. S., San Miguel, T., Ortiz, R., Osgood, T.,

Sun, J. R., Zhu, X., McCarter, J. D., Volak, L. P., Houk, B. E., Fakih, M. G., O'Neil, B. H., Price, T. J., Falchook, G. S., Desai, J., Kuo, J., Govindan, R., Hong, D. S., Ouyang, W., Henary, H., Arvedson, T., Cee, V. J., and Lipford, J. R. (2019). The clinical KRAS(G12C) inhibitor AMG 510 drives anti-tumour immunity. *Nature*, 575(7781):217–223.

Carracedo, A., Ma, L., Teruya-Feldstein, J., Rojo, F., Salmena, L., Alimonti, A., Egia, A., Sasaki, A. T., Thomas, G., Kozma, S. C., Papa, A., Nardella, C., Cantley, L. C., Baselga, J., and Pandolfi, P. P. (2008). Inhibition of mTORC1 leads to MAPK pathway activation through a PI3K-dependent feedback loop in human cancer. *Journal of Clinical Investigation*, 118(9):3065–3074.

Cercek, A., Lumish, M., Sinopoli, J., Weiss, J., Shia, J., Lamendola-Essel, M., El Dika, I. H., Segal, N., Shcherba, M., Sugarman, R., Stadler, Z., Yaeger, R., Smith, J. J., Rousseau, B., Argiles, G., Patel, M., Desai, A., Saltz, L. B., Widmar, M., Iyer, K., Zhang, J., Gianino, N., Crane, C., Romesser, P. B., Pappou, E. P., Paty, P., Garcia-Aguilar, J., Gonen, M., Gollub, M., Weiser, M. R., Schalper, K. A., and Diaz, L. A. (2022). PD-1 Blockade in Mismatch Repair–Deficient, Locally Advanced Rectal Cancer. *New England Journal of Medicine*, 386(25):2363–2376.

Chan, C. W. M., Wong, N. A., Liu, Y., Bicknell, D., Turley, H., Hollins, L., Miller, C. J., Wilding, J. L., and Bodmer, W. F. (2009). Gastrointestinal differentiation marker Cytokeratin 20 is regulated by homeobox gene CDX1. *Proceedings of the National Academy of Sciences*, 106(6):1936–1941.

Chan, E. H., Nousiainen, M., Chalamalasetty, R. B., Schäfer, A., Nigg, E. A., and Sillje, H. H. (2005). The Ste20-like kinase Mst2 activates the human large tumor suppressor kinase Lats1. *Oncogene*, 24(12):2076–2086.

Chapnick, D. A., Warner, L., Bernet, J., Rao, T., and Liu, X. (2011). Partners in crime: The TGFβ and MAPK pathways in cancer progression. *Cell and Bioscience*, 1(1):42.

Chen, L. F. and Greene, W. C. (2004). Shaping the nuclear action of NF-κB. *Nature Reviews Molecular Cell Biology*, 5(5):392–401.

Chen, R., Rabinovitch, P. S., Crispin, D. A., Emond, M. J., Bronner, M. P., and Brentnall, T. A. (2005). The initiation of colon cancer in a chronic inflammatory setting. *Carcinogenesis*, 26(9):1513–1519.

Chen, X. G., Liu, F., Song, X. F., Wang, Z. H., Dong, Z. Q., Hu, Z. Q., Lan, R. Z., Guan, W., Zhou, T. G., Xu, X. M., Lei, H., Ye, Z. Q., Peng, E. J., Du, L. H., and Zhuang, Q. Y. (2010). Rapamycin regulates Akt and ERK phosphorylation through mTORC1 and mTORC2 signaling pathways. *Molecular Carcinogenesis*, 49(6):603–610.

Chevrier, S., Crowell, H. L., Zanotelli, V. R., Engler, S., Robinson, M. D., and Bodenmiller, B. (2018). Compensation of Signal Spillover in Suspension and Imaging Mass Cytometry. *Cell Systems*, 6(5):612–620.e5.

Clevers, H. and Nusse, R. (2012). Wnt/β-catenin signaling and disease. *Cell*, 149(6):1192–1205.

Cloninger, C., Bernath, A., Bashir, T., Holmes, B., and Gera, J. (2011). Inhibition of SAPK2/p38 enhances sensitivity to mTORC1 inhibition by blocking IRES-mediated translation initiation in glioblastoma. *Mol Cancer Therapy*, 10(12):2244–2256.

Cooks, T., Pateras, I. S., Tarcic, O., Solomon, H., Schetter, A. J., Wilder, S., Lozano, G., Pikarsky, E., Forshew, T., Rozenfeld, N., Harpaz, N., Itzkowitz, S., Harris, C. C., Rotter, V., Gorgoulis, V. G., and Oren, M. (2013). Mutant p53 Prolongs NF-κB Activation and Promotes Chronic Inflammation and Inflammation-Associated Colorectal Cancer. *Cancer Cell*, 23(5):634–646.

Corcoran, R. B., Andre, T., Atreya, C. E., Schellens, J. H., Yoshino, T., Bendell, J. C., Hollebecque, A., McRee, A. J., Siena, S., Middleton, G., Muro, K., Gordon, M. S., Tabernero, J., Yaeger, R., O'dwyer, P. J., Humblet, Y., de Vos, F., Jung, A. S., Brase, J. C., Jaeger, S., Bettinger, S., Mookerjee, B., Rangwala, F., and van Cutsem, E. (2018). Combined BRAF, EGFR, and MEK inhibition in patients with BRAF V600E -mutant colorectal cancer. *Cancer Discovery*, 8(4):428–443.

Corcoran, R. B., Ebi, H., Turke, A. B., Coffee, E. M., Cogdill, A. P., Brown, R. D., Pelle, P. D., Dias, D., Hung, K. E., Flaherty, K. T., Piris, A., Wargo, J. A., Settleman, J., Mino-kenudson, M., and Engelman, J. A. (2012). EGFR-mediated re-activation of MAPK signaling contributes to insensitivity of BRAF mutant colorectal cancers to RAF inhibition with vemurafenib. *Cancer Discovery*, 2(3):227–235.

Cordenonsi, M., Zanconato, F., Azzolin, L., Forcato, M., Rosato, A., Frasson, C., Inui, M., Montagner, M., Parenti, A. R., Poletti, A., Daidone, M. G., Dupont, S., Basso, G., Bicciato, S., and Piccolo, S. (2011). The hippo transducer TAZ confers cancer stem cell-related traits on breast cancer cells. *Cell*, 147(4):759–772.

Corrò, C., Novellasdemunt, L., and Li, V. S. (2020). A brief history of organoids. *American Journal of Physiology - Cell Physiology*, 319(1):C151–C165.

De Caestecker, M. P., Parks, W. T., Frank, C. J., Castagnino, P., Bottaro, D. P., Roberts, A. B., and Lechleider, R. J. (1998). Smad2 transduces common signals from receptor serinethreonine and tyrosine kinases. *Genes and Development*, 12(11):1587–1592.

Dekkers, J. F., Berkers, G., Kruisselbrink, E., Vonk, A., De Jonge, H. R., Janssens, H. M., Bronsveld, I., Van De Graaf, E. A., Nieuwenhuis, E. E., Houwen, R. H., Vleggaar, F. P., Escher, J. C., De Rijke, Y. B., Majoor, C. J., Heijerman, H. G., De Winter-De Groot, K. M., Clevers, H., Van Der Ent, C. K., and Beekman, J. M. (2016). Characterizing responses to CFTR-modulating drugs using rectal organoids derived from subjects with cystic fibrosis. *Science Translational Medicine*, 8(344).

Di Agostino, S., Sorrentino, G., Ingallina, E., Valenti, F., Ferraiuolo, M., Bicciato, S., Piazza, S., Strano, S., Del Sal, G., and Blandino, G. (2016). YAP enhances the pro-proliferative transcriptional activity of mutant p53 proteins . *EMBO reports*, 17(2):188–201.

Dietlein, F., Kalb, B., Jokic, M., Noll, E. M., Strong, A., Tharun, L., Ozretić, L., Künstlinger, H., Kambartel, K., Randerath, W. J., Jüngst, C., Schmitt, A., Torgovnick, A., Richters, A., Rauh,

D., Siedek, F., Persigehl, T., Mauch, C., Bartkova, J., Bradley, A., Sprick, M. R., Trumpp, A., Rad, R., Saur, D., Bartek, J., Wolf, J., Büttner, R., Thomas, R. K., and Reinhardt, H. C. (2015). A Synergistic Interaction between Chk1- and MK2 Inhibitors in KRAS-Mutant Cancer. *Cell*, 162(1):146–159.

Ding, Q., Xia, W., Liu, J. C., Yang, J. Y., Lee, D. F., Xia, J., Bartholomeusz, G., Li, Y., Pan, Y., Li, Z., Bargou, R. C., Qin, J., Lai, C. C., Tsai, F. J., Tsai, C. H., and Hung, M. C. (2005). Erk associates with and primes GSK-3β for its inactivation resulting in upregulation of β-catenin. *Molecular Cell*, 19(2):159–170.

Dorel, M., Klinger, B., Sieber, A., Prahallad, A., Gross, T., Bosdriesz, E., Wessels, L., and Bluthgen, N. (2018). Modelling Signalling Networks from Perturbation Data. *bioRxiv*, 10(June):243600.

Drost, J., Van Jaarsveld, R. H., Ponsioen, B., Zimberlin, C., Van Boxtel, R., Buijs, A., Sachs, N., Overmeer, R. M., Offerhaus, G. J., Begthel, H., Korving, J., Van De Wetering, M., Schwank, G., Logtenberg, M., Cuppen, E., Snippert, H. J., Medema, J. P., Kops, G. J., and Clevers, H. (2015). Sequential cancer mutations in cultured human intestinal stem cells. *Nature*, 521(7550):43–47.

Du, L., Wang, H., He, L., Zhang, J., Ni, B., Wang, X., Jin, H., Cahuzac, N., Mehrpour, M., Lu, Y., and Chen, Q. (2008). CD44 is of functional importance for colorectal cancer stem cells. *Clinical Cancer Research*, 14(21):6751–6760.

Fan, F., He, Z., Kong, L.-L., Chen, Q., Yuan, Q., Zhang, S., Ye, J., Liu, H., Sun, X., Geng, J., Yuan, L., Hong, L., Xiao, C., Zhang, W., Sun, X., Li, Y., Wang, P., Huang, L., Wu, X., Ji, Z., Wu, Q., Xia, N.-S., Gray, N. S., Chen, L., Yun, C.-H., Deng, X., and Zhou, D. (2016). Pharmacological targeting of kinases MST1 and MST2 augments tissue repair and regeneration. *Science Translational Medicine*, 8(352):352ra108–352ra108.

Fawkner-Corbett, D., Antanaviciute, A., Parikh, K., Jagielowicz, M., Gerós, A. S., Gupta, T., Ashley, N., Khamis, D., Fowler, D., Morrissey, E., Cunningham, C., Johnson, P. R., Koohy, H., and Simmons, A. (2021). Spatiotemporal analysis of human intestinal development at single-cell resolution. *Cell*, 184(3):810–826.e23.

Fearon, E. R. (2011). Molecular genetics of colorectal cancer. *Annual Review of Pathology: Mechanisms of Disease*, 6:479–507.

Fearon, E. R. and Vogelstein, B. (1990). A genetic model for colorectal tumorigenesis. *Cell*, 61(5):759–67.

Fernández-Zapata, C., Leman, J. K. H., Priller, J., Böttcher, C., Fernández-Zapata, C., Leman, J. K. H., Priller, J., Böttcher, C., Fernández-Zapata, C., Leman, J. K. H., Priller, J., and Böttcher, C. (2020). The use and limitations of single-cell mass cytometry for studying human microglia function. *Brain Pathology*, 30(6):1178–1191.

Fessler, E., Drost, J., Hooff, S. R., Linnekamp, J. F., Wang, X., Jansen, M., De Sousa E Melo, F., Prasetyanti, P. R., IJspeert, J. E., Franitza, M., Nürnberg, P., Noesel, C. J., Dekker, E., Vermeulen,

L., Clevers, H., and Medema, J. P. (2016). TGFβ signaling directs serrated adenomas to the mesenchymal colorectal cancer subtype. *EMBO Molecular Medicine*, 8(7):745–760.

Folkes, A. J., Alderton, W. K., Alix, S., Baker, S. J., Box, G., Chuckowree, I. S., Ahmadi, K., Clarke, P. A., Eccles, S. A., Friedman, L. S., Hayes, A., Hancox, T. C., Depledge, P., Moore, A. K. P., Olivero, A. G., Pang, J., Patel, S., Lensun, L., Pergl-Wilson, G. H., Robson, A., Saghir, N., Salphati, L., Sohal, S., Raynaud, F. I., Ultsch, M. H., Wallweber, H. J., Wan, N. C., Wiesmann, C., Workman, P., Valenti, M., Zhyvoloup, A., Shuttleworth, S. J., and Zvelebil, M. J. (2008). The Identification of 2-(1H-Indazol-4-yl)-6-(4-methanesulfonyl-piperazin-1-ylmethyl)-4-morpholin-4-yl-thieno[3,2-d]pyrimidine (GDC0941) as a Potent, Selective, Orally Bioavailable Inhibitor of Class I PI3 Kinase for the Treatment of Cancer. *Journal of Medicinal Chemistry*, 51:11.

Fritsche-Guenther, R., Witzel, F., Sieber, A., Herr, R., Schmidt, N., Braun, S., Brummer, T., Sers, C., and Blüthgen, N. (2011). Strong negative feedback from Erk to Raf confers robustness to MAPK signalling. *Molecular Systems Biology*, 7(489):1–13.

Fujii, M., Matano, M., Toshimitsu, K., Takano, A., Mikami, Y., Nishikori, S., Sugimoto, S., and Sato, T. (2018). Human Intestinal Organoids Maintain Self-Renewal Capacity and Cellular Diversity in Niche-Inspired Culture Condition. *Cell Stem Cell*, 23(6):787–793.e6.

Fujii, M., Shimokawa, M., Date, S., Takano, A., Matano, M., Nanki, K., Ohta, Y., Toshimitsu, K., Nakazato, Y., Kawasaki, K., Uraoka, T., Watanabe, T., Kanai, T., and Sato, T. (2016). A Colorectal Tumor Organoid Library Demonstrates Progressive Loss of Niche Factor Requirements during Tumorigenesis. *Cell Stem Cell*, 18(6):827–838.

Fumagalli, A., Oost, K. C., Kester, L., Morgner, J., Bornes, L., Bruens, L., Spaargaren, L., Azkanaz, M., Schelfhorst, T., Beerling, E., Heinz, M. C., Postrach, D., Seinstra, D., Sieuwerts, A. M., Martens, J. W., van der Elst, S., van Baalen, M., Bhowmick, D., Vrisekoop, N., Ellenbroek, S. I., Suijkerbuijk, S. J., Snippert, H. J., and van Rheenen, J. (2020). Plasticity of Lgr5-Negative Cancer Cells Drives Metastasis in Colorectal Cancer. *Cell Stem Cell*, 26(4):569–578.e7.

Furth, N., Aylon, Y., and Oren, M. (2018). P53 shades of Hippo. *Cell Death and Differentiation*, 25(1):81–92.

Ganesh, K., Wu, C., O'Rourke, K. P., Szeglin, B. C., Zheng, Y., Sauvé, C. E. G., Adileh, M., Wasserman, I., Marco, M. R., Kim, A. S., Shady, M., Sanchez-Vega, F., Karthaus, W. R., Won, H. H., Choi, S. H., Pelossof, R., Barlas, A., Ntiamoah, P., Pappou, E., Elghouayel, A., Strong, J. S., Chen, C. T., Harris, J. W., Weiser, M. R., Nash, G. M., Guillem, J. G., Wei, I. H., Kolesnick, R. N., Veeraraghavan, H., Ortiz, E. J., Petkovska, I., Cercek, A., Manova-Todorova, K. O., Saltz, L. B., Lavery, J. A., DeMatteo, R. P., Massagué, J., Paty, P. B., Yaeger, R., Chen, X., Patil, S., Clevers, H., Berger, M. F., Lowe, S. W., Shia, J., Romesser, P. B., Dow, L. E., Garcia-Aguilar, J., Sawyers, C. L., and Smith, J. J. (2019). A rectal cancer organoid platform to study individual responses to chemoradiation. *Nature Medicine*, 25(10):1607–1614.

Gilmore, T. D. (2006). Introduction to NF-κB: Players, pathways, perspectives. *Oncogene*, 25(51):6680–6684.

Gregorieff, A., Liu, Y., Inanlou, M. R., Khomchuk, Y., and Wrana, J. L. (2015). Yap-dependent reprogramming of Lgr5+ stem cells drives intestinal regeneration and cancer. *Nature*, 526(7575):715–718.

Grinat, J., Heuberger, J., Vidal, R. O., Goveas, N., Kosel, F., Berenguer-Llergo, A., Kranz, A., Wulf-Goldenberg, A., Behrens, D., Melcher, B., Sauer, S., Vieth, M., Batlle, E., Stewart, A. F., and Birchmeier, W. (2020). The epigenetic regulator Mll1 is required for Wnt-driven intestinal tumorigenesis and cancer stemness. *Nature Communications*, 11(1).

Guinney, J., Dienstmann, R., Wang, X., De Reyniès, A., Schlicker, A., Soneson, C., Marisa, L., Roepman, P., Nyamundanda, G., Angelino, P., Bot, B. M., Morris, J. S., Simon, I. M., Gerster, S., Fessler, E., De Sousa .E Melo, F., Missiaglia, E., Ramay, H., Barras, D., Homicsko, K., Maru, D., Manyam, G. C., Broom, B., Boige, V., Perez-Villamil, B., Laderas, T., Salazar, R., Gray, J. W., Hanahan, D., Tabernero, J., Bernards, R., Friend, S. H., Laurent-Puig, P., Medema, J. P., Sadanandam, A., Wessels, L., Delorenzi, M., Kopetz, S., Vermeulen, L., and Tejpar, S. (2015). The consensus molecular subtypes of colorectal cancer. *Nature Medicine*, 21(11):1350–1356.

Gunnarsson, E. B., De, S., Leder, K., and Foo, J. (2020). Understanding the role of phenotypic switching in cancer drug resistance. *Journal of Theoretical Biology*, 490:110162.

Hadari, Y. R., Gotoh, N., Kouhara, H., Lax, I., and Schlessinger, J. (2001). Critical role for the docking-protein FRS2 in FGF receptor-mediated signal transduction pathways. *PNAS*, 98(15):8578–8583.

Hanahan, D. and Weinberg, R. A. (2000). The Hallmarks of Cancer. *Cell*, 100:57–70.

Harvey, K. F., Pfleger, C. M., and Hariharan, I. K. (2003). The Drosophila Mst ortholog, hippo, restricts growth and cell proliferation and promotes apoptosis. *Cell*, 114(4):457–467.

Herranz, N., Gallage, S., Mellone, M., Wuestefeld, T., Klotz, S., Hanley, C. J., Raguz, S., Acosta, J. C., Innes, A. J., Banito, A., Georgilis, A., Montoya, A., Wolter, K., Dharmalingam, G., Faull, P., Carroll, T., Martínez-Barbera, J. P., Cutillas, P., Reisinger, F., Heikenwalder, M., Miller, R. A., Withers, D., Zender, L., Thomas, G. J., and Gil, J. (2015). mTOR regulates MAPKAPK2 translation to control the senescence-associated secretory phenotype. *Nature Cell Biology*, 17(9):1205–1217.

Herzenberg, L. A., Parks, D., Sahaf, B., Perez, O., Roederer, M., and Herzenberg, L. A. (2002). The History and Future of the Fluorescence Activated Cell Sorter and Flow Cytometry: A View from Stanford. *Clinical Chemistry*, pages 1819–1827.

Herzog, V. A., Reichholf, B., Neumann, T., Rescheneder, P., Bhat, P., Burkard, T. R., Wlotzka, W., Von Haeseler, A., Zuber, J., and Ameres, S. L. (2017). Thiol-linked alkylation of RNA to assess expression dynamics. *Nature Methods*, 14(12):1198–1204.

Hirata, A., Utikal, J., Yamashita, S., Aoki, H., Watanabe, A., Yamamoto, T., Okano, H., Bardeesy, N., Kunisada, T., Ushijima, T., Hara, A., Jaenisch, R., Hochedlinger, K., and Yamada, Y. (2013).

Dose-dependent roles for canonical Wnt signalling in de novo crypt formation and cell cycle properties of the colonic epithelium. *Development (Cambridge)*, 140(1):66–75.

Hobor, S., Van Emburgh, B. O., Crowley, E., Misale, S., Di Nicolantonio, F., and Bardelli, A. (2014). TGFα and amphiregulin paracrine network promotes resistance to EGFR blockade in colorectal cancer cells. *Clinical Cancer Research*, 20(24):6429–6438.

Hong, S. K., Wu, P. K., Karkhanis, M., and Park, J. I. (2015). ERK1/2 can feedback-regulate cellular MEK1/2 levels. *Cellular Signalling*, 27(10):1939–1948.

Hu, M., Huang, H., Zhao, R., Li, P., Li, M., Miao, H., Chen, N., and Chen, M. (2014). AZD8055 induces cell death associated with autophagy and activation of AMPK in hepatocellular carcinoma. *Oncology Reports*, 31(2):649–656.

Hu, Z., Ding, J., Ma, Z., Sun, R., Seoane, J. A., Scott Shaffer, J., Suarez, C. J., Berghoff, A. S., Cremolini, C., Falcone, A., Loupakis, F., Birner, P., Preusser, M., Lenz, H. J., and Curtis, C. (2019). Quantitative evidence for early metastatic seeding in colorectal cancer. *Nature Genetics*, 51(7):1113–1122.

Huang, C. Y. and Tan, T. H. (2012). DUSPs, to MAP kinases and beyond. *Cell and Bioscience*, 2(1):1–10.

Huber, O., Korn, R., McLaughlin, J., Ohsugi, M., Herrmann, B. G., and Kemler, R. (1996). Nuclear localization of β-catenin by interaction with transcription factor LEF-1. *Mechanisms of Development*, 59(1):3–10.

Hveem, T. S., Merok, M. A., Pretorius, M. E., Novelli, M., Bævre, M. S., Sjo, O. H., Clinch, N., Liestøl, K., Svindland, A., Lothe, R. A., Nesbakken, A., and Danielsen, H. E. (2014). Prognostic impact of genomic instability in colorectal cancer. *British journal of cancer*, 110(8):2159–2164.

Ilicic, T., Kim, J. K., Kolodziejczyk, A. A., Bagger, F. O., McCarthy, D. J., Marioni, J. C., and Teichmann, S. A. (2016). Classification of low quality cells from single-cell RNA-seq data. *Genome Biology*, 17(1):1–15.

Jabri, B. and Ebert, E. (2007). Human CD8+ intraepithelial lymphocytes: A unique model to study the regulation of effector cytotoxic T lymphocytes in tissue. *Immunological Reviews*, 215(1):202–214.

Javelaud, D. and Mauviel, A. (2005). Crosstalk mechanisms between the mitogen-activated protein kinase pathways and Smad signaling downstream of TGF-β: Implications for carcinogenesis. *Oncogene*, 24(37):5742–5750.

Jin, L., Chen, Y., Cheng, D., He, Z., Shi, X., Du, B., Xi, X., Gao, Y., and Guo, Y. (2021). YAP inhibits autophagy and promotes progression of colorectal cancer via upregulating Bcl-2 expression. *Cell death And disease*, 12(5):457.

Jing, F., Kim, H. J., Kim, C. H., Kim, Y. J., Lee, J. H., and Kim, H. R. (2015). Colon cancer stem cell markers CD44 and CD133 in patients with colorectal cancer and synchronous hepatic metastases. *International Journal of Oncology*, 46(4):1582–1588.

Joanito, I., Wirapati, P., Zhao, N., Nawaz, Z., Yeo, G., Lee, F., Eng, C. L. P., Macalinao, D. C., Kahraman, M., Srinivasan, H., Lakshmanan, V., Verbandt, S., Tsantoulis, P., Gunn, N., Venkatesh, P. N., Poh, Z. W., Nahar, R., Oh, H. L. J., Loo, J. M., Chia, S., Cheow, L. F., Cheruba, E., Wong, M. T., Kua, L., Chua, C., Nguyen, A., Golovan, J., Gan, A., Lim, W.-J. J., Guo, Y. A., Yap, C. K., Tay, B., Hong, Y., Chong, D. Q., Chok, A.-Y. Y., Park, W.-Y. Y., Han, S., Chang, M. H., Seow-En, I., Fu, C., Mathew, R., Toh, E.-L. L., Hong, L. Z., Skanderup, A. J., DasGupta, R., Ong, C.-A. A. J. A. J., Lim, K. H., Tan, E. K. W., Koo, S.-L. L., Leow, W. Q., Tejpar, S., Prabhakar, S., and Tan, I. B. (2022). Single-cell and bulk transcriptome sequencing identifies two epithelial tumor cell states and refines the consensus molecular classification of colorectal cancer. *Nature Genetics*, 54(7):963–975.

Jonker, D. J., O'Callaghan, C. J., Karapetis, C. S., Zalcberg, J. R., Tu, D., Au, H.-J., Berry, S. R., Krahn, M., Price, T., Simes, R. J., Tebbutt, N. C., van Hazel, G., Wierzbicki, R., Langer, C., and Moore, M. J. (2007). Cetuximab for the Treatment of Colorectal Cancer. *New England Journal of Medicine*, 357(20):2040–2048.

Juo, Y. Y., Johnston, F. M., Zhang, D. Y., Juo, H. H., Wang, H., Pappou, E. P., Yu, T., Easwaran, H., Baylin, S., van Engeland, M., and Ahuja, N. (2014). Prognostic value of CpG island methylator phenotype among colorectal cancer patients: A systematic review and meta-analysis. *Annals of Oncology*, 25(12):2314–2327.

Kane, M. F., Loda, M., Gaida, G. M., Lipman, J., Mishra, R., Goldman, H., Jessup, J. M., and Kolodner, R. (1997). Methylation of the hMLH1 promoter correlates with lack of expression of hMLH1 in sporadic colon tumors and mismatch repair-defective human tumor cell lines. *Cancer Research*, 57(5):808–811.

Karapetis, C. S., Khambata-Ford, S., Jonker, D. J., O'Callaghan, C. J., Tu, D., Tebbutt, N. C., Simes, R. J., Chalchal, H., Shapiro, J. D., Robitaille, S., Price, T. J., Shepherd, L., Au, H.-J., Langer, C., Moore, M. J., and Zalcberg, J. R. (2008). K-ras Mutations and Benefit from Cetuximab in Advanced Colorectal Cancer. *New England Journal of Medicine*, 359(17):1757–1765.

Kaufmann, S. H., Desnoyers, S., Ottaviano, Y., Davidson, N. E., and Poirier, G. G. (1993). Specific proteolytic cleavage of poly(ADP-ribose) polymerase: an early marker of chemotherapy-induced apoptosis. *Cancer research*, 53(17):3976–85.

Kawarada, Y., Inoue, Y., Kawasaki, F., Fukuura, K., Sato, K., Tanaka, T., Itoh, Y., and Hayashi, H. (2016). TGF-β induces p53/Smads complex formation in the PAI-1 promoter to activate transcription. *Scientific Reports*, 6(September):1–13.

Kirouac, D. C., Saez-Rodriguez, J., Swantek, J., Burke, J. M., Lauffenburger, D. A., and Sorger, P. K. (2012). Creating and analyzing pathway and protein interaction compendia for modelling signal transduction networks. *BMC Systems Biology*, 6.

Klingbiel, D., Saridaki, Z., Roth, A. D., Bosman, F. T., Delorenzi, M., and Tejpar, S. (2015). Prognosis of stage II and III colon cancer treated with adjuvant 5-fluorouracil or FOLFIRI in relation to microsatellite status: Results of the PETACC-3 trial. *Annals of Oncology*, 26(1):126–132.

Klinger, B., Sieber, A., Fritsche-Guenther, R., Witzel, F., Berry, L., Schumacher, D., Yan, Y., Durek, P., Merchant, M., Schäfer, R., Sers, C., and Blüthgen, N. (2013). Network quantification of EGFR signaling unveils potential for targeted combination therapy. *Molecular Systems Biology*, 9(1).

Klotz-Noack, K., Klinger, B., Rivera, M., Bublitz, N., Uhlitz, F., Riemer, P., Lüthen, M., Sell, T., Kasack, K., Gastl, B., Ispasanie, S. S., Simon, T., Janssen, N., Schwab, M., Zuber, J., Horst, D., Blüthgen, N., Schäfer, R., Morkel, M., and Sers, C. (2020). SFPQ Depletion Is Synthetically Lethal with BRAFV600E in Colorectal Cancer Cells. *Cell Reports*, 32(12).

Kolahi, K. S., Nakano, M., and Kuo, C. J. (2020). Organoids as Oracles for Precision Medicine in Rectal Cancer. *Cell Stem Cell*, 26(1):4–6.

Kopetz, S., Grothey, A., Yaeger, R., Van Cutsem, E., Desai, J., Yoshino, T., Wasan, H., Ciardiello, F., Loupakis, F., Hong, Y. S., Steeghs, N., Guren, T. K., Arkenau, H.-T., Garcia-Alfonso, P., Pfeiffer, P., Orlov, S., Lonardi, S., Elez, E., Kim, T.-W., Schellens, J. H., Guo, C., Krishnan, A., Dekervel, J., Morris, V., Calvo Ferrandiz, A., Tarpgaard, L., Braun, M., Gollerkeri, A., Keir, C., Maharry, K., Pickard, M., Christy-Bittel, J., Anderson, L., Sandor, V., and Tabernero, J. (2019). Encorafenib, Binimetinib, and Cetuximab in BRAF V600E–Mutated Colorectal Cancer. *New England Journal of Medicine*, 381(17):1632–1643.

Korinek, V., Barker, N., Morin, P. J., Van Wichen, D., De Weger, R., Kinzler, K. W., Vogelstein, B., and Clevers, H. (1997). Constitutive transcriptional activation by a β-catenin-Tcf complex in APC(-/-) colon carcinoma. *Science*, 275(5307):1784–1787.

Koveitypour, Z., Panahi, F., Vakilian, M., Peymani, M., Seyed Forootan, F., Nasr Esfahani, M. H., and Ghaedi, K. (2019). Signaling pathways involved in colorectal cancer progression. *Cell and Bioscience*, 9(1):1–14.

Krishna, M. and Narang, H. (2008). The complexity of mitogen-activated protein kinases (MAPKs) made simple. *Cellular and Molecular Life Sciences*, 65(22):3525–3544.

Kuipers, E. J., Grady, W. M., Lieberman, D., Seufferlein, T., Sung, J. J., Boelens, P. G., van de Velde, C. J. H., Watanabe, T., van de Velde, C. J. H., Watanabe, T., van de Velde, C. J. H., Watanabe, T., van de Velde, C. J. H., Watanabe, T., van de Velde, C. J. H., Watanabe, T., van de Velde, C. J. H., Watanabe, T., van de Velde, C. J. H., Watanabe, T., van de Velde, C. J. H., Watanabe, T., van de Velde, C. J. H., Watanabe, T., van de Velde, C. J. H., Watanabe, T., van de Velde, C. J. H., Watanabe, T., van de Velde, C. J. H., Watanabe, T., van de Velde, C. J. H., Watanabe, T., van de Velde, C. J. H., Watanabe, T., van de Velde, C. J. H., and Watanabe, T. (2015). Colorectal cancer. *Nature Reviews Disease Primers*, 1:15065.

Kullback, S. and Leibler, R. (1951). On Information and Sufficiency. *The Annals of Mathematical Statistics*, 22(1):79 – 86.

Lake, D., Corrêa, S. A., and Müller, J. (2016). Negative feedback regulation of the ERK1/2 MAPK pathway. *Cellular and Molecular Life Sciences*, 73(23):4397–4413.

Leach, J. D. G., Vlahov, N., Tsantoulis, P., Ridgway, R. A., Flanagan, D. J., Gilroy, K., Sphyris, N., Vázquez, E. G., Vincent, D. F., Faller, W. J., Hodder, M. C., Raven, A., Fey, S., Najumudeen, A. K., Strathdee, D., Nixon, C., Hughes, M., Clark, W., Shaw, R., consortium, S., van Hooff, S. R., Huels, D. J., Medema, J. P., Barry, S. T., Frame, M. C., Unciti-Broceta, A., Leedham, S. J., Inman, G. J., Jackstadt, R., Thompson, B. J., Campbell, A. D., Tejpar, S., and Sansom, O. J. (2021). Oncogenic BRAF, unrestrained by TGFβ-receptor signalling, drives right-sided colonic tumorigenesis. *Nature communications*, 12(1):3464.

Lee, K. W., Lee, S. S., Kim, S. B., Sohn, B. H., Lee, H. S., Jang, H. J., Park, Y. Y., Kopetz, S., Kim, S. S., Oh, S. C., and Lee, J. S. (2015). Significant association of oncogene YAP1 with poor prognosis and cetuximab resistance in colorectal cancer patients. *Clinical Cancer Research*, 21(2):357–364.

Lee, M. C. W., Lopez-Diaz, F. J., Khan, S. Y., Tariq, M. A., Dayn, Y., Vaske, C. J., Radenbaugh, A. J., Kim, H. J., Emerson, B. M., and Pourm, N. (2014). Single-cell analyses of transcriptional heterogeneity during drug tolerance transition in cancer cells by RNA sequencing. *Proceedings of the National Academy of Sciences of the United States of America*, 111(44):E4726–E4735.

Lenos, K. J., Miedema, D. M., Lodestijn, S. C., Nijman, L. E., van den Bosch, T., Romero Ros, X., Lourenço, F. C., Lecca, M. C., van der Heijden, M., van Neerven, S. M., van Oort, A., Leveille, N., Adam, R. S., de Sousa E Melo, F., Otten, J., Veerman, P., Hypolite, G., Koens, L., Lyons, S. K., Stassi, G., Winton, D. J., Medema, J. P., Morrissey, E., Bijlsma, M. F., and Vermeulen, L. (2018). Stem cell functionality is microenvironmentally defined during tumour expansion and therapy response in colon cancer. *Nature Cell Biology*, 20(10):1193–1202.

Li, S., Schmitz, K. R., Jeffrey, P. D., Wiltzius, J. J., Kussie, P., and Ferguson, K. M. (2005). Structural basis for inhibition of the epidermal growth factor receptor by cetuximab. *Cancer Cell*, 7(4):301–311.

Li, Y., Zhao, Z., Xu, C., Zhou, Z., Zhu, Z., and You, T. (2014). HMGA2 induces transcription factor Slug expression to promote epithelial-to-mesenchymal transition and contributes to colon cancer progression. *Cancer Letters*, 355(1):130–140.

Liang, S. I., van Lengerich, B., Eichel, K., Cha, M., Patterson, D. M., Yoon, T. Y., von Zastrow, M., Jura, N., and Gartner, Z. J. (2018). Phosphorylated EGFR Dimers Are Not Sufficient to Activate Ras. *Cell Reports*, 22(10):2593–2600.

Liberzon, A., Birger, C., Thorvaldsdóttir, H., Ghandi, M., Mesirov, J. P., and Tamayo, P. (2015). The Molecular Signatures Database Hallmark Gene Set Collection. *Cell Systems*, 1(6):417–425.

Lim, Z. F. and Ma, P. C. (2019). Emerging insights of tumor heterogeneity and drug resistance mechanisms in lung cancer targeted therapy. *Journal of Hematology and Oncology*, 12(1):1–18.

Litvinov, S. V., Velders, M. P., Bakker, H. A., Fleuren, G. J., and Warnaar, S. O. (1994). Ep-CAM: a human epithelial antigen is a homophilic cell-cell adhesion molecule. *Journal of Cell Biology*, 125(2):437–446.

Liu, C. Y., Zha, Z. Y., Zhou, X., Zhang, H., Huang, W., Zhao, D., Li, T., Chan, S. W., Lim, C. J., Hong, W., Zhao, S., Xiong, Y., Lei, Q. Y., and Guan, K. L. (2010). The hippo tumor pathway promotes TAZ degradation by phosphorylating a phosphodegron and recruiting the SCFβ-TrCP E3 ligase. *Journal of Biological Chemistry*, 285(48):37159–37169.

Lu, T., Tian, L., Han, Y., Vogelbaum, M., and Stark, G. R. (2007). Dose-dependent cross-talk between the transforming growth factor-β and interleukin-1 signaling pathways. *Proceedings of the National Academy of Sciences of the United States of America*, 104(11):4365–4370.

Luecken, M. D. and Theis, F. J. (2019). Current best practices in single-cell RNA-seq analysis: a tutorial. *Molecular Systems Biology*, 15(6).

Lukonin, I., Serra, D., Challet Meylan, L., Volkmann, K., Baaten, J., Zhao, R., Meeusen, S., Colman, K., Maurer, F., Stadler, M. B., Jenkins, J., and Liberali, P. (2020). Phenotypic landscape of intestinal organoid regeneration. *Nature*, 586(7828):275–280.

Lupo, B., Sassi, F., Pinnelli, M., Galimi, F., Zanella, E. R., Vurchio, V., Migliardi, G., Gagliardi, P. A., Puliafito, A., Manganaro, D., Luraghi, P., Kragh, M., Pedersen, M. W., Horak, I. D., Boccaccio, C., Medico, E., Primo, L., Nichol, D., Spiteri, I., Heide, T., Vatsiou, A., Graham, T. A., Élez, E., Argiles, G., Nuciforo, P., Sottoriva, A., Dienstmann, R., Pasini, D., Grassi, E., Isella, C., Bertotti, A., and Trusolino, L. (2020). Colorectal cancer residual disease at maximal response to EGFR blockade displays a druggable Paneth cell–like phenotype. *Science Translational Medicine*, 12(555).

Lustig, B., Jerchow, B., Sachs, M., Weiler, S., Pietsch, T., Karsten, U., van de Wetering, M., Clevers, H., Schlag, P. M., Birchmeier, W., and Behrens, J. (2002). Negative feedback loop of Wnt signaling through upregulation of conductin/axin2 in colorectal and liver tumors. *Molecular and cellular biology*, 22(4):1184–1193.

Madrid, L. V., Mayo, M. W., Reuther, J. Y., and Baldwin, A. S. (2001). Akt Stimulates the Transactivation Potential of the RelA/p65 Subunit of NF-κB through Utilization of the IκB Kinase and Activation of the Mitogen-activated Protein Kinase p38. *Journal of Biological Chemistry*, 276(22):18934–18940.

Mair, F., Erickson, J. R., Voillet, V., Simoni, Y., Bi, T., Tyznik, A. J., Martin, J., Gottardo, R., Newell, E. W., and Prlic, M. (2020). A Targeted Multi-omic Analysis Approach Measures Protein Expression and Low-Abundance Transcripts on the Single-Cell Level. *Cell Reports*, 31(1):107499.

Malesci, A., Laghi, L., Bianchi, P., Delconte, G., Randolph, A., Torri, V., Carnaghi, C., Doci, R., Rosati, R., Montorsi, M., Roncalli, M., Gennari, L., and Santoro, A. (2007). Reduced likelihood of metastases in patients with microsatellite-unstable colorectal cancer. *Clinical Cancer Research*, 13(13):3831–3839.

Mariotto, A. B., Robin Yabroff, K., Shao, Y., Feuer, E. J., and Brown, M. L. (2011). Projections of the cost of cancer care in the United States: 2010-2020. *Journal of the National Cancer Institute*, 103(2):117–128.

Massagué, J. (2012). TGFβ signalling in context. *Nature Reviews Molecular Cell Biology*, 13(10):616–630.

McCarthy, R. L., Mak, D. H., Burks, J. K., and Barton, M. C. (2017). Rapid monoisotopic cisplatin based barcoding for multiplexed mass cytometry. *Scientific Reports*, 7(1):1–6.

McFall, T., Diedrich, J. K., Mengistu, M., Littlechild, S. L., Paskvan, K. V., Sisk-Hackworth, L., Moresco, J. J., Shaw, A. S., and Stites, E. C. (2019). A systems mechanism for KRAS mutant allele–specific responses to targeted therapy. *Science Signaling*, 12(600):eaaw8288.

Medunjanin, S., Schleithoff, L., Fiegehenn, C., Weinert, S., Zuschratter, W., and Braun-Dullaeus, R. C. (2016). GSK-3β controls NF-kappaB activity via IKKγ/NEMO. *Scientific Reports*, 6(November):1–11.

Merlos-Suárez, A., Barriga, F. M., Jung, P., Iglesias, M., Céspedes, M. V., Rossell, D., Sevillano, M., Hernando-Momblona, X., da Silva-Diz, V., Muñoz, P., Clevers, H., Sancho, E., Mangues, R., and Batlle, E. (2011). The Intestinal Stem Cell Signature Identifies Colorectal Cancer Stem Cells and Predicts Disease Relapse. *Cell Stem Cell*, 8(5):511–524.

Misale, S., Di Nicolantonio, F., Sartore-Bianchi, A., Siena, S., and Bardelli, A. (2014). Resistance to Anti-EGFR therapy in colorectal cancer: From heterogeneity to convergent evolution. *Cancer Discovery*, 4(11):1269–1280.

Misale, S., Yaeger, R., Hobor, S., Scala, E., Janakiraman, M., Liska, D., Valtorta, E., Schiavo, R., Buscarino, M., Siravegna, G., Bencardino, K., Cercek, A., Chen, C. T., Veronese, S., Zanon, C., Sartore-Bianchi, A., Gambacorta, M., Gallicchio, M., Vakiani, E., Boscaro, V., Medico, E., Weiser, M., Siena, S., Di Nicolantonio, F., Solit, D., and Bardelli, A. (2012). Emergence of KRAS mutations and acquired resistance to anti-EGFR therapy in colorectal cancer. *Nature*, 486(7404):532–536.

Mo, J. S., Meng, Z., Kim, Y. C., Park, H. W., Hansen, C. G., Kim, S., Lim, D. S., and Guan, K. L. (2015). Cellular energy stress induces AMPK-mediated regulation of YAP and the Hippo pathway. *Nature Cell Biology*, 17(4):500–510.

Molinelli, E. J., Korkut, A., Wang, W., Miller, M. L., Gauthier, N. P., Jing, X., Kaushik, P., He, Q., Mills, G., Solit, D. B., Pratilas, C. A., Weigt, M., Braunstein, A., Pagnani, A., Zecchina, R., and

Sander, C. (2013). Perturbation Biology: Inferring Signaling Networks in Cellular Systems. *PLoS Computational Biology*, 9(12).

Montinaro, A., Areso Zubiaur, I., Saggau, J., Kretz, A. L., Ferreira, R. M., Hassan, O., Kitzig, E., Müller, I., El-Bahrawy, M. A., von Karstedt, S., Kulms, D., Liccardi, G., Lemke, J., and Walczak, H. (2022). Potent pro-apoptotic combination therapy is highly effective in a broad range of cancers. *Cell Death and Differentiation*, 29(3):492–503.

Morin, P. J., Sparks, A. B., Korinek, V., Barker, N., Clevers, H., Vogelstein, B., and Kinzler, K. W. (1997). Activation of β-catenin-Tcf signaling in colon cancer by mutations in β-catenin or APC. *Science*, 275(5307):1787–1790.

Morkel, M., Riemer, P., Bläker, H., and Sers, C. (2015). Similar but different: distinct roles for KRAS and BRAF oncogenes in colorectal cancer development and therapy resistance. *Oncotarget*, 6(25):20785–20800.

Morris, L. G., Riaz, N., Desrichard, A., Şenbabaoğlu, Y., Hakimi, A. A., Makarov, V., Reis-Filho, J. S., and Chan, T. A. (2016). Pan-cancer analysis of intratumor heterogeneity as a prognostic determinant of survival. *Oncotarget*, 7(9):10051–10063.

Moya, I. M. and Halder, G. (2019). Hippo–YAP/TAZ signalling in organ regeneration and regenerative medicine. *Nature Reviews Molecular Cell Biology*, 20(4):211–226.

Muñoz, J., Stange, D. E., Schepers, A. G., Van De Wetering, M., Koo, B. K., Itzkovitz, S., Volckmann, R., Kung, K. S., Koster, J., Radulescu, S., Myant, K., Versteeg, R., Sansom, O. J., Van Es, J. H., Barker, N., Van Oudenaarden, A., Mohammed, S., Heck, A. J. R., and Clevers, H. (2012). The Lgr5 intestinal stem cell signature: Robust expression of proposed quiescent +4 cell markers. *EMBO Journal*, 31(14):3079–3091.

Nelson, D. E., Ihekwaba, A. E., Elliott, M., Johnson, J. R., Gibney, C. A., Foreman, B. E., Nelson, C., See, V., Horton, C. A., Spiller, D. G., Edwards, S. W., McDowell, H. P., Unitt, J. F., Sullivan, E., Grimley, R., Benson, N., Broomhead, D., Kell, D. B., and White, M. R. (2004). Oscillations in NF-κB signaling control the dynamics of gene expression. *Science*, 306(5696):704–708.

Novak, A. and Dedhar, S. (1999). Signaling through β-catenin and Lef/Tcf. *Cellular and Molecular Life Sciences CMLS*, 56(5):523–537.

Ooft, S. N., Weeber, F., Dijkstra, K. K., McLean, C. M., Kaing, S., van Werkhoven, E., Schipper, L., Hoes, L., Vis, D. J., van de Haar, J., Prevoo, W., Snaebjornsson, P., van der Velden, D., Klein, M., Chalabi, M., Boot, H., van Leerdam, M., Bloemendal, H. J., Beerepoot, L. V., Wessels, L., Cuppen, E., Clevers, H., and Voest, E. E. (2019). Patient-derived organoids can predict response to chemotherapy in metastatic colorectal cancer patients. *Science Translational Medicine*, 11(513):1–10.

Oren, Y., Tsabar, M., Cuoco, M. S., Amir-Zilberstein, L., Cabanos, H. F., Hütter, J. C., Hu, B., Thakore, P. I., Tabaka, M., Fulco, C. P., Colgan, W., Cuevas, B. M., Hurvitz, S. A., Slamon, D. J.,

Deik, A., Pierce, K. A., Clish, C., Hata, A. N., Zaganjor, E., Lahav, G., Politi, K., Brugge, J. S., and Regev, A. (2021). Cycling cancer persister cells arise from lineages with distinct programs. *Nature*, 596(7873):576–582.

Pages, G., Lenormand, P., L'Allemain, G., Chambard, J.-C. C., Meloche, S., Pouyssagurt, J., Fenton, W., and Pouyssegur, J. (1993). Mitogen-activated protein kinases p42(mapk) and p44(mapk) are required for fibroblast proliferation. *Proceedings of the National Academy of Sciences of the United States of America*, 90(18):8319–8323.

Park, H. W., Kim, Y. C., Yu, B., Moroishi, T., Mo, J. S., Plouffe, S. W., Meng, Z., Lin, K. C., Yu, F. X., Alexander, C. M., Wang, C. Y., and Guan, K. L. (2015). Alternative Wnt Signaling Activates YAP/TAZ. *Cell*, 162(4):780–794.

Parsons, D. W., Wang, T.-L., Samuels, Y., Bardelli, A., Cummins, J. M., DeLong, L., Silliman, N., Ptak, J., Szabo, S., Willson, J. K. V., Markowitz, S., Kinzler, K. W., Vogelstein, B., Lengauer, C., and Velculescu, V. E. (2005). Mutations in a signalling pathway. *Nature*, 436(7052):792–792.

Piccolo, S., Dupont, S., and Cordenonsi, M. (2014). The biology of YAP/TAZ: Hippo signaling and beyond. *Physiological Reviews*, 94(4):1287–1312.

Pietrantonio, F., Petrelli, F., Coinu, A., Di Bartolomeo, M., Borgonovo, K., Maggi, C., Cabiddu, M., Iacovelli, R., Bossi, I., Lonati, V., Ghilardi, M., De Braud, F., and Barni, S. (2015). Predictive role of BRAF mutations in patients with advanced colorectal cancer receiving cetuximab and panitumumab: A meta-analysis. *European Journal of Cancer*, 51(5):587–594.

Pinto, D., Gregorieff, A., Begthel, H., and Clevers, H. (2003). Canonical Wnt signals are essential for homeostasis of the intestinal epithelium. *Genes and Development*, 17(14):1709–1713.

Poulikakos, P. I., Zhang, C., Bollag, G., Shokat, K. M., and Rosen, N. (2010). RAF inhibitors transactivate RAF dimers and ERK signalling in cells with wild-type BRAF. *Nature*, 464(7287):427–430.

Qian, J., Olbrecht, S., Boeckx, B., Vos, H., Laoui, D., Etlioglu, E., Wauters, E., Pomella, V., Verbandt, S., Busschaert, P., Bassez, A., Franken, A., Bempt, M. V., Xiong, J., Weynand, B., van Herck, Y., Antoranz, A., Bosisio, F. M., Thienpont, B., Floris, G., Vergote, I., Smeets, A., Tejpar, S., and Lambrechts, D. (2020). A pan-cancer blueprint of the heterogeneous tumor microenvironment revealed by single-cell profiling. *Cell Research*, 30(9):745–762.

Qin, X., Sufi, J., Vlckova, P., Kyriakidou, P., Acton, S. E., Li, V. S. W., Nitz, M., and Tape, C. J. (2020). Cell-type-specific signaling networks in heterocellular organoids. *Nature Methods*, pages 1–8.

Raatz, M., Shah, S., Chitadze, G., Brüggemann, M., and Traulsen, A. (2021). The impact of phenotypic heterogeneity of tumour cells on treatment and relapse dynamics. *PLOS Computational Biology*, 17(2):e1008702.

Rad, R., Cadiñanos, J., Rad, L., Varela, I., Strong, A., Kriegl, L., Constantino-Casas, F., Eser, S., Hieber, M., Seidler, B., Price, S., Fraga, M. F., Calvanese, V., Hoffman, G., Ponstingl, H., Schneider, G., Yusa, K., Grove, C., Schmid, R. M., Wang, W., Vassiliou, G., Kirchner, T., McDermott, U., Liu, P., Saur, D., and Bradley, A. (2013). A Genetic Progression Model of Braf V600E-Induced Intestinal Tumorigenesis Reveals Targets for Therapeutic Intervention. *Cancer Cell*, 24(1):15–29.

Raj, A., Peskin, C. S., Tranchina, D., Vargas, D. Y., and Tyagi, S. (2006). Stochastic mRNA synthesis in mammalian cells. *PLoS Biology*, 4(10):1707–1719.

Rao, T. P. and Kühl, M. (2010). An updated overview on Wnt Signaling Pathways: A prelude for more. *Circulation Research*, 106(12):1798–1806.

Reimegård, J., Tarbier, M., Danielsson, M., Schuster, J., Baskaran, S., Panagiotou, S., Dahl, N., Friedländer, M. R., and Gallant, C. J. (2021). A combined approach for single-cell mRNA and intracellular protein expression analysis. *Communications Biology*, 4(1):1–11.

Remy, I., Montmarquette, A., and Michnick, S. W. (2004). PKB/Akt modulates TGF-β signalling through a direct interaction with Smad3. *Nature Cell Biology*, 6(4):358–365.

Riemer, P., Rydenfelt, M., Marks, M., van Eunen, K., Thedieck, K., Herrmann, B. G., Blüthgen, N., Sers, C., and Morkel, M. (2017). Oncogenic β-catenin and PIK3CA instruct network states and cancer phenotypes in intestinal organoids. *Journal of Cell Biology*, 216(6):1567–1577.

Riemer, P., Sreekumar, A., Reinke, S., Rad, R., Schäfer, R., Sers, C., Bläker, H., Herrmann, B. G., and Morkel, M. (2015). Transgenic expression of oncogenic BRAF induces loss of stem cells in the mouse intestine, which is antagonized by β-catenin activity. *Oncogene*, 34(24):3164–3175.

Röck, R., Mayrhofer, J. E., Torres-Quesada, O., Enzler, F., Raffeiner, A., Raffeiner, P., Feichtner, A., Huber, R. G., Koide, S., Taylor, S. S., Troppmair, J., and Stefan, E. (2019). BRAF inhibitors promote intermediate BRAF(V600E) conformations and binary interactions with activated RAS. *Science Advances*, 5(8):14–16.

Roulis, M., Kaklamanos, A., Schernthanner, M., Bielecki, P., Zhao, J., Kaffe, E., Frommelt, L.-S., Qu, R., Knapp, M. S., Henriques, A., Chalkidi, N., Koliaraki, V., Jiao, J., Brewer, J. R., Bacher, M., Blackburn, H. N., Zhao, X., Breyer, R. M., Aidinis, V., Jain, D., Su, B., Herschman, H. R., Kluger, Y., Kollias, G., and Flavell, R. A. (2020). Paracrine orchestration of intestinal tumorigenesis by a mesenchymal niche. *Nature*.

Russo, M., Crisafulli, G., Sogari, A., Reilly, N. M., Arena, S., Lamba, S., Bartolini, A., Amodio, V., Magrì, A., Novara, L., Sarotto, I., Nagel, Z. D., Piett, C. G., Amatu, A., Sartore-Bianchi, A., Siena, S., Bertotti, A., Trusolino, L., Corigliano, M., Gherardi, M., Lagomarsino, M. C., Nicolantonio, F. D., Bardelli, A., Di Nicolantonio, F., and Bardelli, A. (2019). Adaptive mutability of colorectal cancers in response to targeted therapies. *Science*, 366(6472):1473–1480.

Sabine, V. S., Faratian, D., Kirkegaard-Clausen, T., and Bartlett, J. M. (2012). Validation of activated caspase-3 antibody staining as a marker of apoptosis in breast cancer. *Histopathology*, 60(2):369–371.

Sato, T., Stange, D. E., Ferrante, M., J Vries, R. G., Van Es, J. H., Van Den Brink, S., Van Houdt, W. J., Pronk, A., Van Gorp, J., Siersema, P. D., and Clevers, H. (2011a). Long-term Expansion of Epithelial Organoids From Human Colon, Adenoma, Adenocarcinoma, and Barrett's Epithelium. *Gastroenterology*, 141:1762–1772.

Sato, T., Van Es, J. H., Snippert, H. J., Stange, D. E., Vries, R. G., Van Den Born, M., Barker, N., Shroyer, N. F., Van De Wetering, M., and Clevers, H. (2011b). Paneth cells constitute the niche for Lgr5 stem cells in intestinal crypts. *Nature*, 469(7330):415–418.

Sato, T., Vries, R. G., Snippert, H. J., Van De Wetering, M., Barker, N., Stange, D. E., Van Es, J. H., Abo, A., Kujala, P., Peters, P. J., and Clevers, H. (2009). Single Lgr5 stem cells build crypt-villus structures in vitro without a mesenchymal niche. *Nature*, 459(7244):262–265.

Schlegelmilch, K., Mohseni, M., Kirak, O., Pruszak, J., Rodriguez, J. R., Zhou, D., Kreger, B. T., Vasioukhin, V., Avruch, J., Brummelkamp, T. R., and Camargo, F. D. (2011). Yap1 acts downstream of α-catenin to control epidermal proliferation. *Cell*, 144(5):782–795.

Schmidt, E. M., Lamprecht, S., Blaj, C., Schaaf, C., Krebs, S., Blum, H., Hermeking, H., Jung, A., Kirchner, T., and Horst, D. (2018). Targeting tumor cell plasticity by combined inhibition of NOT CH and MAPK signaling in colon cancer. *Journal of Experimental Medicine*, 215(6):1693–1708.

Schnalzger, T. E., Groot, M. H., Zhang, C., Mosa, M. H., Michels, B. E., Röder, J., Darvishi, T., Wels, W. S., and Farin, H. F. (2019). 3D model for CAR -mediated cytotoxicity using patient-derived colorectal cancer organoids. *The EMBO Journal*, 38(12):1–15.

Schubert, M., Klinger, B., Klünemann, M., Sieber, A., Uhlitz, F., Sauer, S., Garnett, M. J., Blüthgen, N., and Saez-Rodriguez, J. (2018). Perturbation-response genes reveal signaling footprints in cancer gene expression. *Nature Communications*, 9(1).

Schumacher, D., Andrieux, G., Boehnke, K., Keil, M., Silvestri, A., Silvestrov, M., Keilholz, U., Haybaeck, J., Erdmann, G., Sachse, C., Templin, M., Hoffmann, J., Boerries, M., Schäfer, R., and Regenbrecht, C. R. (2019). Heterogeneous pathway activation and drug response modelled in colorectal-tumor-derived 3D cultures. *PLoS Genetics*, 15(3).

Schütte, M., Risch, T., Abdavi-Azar, N., Boehnke, K., Schumacher, D., Keil, M., Yildiriman, R., Jandrasits, C., Borodina, T., Amstislavskiy, V., Worth, C. L., Schweiger, C., Liebs, S., Lange, M., Warnatz, H. J., Butcher, L. M., Barrett, J. E., Sultan, M., Wierling, C., Golob-Schwarzl, N., Lax, S., Uranitsch, S., Becker, M., Welte, Y., Regan, J. L., Silvestrov, M., Kehler, I., Fusi, A., Kessler, T., Herwig, R., Landegren, U., Wienke, D., Nilsson, M., Velasco, J. A., Garin-Chesa, P., Reinhard, C., Beck, S., Schäfer, R., Regenbrecht, C. R., Henderson, D., Lange, B., Haybaeck, J., Keilholz, U., Hoffmann, J., Lehrach, H., and Yaspo, M. L. (2017). Molecular dissection of colorectal cancer in pre-clinical models identifies biomarkers predicting sensitivity to EGFR inhibitors. *Nature Communications*, 8.

Schwanhäusser, B., Busse, D., Li, N., Dittmar, G., Schuchhardt, J., Wolf, J., Chen, W., and Selbach, M. (2011). Global quantification of mammalian gene expression control. *Nature*, 473(7347):337–342.

Schwitalla, S., Fingerle, A. A., Cammareri, P., Nebelsiek, T., Göktuna, S. I., Ziegler, P. K., Canli, O., Heijmans, J., Huels, D. J., Moreaux, G., Rupec, R. A., Gerhard, M., Schmid, R., Barker, N., Clevers, H., Lang, R., Neumann, J., Kirchner, T., Taketo, M. M., van den Brink, G. R., Sansom, O. J., Arkan, M. C., and Greten, F. R. (2013). Intestinal Tumorigenesis Initiated by Dedifferentiation and Acquisition of Stem-Cell-like Properties. *Cell*, 152(1-2):25–38.

Serra, D., Mayr, U., Boni, A., Lukonin, I., Rempfler, M., Challet Meylan, L., Stadler, M. B., Strnad, P., Papasaikas, P., Vischi, D., Waldt, A., Roma, G., and Liberali, P. (2019). Self-organization and symmetry breaking in intestinal organoid development. *Nature*.

Shashkova, E. V., Trivedi, J., Cline-Smith, A. B., Ferris, C., Buchwald, Z. S., Gibbs, J., Novack, D., and Aurora, R. (2016). Osteoclast-Primed Foxp3+ CD8 T Cells Induce T-bet, Eomesodermin, and IFN-γ To Regulate Bone Resorption. *Journal of immunology (Baltimore, Md. : 1950)*, 197(3):726–35.

Shum, E. Y., Walczak, E. M., Chang, C., and Christina Fan, H. (2019). Quantitation of mRNA Transcripts and Proteins Using the BD Rhapsody™ Single-Cell Analysis System. *Advances in Experimental Medicine and Biology*, 1129:63–79.

Simons, C. C., Hughes, L. A., Smits, K. M., Khalid-de Bakker, C. A., de Bruïne, A. P., Carvalho, B., Meijer, G. A., Schouten, L. J., van den Brandt, P. A., Weijenberg, M. P., and van Engeland, M. (2013). A novel classification of colorectal tumors based on microsatellite instability, the CpG island methylator phenotype and chromosomal instability: Implications for prognosis. *Annals of Oncology*, 24(8):2048–2056.

Smillie, C. S., Biton, M., Ordovas-Montanes, J., Sullivan, K. M., Burgin, G., Graham, D. B., Herbst, R. H., Rogel, N., Slyper, M., Waldman, J., Sud, M., Andrews, E., Velonias, G., Haber, A. L., Jagadeesh, K., Vickovic, S., Yao, J., Stevens, C., Dionne, D., Nguyen, L. T., Villani, A. C., Hofree, M., Creasey, E. A., Huang, H., Rozenblatt-Rosen, O., Garber, J. J., Khalili, H., Desch, A. N., Daly, M. J., Ananthakrishnan, A. N., Shalek, A. K., Xavier, R. J., and Regev, A. (2019). Intra- and Inter-cellular Rewiring of the Human Colon during Ulcerative Colitis. *Cell*, 178(3):714–730.e22.

Sun, C., Hobor, S., Bertotti, A., Zecchin, D., Huang, S., Galimi, F., Cottino, F., Prahallad, A., Grernrum, W., Tzani, A., Schlicker, A., Wessels, L. F., Smit, E. F., Thunnissen, E., Halonen, P., Lieftink, C., Beijersbergen, R. L., DiNicolantonio, F., Bardelli, A., Trusolino, L., and Bernards, R. (2014). Intrinsic resistance to MEK inhibition in kras mutant lung and colon cancer through transcriptional induction of ERBB3. *Cell Reports*, 7(1):86–93.

Sun, S. Y., Rosenberg, L. M., Wang, X., Zhou, Z., Yue, P., Fu, H., and Khuri, F. R. (2005). Activation of Akt and eIF4E survival pathways by rapamycin-mediated mammalian target of rapamycin inhibition. *Cancer Research*, 65(16):7052–7058.

Tanner, S. D., Ornatsky, O., Bandura, D. R., and Baranov, V. I. (2007). Multiplex bio-assay with inductively coupled plasma mass spectrometry: Towards a massively multivariate single-cell technology. *Spectrochimica Acta - Part B Atomic Spectroscopy*, 62(3 SPEC. ISS.):188–195.

Tariq, K. and Ghias, K. (2016). Colorectal cancer carcinogenesis: a review of mechanisms. *Cancer Biology And Medicine*, 13(1):120–35.

Turke, A. B., Song, Y., Costa, C., Cook, R., Arteaga, C. L., Asara, J. M., and Engelman, J. A. (2012). MEK inhibition leads to PI3K/AKT activation by relieving a negative feedback on ERBB receptors. *Cancer Research*, 72(13):3228–3237.

Uhlitz, F., Bischoff, P., Peidli, S., Sieber, A., Trinks, A., Lüthen, M., Obermayer, B., Blanc, E., Ruchiy, Y., Sell, T., Mamlouk, S., Arsie, R., Wei, T., Klotz-Noack, K., Schwarz, R. F., Sawitzki, B., Kamphues, C., Beule, D., Landthaler, M., Sers, C., Horst, D., Blüthgen, N., and Morkel, M. (2021). Mitogen-activated protein kinase activity drives cell trajectories in colorectal cancer. *EMBO Molecular Medicine*, 13(10):2172–2194.

Van Cutsem, E., Köhne, C.-H., Hitre, E., Zaluski, J., Chang Chien, C.-R., Makhson, A., D'Haens, G., Pintér, T., Lim, R., Bodoky, G., Roh, J. K., Folprecht, G., Ruff, P., Stroh, C., Tejpar, S., Schlichting, M., Nippgen, J., and Rougier, P. (2009). Cetuximab and Chemotherapy as Initial Treatment for Metastatic Colorectal Cancer. *New England Journal of Medicine*, 360(14):1408–1417.

Van Cutsem, E., Peeters, M., Siena, S., Humblet, Y., Hendlisz, A., Neyns, B., Canon, J. L., Van Laethem, J. L., Maurel, J., Richardson, G., Wolf, M., and Amado, R. G. (2007). Open-label phase III trial of panitumumab plus best supportive care compared with best supportive care alone in patients with chemotherapy- refractory metastatic colorectal cancer. *Journal of Clinical Oncology*, 25(13):1658–1664.

van de Wetering, M., Francies, H. E., Francis, J. M., Bounova, G., Iorio, F., Pronk, A., van Houdt, W., van Gorp, J., Taylor-Weiner, A., Kester, L., McLaren-Douglas, A., Blokker, J., Jaksani, S., Bartfeld, S., Volckman, R., van Sluis, P., Li, V. S., Seepo, S., Sekhar Pedamallu, C., Cibulskis, K., Carter, S. L., McKenna, A., Lawrence, M. S., Lichtenstein, L., Stewart, C., Koster, J., Versteeg, R., van Oudenaarden, A., Saez-Rodriguez, J., Vries, R. G., Getz, G., Wessels, L., Stratton, M. R., McDermott, U., Meyerson, M., Garnett, M. J., and Clevers, H. (2015). Prospective Derivation of a Living Organoid Biobank of Colorectal Cancer Patients. *Cell*, 161(4):933–945.

Van de Wetering, M., Sancho, E., Verweij, C., De Lau, W., Oving, I., Hurlstone, A., Van der Horn, K., Batlle, E., Coudreuse, D., Haramis, A. P., Tjon-Pon-Fong, M., Moerer, P., Van den Born, M., Soete, G., Pals, S., Eilers, M., Medema, R., and Clevers, H. (2002). The β-catenin/TCF-4 complex imposes a crypt progenitor phenotype on colorectal cancer cells. *Cell*, 111(2):241–250.

van der Flier, L. G. and Clevers, H. (2009). Stem Cells, Self-Renewal, and Differentiation in the Intestinal Epithelium. *Annual Review of Physiology*, 71:241 – 260.

Varelas, X., Samavarchi-Tehrani, P., Narimatsu, M., Weiss, A., Cockburn, K., Larsen, B. G., Rossant, J., and Wrana, J. L. (2010). The Crumbs Complex Couples Cell Density Sensing to Hippo-Dependent Control of the TGF-β-SMAD Pathway. *Developmental Cell*, 19(6):831–844.

Vermeulen, L., De Sousa E Melo, F., Van Der Heijden, M., Cameron, K., De Jong, J. H., Borovski, T., Tuynman, J. B., Todaro, M., Merz, C., Rodermond, H., Sprick, M. R., Kemper, K., Richel, D. J., Stassi, G., and Medema, J. P. (2010). Wnt activity defines colon cancer stem cells and is regulated by the microenvironment. *Nature Cell Biology*, 12(5):468–476.

Verrecchia, F., Chu, M. L., and Mauviel, A. (2001). Identification of Novel TGF-β/Smad Gene Targets in Dermal Fibroblasts using a Combined cDNA Microarray/Promoter Transactivation Approach. *Journal of Biological Chemistry*, 276(20):17058–17062.

Vlachogiannis, G., Hedayat, S., Vatsiou, A., Jamin, Y., Fernández-Mateos, J., Khan, K., Lampis, A., Eason, K., Huntingford, I., Burke, R., Rata, M., Koh, D.-M., Tunariu, N., Collins, D., Hulkki-Wilson, S., Ragulan, C., Spiteri, I., Moorcraft, S. Y., Chau, I., Rao, S., Watkins, D., Fotiadis, N., Bali, M., Darvish-Damavandi, M., Lote, H., Eltahir, Z., Smyth, E. C., Begum, R., Clarke, P. A., Hahne, J. C., Dowsett, M., De Bono, J., Workman, P., Sadanandam, A., Fassan, M., Sansom, O. J., Eccles, S., Starling, N., Braconi, C., Sottoriva, A., Robinson, S. P., Cunningham, D., and Valeri, N. (2018). Patient-derived organoids model treatment response of metastatic gastrointestinal cancers. *Science*, 6378(359):920 – 926.

Wan, P. T., Garnett, M. J., Roe, S. M., Lee, S., Niculescu-Duvaz, D., Good, V. M., Project, C. G., Jones, C. M., Marshall, C. J., Springer, C. J., Barford, D., and Marais, R. (2004). Mechanism of activation of the RAF-ERK signaling pathway by oncogenic mutations of B-RAF. *Cell*, 116(6):855–867.

Wan, X., Harkavy, B., Shen, N., Grohar, P., and Helman, L. J. (2007). Rapamycin induces feedback activation of Akt signaling through an IGF-1R-dependent mechanism. *Oncogene*, 26(13):1932–1940.

Wei, Z. and Liu, H. T. (2002). MAPK signal pathways in the regulation of cell proliferation in mammalian cells. *Cell Research*, 12(1):9–18.

Woolston, A., Khan, K., Cunningham, D., and Gerlinger, M. (2019). Genomic and Transcriptomic Determinants of Therapy Resistance and Immune Landscape Evolution during Anti-EGFR Treatment in Colorectal Cancer. *Cancer Cell*, 36:35–50.

Xi, Y. and Xu, P. (2021). Global colorectal cancer burden in 2020 and projections to 2040. *Translational Oncology*, 14(10):101174.

Yachida, S., Mudali, S., Martin, S. A., Montgomery, E. A., and Iacobuzio-Donahue, C. A. (2009). Beta-catenin nuclear labeling is a common feature of sessile serrated adenomas and correlates with early neoplastic progression after BRAF activation. *American Journal of Surgical Pathology*, 33(12):1823–1832.

Yao, Y., Xu, X., Yang, L., Zhu, J., Wan, J., Shen, L., Xia, F., Fu, G., Deng, Y., Pan, M., Guo, Q., Gao, X., Li, Y., Rao, X., Zhou, Y., Liang, L., Wang, Y., Zhang, J., Zhang, H., Li, G., Zhang, L., Peng, J., Cai, S., Hu, C., Gao, J., Clevers, H., Zhang, Z., and Hua, G. (2020). Patient-Derived Organoids Predict Chemoradiation Responses of Locally Advanced Rectal Cancer. *Cell Stem Cell*, 26(1):17–26.e6.

Yu, H., Lin, L., Zhang, Z., Zhang, H., and Hu, H. (2020). Targeting NF-κB pathway for the therapy of diseases: mechanism and clinical study. *Signal Transduction and Targeted Therapy*, 5(1).

Yuan, B., Shen, C., Luna, A., Korkut, A., Marks, D. S., Ingraham, J., and Sander, C. (2021). CellBox: Interpretable Machine Learning for Perturbation Biology with Application to the Design of Cancer Combination Therapy. *Cell Systems*, 12(2):128–140.e4.

Zhan, T., Ambrosi, G., Wandmacher, A. M., Rauscher, B., Betge, J., Rindtorff, N., Häussler, R. S., Hinsenkamp, I., Bamberg, L., Hessling, B., Müller-Decker, K., Erdmann, G., Burgermeister, E., Ebert, M. P., and Boutros, M. (2019). MEK inhibitors activate Wnt signalling and induce stem cell plasticity in colorectal cancer. *Nature Communications*, 10(1):2197.

Zhao, J., Yuan, X., Frödin, M., and Grummt, I. (2003). ERK-Dependent Phosphorylation of the Transcription Initiation Factor TIF-IA Is Required for RNA Polymerase I Transcription and Cell Growth. *Molecular Cell*, 11(2):405–413.

Zheng, C. F. and Guan, K. L. (1993). Properties of MEKs, the kinases that phosphorylate and activate the extracellular signal-regulated kinases. *Journal of Biological Chemistry*, 268(32):23933–23939.

Zhou, J., Li, C., Sachs, N., Chiu, M. C., Wong, B. H. Y., Chu, H., Poon, V. K. M., Wang, D., Zhao, X., Wen, L., Song, W., Yuan, S., Wong, K. K. Y., Chan, J. F. W., To, K. K. W., Chen, H., Clevers, H., and Yuen, K. Y. (2018). Differentiated human airway organoids to assess infectivity of emerging influenza virus. *Proceedings of the National Academy of Sciences of the United States of America*, 115(26):6822–6827.

Zimmermann, S. and Moelling, K. (1999). Phosphorylation and Regulation of Raf by Akt (Protein Kinase B). *Science*, 286(5445):1741–1744.

Zunder, E. R., Finck, R., Behbehani, G. K., Amir, E. A. D., Krishnaswamy, S., Gonzalez, V. D., Lorang, C. G., Bjornson, Z., Spitzer, M. H., Bodenmiller, B., Fantl, W. J., Pe'Er, D., and Nolan, G. P. (2015). Palladium-based mass tag cell barcoding with a doublet-filtering scheme and single-cell deconvolution algorithm. *Nature Protocols*, 10(2):316 – 333.

8 Publications

Benary, M., Bohn, S., **Lüthen, Mareen**, Nolis, I. K., Blüthgen, N., and Loewer, A. (2020). Disentangling Pro-mitotic Signaling during Cell Cycle Progression using Time-Resolved Single-Cell Imaging. *Cell Reports*, 31(2).

Brandt, R., Sell, T., **Lüthen, Mareen**, Uhlitz, F., Klinger, B., Riemer, P., Giesecke-Thiel, C., Schulze, S., El-shimy, I. A., Kunkel, D., Fauler, B., Mielke, T., Mages, N., Herrmann, B. G., Sers, C., Blüthgen, N., and Morkel, M. (2019). Cell type-dependent differential activation of ERK by oncogenic KRAS in colon cancer and intestinal epithelium. *Nature Communications*, 10(1):2919.

Goodwin, C. M., Waters, A. M., Klomp, J. E., Javaid, S., Bryant, K. L., Stalnecker, C. A., Drizyte-Miller, K., Papke, B., Yang, R., Amparo, A. M., Ozkan-Dagliyan, I., Baldelli, E., Calvert, V., Pierobon, M., Sorrentino, J. A., Beelen, A. P., Bublitz, N., **Lüthen, Mareen**, Wood, K. C., Petricoin, E. F., Sers, C., McRee, A. J., Cox, A. D., and Der, C. J. (2022). Combination Therapies with CDK4/6 Inhibitors to Treat KRAS-mutant Pancreatic Cancer. *Cancer Research*.

Klotz-Noack, K., Klinger, B., Rivera, M., Bublitz, N., Uhlitz, F., Riemer, P., **Lüthen, Mareen**, Sell, T., Kasack, K., Gastl, B., Ispasanie, S. S., Simon, T., Janssen, N., Schwab, M., Zuber, J., Horst, D., Blüthgen, N., Schäfer, R., Morkel, M., and Sers, C. (2020). SFPQ Depletion Is Synthetically Lethal with BRAFV600E in Colorectal Cancer Cells. *Cell Reports*, 32(12).

Uhlitz, F., Bischoff, P., Peidli, S., Sieber, A., Trinks, A., **Lüthen, Mareen**, Obermayer, B., Blanc, E., Ruchiy, Y., Sell, T., Mamlouk, S., Arsie, R., Wei, T., Klotz-Noack, K., Schwarz, R. F., Sawitzki, B., Kamphues, C., Beule, D., Landthaler, M., Sers, C., Horst, D., Blüthgen, N., and Morkel, M. (2021). Mitogen-activated protein kinase activity drives cell trajectories in colorectal cancer. *EMBO Molecular Medicine*, 13(10):2172–2194.